Edited by
Sabu Thomas
Didier Rouxel
Deepalekshmi Ponnamma

SPECTROSCOPY OF POLYMER NANOCOMPOSITES

Micro & Nano Technologies Series

Contents

Preface

Recent years have witnessed the steep growth of polymer-based industries; particularly those related to nanotechnology. Various fillers of nanodimensions impart abnormal properties when incorporated into polymers. For instance, the insulating polymers turn conducting, flexible elastomer chains become rigid, brittle materials become tougher, and so on. This substantiates the significance of nanoscience in the polymer industry and explains how various molecular properties can be tailored to achieve ultimately superior performance.

However, quality measurement of the materials synthesized has much more significance as far as determining the usefulness of a particular material is concerned. In this regard, spectroscopy has the utmost importance because it investigates both structural and functional features of materials. This book is written as a unique source by which the reader should understand the importance of all kinds of spectroscopic techniques in the field of polymer nanocomposites. It contains two parts; the first being Chapters 1−3, which give information about the significance of spectroscopic techniques in characterizing the nanocomposites, the meaning, definition, and types of nanocomposites, and the thermodynamics within the polymer nanocomposite systems. This part is particularly aimed at beginners in the field of material science, through which all basics of spectroscopy and the mode of characterization of polymer-based materials by this technique must be well understood.

The second part contains the remaining 12 chapters, each of which tells about particular spectroscopic techniques. The very common methods, such as infrared (IR) spectroscopy, ultraviolet (UV) spectroscopy, nuclear magnetic resonance (NMR) spectroscopy, Raman, and x-ray photoelectron spectroscopy are discussed in detail, with the basic mechanisms and proper examples from polymer science and nanotechnology. Some other techniques, such as Brillouin spectroscopy (BS), dielectric spectroscopy, photothermal, and Mossbaeur spectroscopy, are also incorporated so that the whole book has become an encyclopedia in the area of polymer nanocomposite spectroscopy.

The authors were selected according to their expertise in specific techniques, and all of them deserve special thanks in making the contribution valuable.

Sabu Thomas
Didier Rouxel
Deepalekshmi Ponnamma

CHAPTER

9 EPR spectroscopy of polymer:fullerene nanocomposites[1]

V.I. Krinichnyi
Institute of Problems of Chemical Physics, Chernogolovka, Russian Federation

9.1 INTRODUCTION

Nanoscale composites with a π-conjugated polymer matrix have attracted a lot of attention in recent years due to potential use of their unique physical and chemical properties in molecular electronics [1–3] and spintronics [4] for energy conversion and transport. Among elements of organic electronics based on nanomodified polymers, polymer:fullerene composites seem to be most suitable for polymer photovoltaics which explains their wide investigation [5–8]. Fullerene molecules embedded into polymer matrix of such systems form so-called bulk heterojunctions (BHJ) and perform as electron acceptors (electron transporter, *n*-type material) and as electron donors (hole transporter, *p*-type material), respectively. Composites of soluble derivatives of conjugated polymers and fullerene were proved [8] to be the most efficient systems for utilization in plastic devices. Beyond photoinduced charge exciting and separation, positive carriers are transported to electrodes by polarons diffusing in the polymer phase and electrons hopping between fullerene domains embedded into the polymer matrix. A definitive advantage of BHJ is that it can be made by simply mixing the materials in an organic solvent, and casting with standard solution deposition techniques, such as spin coating [9].

The irradiation of such BHJ by visible light with photon energy $h\nu_{ph}$ higher than the π–π^* energy gap E_g of the polymer matrix leads to the formation of ion radical quasipairs, polaron $P^{+\bullet}$ on a polymer chain (donor, D) and fullerene $F_{60}^{-\bullet}$ (acceptor, A), and charge separation during the following successive stages [10]:

(i) excitation of polaron on polymer chain: $D + A \xrightarrow{h\nu} D^* + A$,
(ii) excitation delocalization on the complex: $D^* + A \xrightarrow{h\nu} (D + A)^*$,
(iii) initiation of charge transfer: $(D{-}A)^* \rightarrow (D^{\delta+}{-}A^{\delta-})$,

[1]This chapter is dedicated to my beautiful daughters, Natalia and Ksenia.

Spectroscopy of Polymer Nanocomposites. DOI: http://dx.doi.org/10.1016/B978-0-323-40183-8.00009-4

(iv) formation of ion-radical pair: $(D^{\delta+}-A^{\delta-})^* \rightarrow (D^{+\bullet}-A^{-\bullet})$,
(v) charge separation: $(D^{+\bullet}-A^{-\bullet}) \rightarrow D^{+\bullet}-A^{-\bullet}$.

The donor and acceptor units are spatially close, but not covalently bonded. At each step, the *D-A* system can relax back to the ground state, releasing energy to the "lattice" in the form of either heat or emitted light. This process, revealed by time-resolved optical spectroscopy occurs in the femtosecond time domain [11,12] (e.g., about 100 fs in optimized polymer:fullerene BHJ [13], whereas the electron back transfer with charge annihilation is much slower, possibly due to dynamics and the relatively slow structural relaxation in such a system of lowered dimensionality. Understanding of photoexcitation, recombination of charge carriers, and other electronic processes realized in conjugated polymers is of fundamental interest for both material characterization and molecular device fabrication.

BHJs are characterized by efficient light-excited charge generation at the interface between two organic materials with different electron affinities. Figure 9.1 illustrates the energy diagram of two intrinsic semiconductors, poly(3-alkylthiophene) (P3AT) and [6,6]-phenyl-C_{61}-butanoic acid methyl ester ($PC_{61}BM$), most widely used in polymer:fullerene composites, before making a contact between

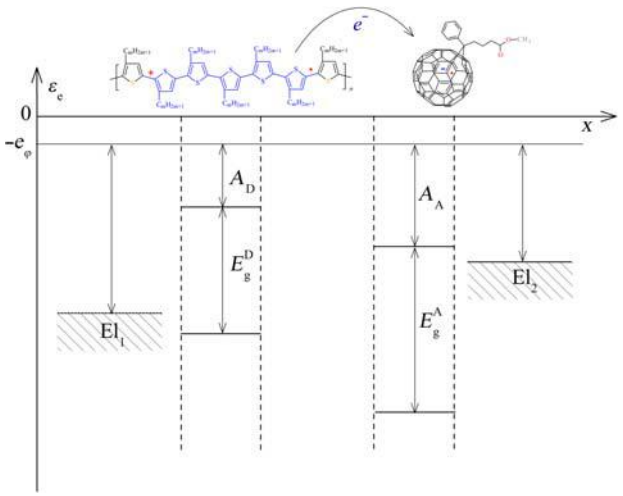

FIGURE 9.1

Schematic band diagram of two semiconductors with different electron affinities before forming the BHJ between them. The electron donor (A_D) and electron acceptor (A_A) affinities are defined as compared with the electron energy in vacuum at the same electrical potential. E_g^D and E_g^A are the band gap energies of the electron donor and electron acceptor, respectively. At the top of the figure, the P3AT and PC61BM are schematically shown as electron donor and electron acceptor, respectively. The appearance of the polaron quasiparticle with a spin $S = ½$ and an elemental positive charge in a P3AT chain and ion radical with an elemental negative charge and a spin $S = ½$ on a $PC_{61}BM$ are also shown.

them. A heterojunction formed by these materials inserted between a high work-function electrode (El_1) matching the highest occupied molecular orbital level of the donor ($HOMO_D$) and a low work-function electrode (El_2) matching the lowest unoccupied molecular orbital level of the electron acceptor ($LUMO_A$) should, in principle, act as a diode with rectifying current−voltage characteristics. Under the forward bias (the low work-function electrode is biased negative in respect to the high work-function electrode) the electron injection into the $LUMO_A$ layer from the low work-function electrode as well as the electron extraction out of the $HOMO_D$ by the high work-function electrode is energetically possible and a high current may flow through the heterojunction. Under reverse bias (the low work-function electrode is biased positive in respect to the high work-function electrode), the electron removal from the electron donor and electron injection to the electron acceptor is energetically unfavorable. The formation of the polaron $P^{+\bullet}$ and fullerene $F_{61}^{-\bullet}$ charge carriers is shown in Fig. 9.1.

The mobility and stability of charge carriers was found [14] to be considerably higher in the BHJ formed by poly(3-hexylthiophene) (P3HT) with $PC_{61}BM$ globes as compared with other polymer:fullerene composites. The much longer charge carrier lifetime achieved in the P3HT:$PC_{61}BM$ films should, therefore, lead to a higher concentration of charge carriers and their reduced recombination rate. Specific nanomorphology of such composites could result in screened Coulomb potential between the radical pairs photoexcited in their BHJ and facilitate their splitting into noninteracting charge carriers with a reduced probability of their further annihilation. An example of such nanomorphology is better structural order in the presence of interface dipoles, which would provoke the creation of a potential barrier for carrier recombination in this composite. This implies that longer charge carrier lifetime can be achieved at the same concentrations which finally result in higher photocurrent and larger power-conversion efficiency of such solar cells. For these reasons, PCBM has appeared to be most suitable electron acceptor to be used for an extended time in plastic solar-cell prototypes.

Efficiency of light conversion has already attained about 3% for the P3HT:$PC_{61}BM$ BHJ [15] and around 6−8% for other organic solar cells [16]. This parameter is governed by different factors. The first limitation originated from the high binding energy of polarons photoinduced in conjugated polymers upon light excitation, so by adding an electron acceptor, it becomes energetically favorable for the electron to escape a polymer macromolecule and to transfer to an acceptor. This requires the $LUMO_D$ to be 0.3−0.5 eV higher than the $LUMO_A$ [17,18]. However, such energy difference can be much higher for some polymer matrices, which decreases optimal open-circuit voltage, since the latter is ultimately limited by the difference between the $HOMO_D$ and $LUMO_A$ [19,20]. Raising the $LUMO_A$, for example, the efficiency factor of plastic solar cells increases without affecting their light absorption. This approach is theoretically more beneficial for a single-layer solar cell, and results in an estimated efficiency of 8.4% when the LUMO offset is reduced to 0.5 eV [21]. The structure of donor and acceptor as well as the conformation of respective BHJ can also affect charge

transport and recombination [22]. Lenes et al. [23] have suggested *bis*-$PC_{62}BM$ methanofullerene, $bmF_{62}^{-\bullet}$, to use as electron acceptor, in which the fullerene cage is functionalized by two methanobridged PBM side groups, with a higher (by $\sim$0.1 eV) $LUMO_A$ than that of $PC_{61}BM$. Indeed, quantum efficiency of plastic solar cells appeared [24,25] to be improved when $PC_{61}BM$ is replaced by *bis*-PC62BM. However, it was shown [26] that the photoluminescence dynamics became slower after the replacement due to the reorganization of BHJ. Quantum efficiency can also be reduced due to possible formation of triplets from intersystem crossing of the excitons or by intersystem crossing of the charge-separated states followed by charge recombination [27]. Another way to improve this important parameter is by decreasing the band gap of the active polymer matrix (near 1.9 eV for P3HT), which limits the absorbance of light photons with higher energy. Thus, to harvest more solar photons, which increases the power-conversion efficiency, one should use polymers with lower band gaps in such devices. Poly[*N*-9″-hepta-decanyl-2,7-carbazole-alt-5,5-(4′,7′-di-2-thienyl-2′,1′,3′-benzothiadiazole)] (PCDTBT), with band gap less than 1.9 eV [28,29], was discovered [30] to be one of the most efficient low-band gap semiconducting polymers for use in organic thin film field-effect transistors and solar cells [31–33]. The light conversion efficiency of the PCDTBT:$PC_{71}BM$ composite layer reached 7.2% [34] due to a relatively low $HOMO_D$ level and an internal quantum efficiency approaching 100% [35]. Such outstanding results were explained [13] mainly by ultrafast charge separation in the PCDTBT:$PC_{71}BM$ composite before localization of the primary excitation to form a bound exciton in contrast with, for example, a P3HT-based one, where photoinduced charge separation happens after diffusion of the polymer exciton to a fullerene interface. The other important property, the morphology of the PCDTBT:$PC_{71}BM$ BHJ is [34,36] laterally oriented with a column-like, bilayer-ordered polymer matrix with methanofullerene embedded between its chains that improves the carrier mobility, and, in particular, its electron mobility [37]. The dimensionality of the PCDTBT backbone with such morphology should be higher than that of P3AT matrices. Gutzler and Perepichka [38] showed that higher π-overlapping in two-dimensional (2D) thiophene-based polymers hinders their torsional twisting and, therefore, lowers their band gap. This allows holes to form through such well-ordered bilayer PCDTBT surfaces so the anode and electrons can move to the cathode inside methanofullerene pools located between these bilayers. This is evidence that charge dynamics is another important parameter affecting device light conversion efficiency. Higher charge carrier mobility of the polymer increases the diffusion length of electrons and photoinitiated holes and decreases the probability of their recombination in the active layer.

A real polymer:fullerene system consists of domains with different band gaps (i.e., different $LUMO_A$–$HOMO_D$) determining its energetic disorder with Gaussian distributed density of states [39]. Another constraint comes due to the finite number and mobility of charge carriers in organic solar cells which are lower when compared with conventional semiconductors. These main parameters depend on the

structure and properties of a polymer matrix and fullerene derivative embedded [23,40–43]. This why their power-conversion efficiency is appears to be governed by an ultrafast electron transfer from photoexcited polymer to fullerene [12], a large interfacial area for charge separation due to intimate blending of the materials [9], and efficient carrier transport across a thin film. Unambiguously, to increase power-conversion efficiency it is necessary to photoinitiate a higher density of charge carriers. However, an increased carrier density causes a reduced lifetime due to bimolecular recombination and the efficiency of solar cells might be reduced [43].

Planarity and regioregularity of polymer matrix, which are governed by the structure of the polymer and methanofullerene side substitutes, play an important role in charge separation and transition in the polymer:fullerene composites. The presence of substituents additionally affects torsional and energetic disorder of polymer chains, thereby changing effective mobility of charge carriers. Side chain groups accelerate torsional and librational chain dynamics, modulating intrachain and interchain charge transfer, respectively. Ginder et al. [44] showed that the torsional reordering of the backbone rings of conjugated polymers determines their electronic structure and charge transfer mechanism. Sensitivity of the average ring torsion angle between adjacent thiophene rings θ to steric repulsion and electron delocalization is manifested in the effects of derivatization and temperature on optical spectra of these materials. The less a torsion angle θ, the higher transfer integral and effective crystallinity can be reached. The increase in planarity reduces band gap, increases charge mobility, stability, and interactions between parallel polymer planes. Modification of the P3HT:$PC_{61}BM$ composite with N- or B-doped carbon nanotubes [45] and self-assembled dipole molecule deposition in plastic light-emitting diodes [46] can, in principle, to enhance their power-conversion efficiency. Thermal annealing can also modify morphological structure of BHJ and increase its light conversing efficiency [47]. Such a treatment leads to the formation of crystalline regions in an amorphous polymer matrix that is accompanied by the shift of its light absorption maximum (e.g., of the P3HT:$PC_{61}BM$ composite from $h\nu_{ph} \approx 2.5–2.8$ eV to the lower photon energies, 1.9–2.3 eV). The observed shift should also evidence the increase in the conjugation length in crystallites, because the polymer molecules within such crystallites are perfectly oriented and there are no defects like chain kinks, which limit the conjugation length. This process can be controlled, by UV/vis spectroscopy, grazing-incidence X-ray diffraction, and atomic force microscopy [48–50].

Charge recombination is considered to be predominantly nongeminate process governing the efficiency of polymer:fullerene solar cells [51–53]. Normally, the delay of charge carriers consists of prompt and persistent contributions [54,55]. The excitation light intensity dependence of prompt process is of activation bimolecular type and implies mutual annihilation within the initially created radical pair [56]. The persistent contribution is independent on the excitation intensity and originates from deep traps due to disorder [54]. Bimolecular and quadrimolecular recombination was shown [57] to be dominant in the P3AT:fullerene composites at the lower and higher intensity of the excited light, respectively.

The lifetime of charge carriers is usually estimated from photocurrent transients after the excitation by a short light pulse. However, this method seems to be inaccurate in the case of organic materials because the photocurrent transients depend not only on the decay of charge carrier concentration, but also on the mobility relaxation within the broad density of states [58]. An estimate of lifetimes from transient absorption techniques is difficult to make because of the very large dispersion observed leading to power law decays [51]. Thus, the photoexciting of charge carriers and their recombination are the most interesting points.

Both the $P^{+\bullet}$ and $F_{61}^{-\bullet}$ charge carriers possess uncompensated spin $S = ½$. This accounts for the wide use of light-induced electron paramagnetic resonance (LEPR) spectroscopy as a direct method for the investigation of charge photoexciting, separation, transfer, and recombination in fullerene-modified conjugated polymers [56,57,59]. Intramolecular quasi-one-dimensional (Q1D) charge transfer by polaron along polymer chains and its quasi-three-dimensional (Q3D) hopping between polymer and/or fullerene domains, as well as a rotational librative motion of fullerene globes are realized in the polymer:fullerene system. All spin-assisted molecular and electronic processes are expected to correlate. LEPR measurements revealed the existence of two radicals with different line shapes, magnetic resonance parameters, and saturation behaviors. The photoinduced spins should coact with their own charged microenvironment through exchange or dipole−dipole interaction. Such interactions do not register in LEPR spectra of plastic solar cells, which can be interpreted as the recession of mobile polarons on a conjugated polymer backbone and the fullerene anions with the rate faster than 10^{-9} s. That is the reason why both the charge carriers excited in main polymer:fullerene composites are characterized by considerably long lifetimes and can be registered separately. Understanding the basic physics underlying the electron relaxation and dynamic behavior of fullerene-modified organic polymers is essential for the optimization of devices based on these materials.

The optimization of structure and nanomorphology of BHJ as well as the understanding of photoexcitation, dynamics, and recombination of charge carriers in such systems is of fundamental interest for controlled fabrication of optimal molecular photovoltaic devices. Understanding the charge separation and charge transport in such materials at a molecular level is crucial for improving the efficiency of the solar cells. However, they are not yet understood in detail and there is no generally applicable model describing molecular, electronic, and relaxation processes in different polymer:fullerene composites and there are no generally applicable models available.

This chapter describes a multifrequency (9.7−140 GHz) LEPR study of magnetic, relaxation and charge transport properties of spin charge carriers stabilized and photoinduced in different organic polymer:fullerene composites that was mainly conducted at the Institute of Problems of Chemical Physics of the Russian Academy of Sciences.

It starts with a brief theoretical background necessary for the interpretation of main spectroscopic parameters of spin carriers transferring a charge cross polymer:fullerene BHJ. The main results obtained by the LEPR spectroscopy in

combination with the steady-state saturation of spin-packets in the study of the nature, relaxation, and dynamics of both types of spin charge carriers are summarized and analyzed in the next section. Some examples of the utilization of multispin polymer/polymer:fullerene composites in molecular electronics and spintronics finalize their review.

9.2 THEORETICAL BACKGROUNDS OF ELECTRON PARAMAGNETIC RESONANCE IN POLYMER COMPOSITES

Electron paramagnetic resonance (EPR) spectroscopy is one of the most widely used and productive methods in structural and dynamic studies of various model, biological and physical solids containing free radicals, ion radicals, molecules in triplet states, transition metal complexes, and other paramagnetic centers (PC) [60–67]. The method is based on the interactions of unpaired electron spins in a sample with microwave irradiation in a magnetic field. Electrons possess a property called "spin," resulting in an angular momentum. Because the electron is charged, there is a magnetic moment which points in the opposite direction to the angular momentum vector associated with the angular momentum. In an external magnetic field, the spin processes around the field direction at the Larmor frequency and thus a component of the magnetic moment is either parallel or antiparallel to the field direction. If a microwave field of this frequency is applied to a spin containing sample, then the spins can change their direction relative to the magnetic field. This results in absorption of the microwave field, which may be measured. Spin reorientation is also affected by microenvironment. Microwave absorption depends on the fundamental properties of spin reservoir previously described. Thus, EPR spectra can yield detailed information not only about spin properties of a sample, but also about its structure and composition.

A typical continuous wave (CW) EPR spectrometer consists of a source of microwave radiation, a cavity into which the sample is placed (to enhance the size of the microwave field), a detector to measure the microwave signal reflected from the cavity, and a magnet to induce the external field. A small modulation field allows the use of phase sensitive detection for the increased signal/noise ratio. In some cases pulse EPR techniques, accompanied by the Fourier transformation of the signal [68–71], can be used for the study of fast dynamics and spin transitions. Such techniques, which involve illuminating the sample with a sequence of short pulses and then observing what it reradiates, offer time-resolved experiments, the ability to resolve closely spaced lines, and are good for measuring relaxation. To excite the whole spectrum at once, however, requires very short, very high power pulses and requires the system dead-time (the time after the last illuminating pulse before measurement can begin) to be minimized. The system dead-time often means that the signal from any broad lines has decayed before measurement starts.

The parameters which can be directly obtained from CW EPR spectra of PC stabilized or initiated in polymer systems are described next.

9.2.1 LANDÉ FACTOR

The main magnetic resonance parameters directly obtained by EPR spectroscopy for PC in condensed systems are the Landé factor (or g-factor: that is the ratio of electron mechanic momentum to a magnetic moment), spin susceptibility, and line width. The first of them is characterized by the Zeeman interaction of an unpaired electron with an external magnetic field. If the fundamental resonance condition [72] is fulfilled, an unpaired electron absorbs an energy quantum and is transferred to a higher excited state. It can be seen that the higher B_0 (or ω_e) value, the higher excited state an electron can reach and the higher spectral resolution can therefore be realized. It is stipulated by the distribution of spin density in a polymer unit, the energy of exited configurations, and its interaction with nearest nuclear. If the spin of polaron weakly interacts with own environments, its Landé-factor lies near g-factor of free electron, $g_e = 2.00232$. At higher interaction, environmental nuclei induce an additional magnetic field resulting tensoric character of its Landé-factor [63,73,74].

$$\hbar\omega_e = \gamma_e \hbar B_0 = g\mu_B B_0 \tag{9.1}$$

where $\hbar = h/2\pi$ is the Planck constant, $\omega_e = 2\pi\nu_e$ is the Larmor or electron spin precession angular frequency, γ_e is the hyromagnetic ratio for electron, B_0 is the strength of an external magnetic field, and μ_B is the Bohr magneton.

$$\mathbf{g} = \begin{vmatrix} g_{xx} & & \\ & g_{yy} & \\ & & g_{zz} \end{vmatrix} = \begin{vmatrix} 2\left(1 + \dfrac{\lambda\rho(0)}{\Delta E_{n\pi^*}}\right) & & \\ & 2\left(1 + \dfrac{\lambda\rho(0)}{\Delta E_{\sigma\pi^*}}\right) & \\ & & 2 \end{vmatrix}, \tag{9.2}$$

where λ is the spin-orbit coupling constant, $\rho(0)$ is the spin density, $\Delta E_{n\pi^*}$ and $\Delta E_{\sigma\pi^*}$ are the energies of the unpaired electron $n \to \pi^*$ and $\sigma \to \pi^*$ transitions, respectively. Normally, polarons in organic conjugated polymers require a small energy of $n \to \pi^*$ transition. This leads to deviation of its g_{xx} and g_{yy} values from g_e, so then the inequality $g_{xx} > g_{yy} > g_{zz} \approx g_e$ holds for these PC.

Weak interaction of an unpaired electron delocalized on polaron over L lattice units with heteroatoms involved in a polymer backbone provokes rhombic symmetry of spin density and, therefore, anisotropy of its magnetic resonance parameters. Since the backbone of a polymer can be expected to lie preferably parallel to the film substrate [75], the lowest principal g-value is associated with the polymer backbone. The macromolecule can take any orientation relative to the z-axis, that is, the polymer backbone direction as is derives from the presence

of both the g_{xx} and g_{yy} components in the spectra for all orientations of the film. Thus, the g-factor anisotropy is the result of inhomogeneous distribution of additional fields in such systems along the x and y directions within the plane of their σ-skeleton rather than along its perpendicular z direction. Multifrequency EPR spectroscopy allows the resolution of some PC with near g-factors or spectral components of PC with anisotropic g-factor [63,74,76–78]. Harmonic librations of polymer chains with localized polarons can modulate the charge transfer integrals in polymer composites as it is typical for organic molecular ordered systems [79]. This should change the effective g-factor as:

$$g = g_0 + \frac{A}{\hbar\omega_l}\coth\left(\frac{\hbar\omega_l}{2k_BT}\right), \tag{9.3}$$

where g_0 and A are constants, $\omega_l = \omega_0 \exp(-E_l/k_BT)$ is librational frequency, E_l is the energy required for activation of such a motion, k_B is the Boltzmann constant, and T is the temperature.

9.2.2 SPIN SUSCEPTIBILITY

A static paramagnetic susceptibility χ is also an important characteristic of a paramagnetic system. Generally, this parameter of N spins consists of temperature-independent Pauli susceptibility of the Fermi gas χ_P and temperature-dependent contributions of localized Curie PC χ_C [80]. However, such a simple system has been questioned, especially for conjugated polymers and their composites. These systems are characterized by significant disorder which localizes spins [81,82]. This originates the appearance in effective χ of additional contribution χ_{ST} which may be due to a possible singlet-triplet spin equilibrium in the system [80], contribution χ_{ECP} described in terms of an exchange-coupled pairs (ECP) model of spin exchange interaction in pairs randomly distributed in a polymer matrix [83,84], and contribution χ_m coming due to polaron Q1D mobility characterized by mid-gap energy $E_g = 2E_a$ near the Fermi level ε_F [85,86]. Finally, one can write the equation for sum χ as:

$$\begin{aligned}\chi = \chi_P + \chi_C + \chi_{ST} + \chi_m + \chi_{ECP} = N_A\mu_{eff}^2 n(\varepsilon_F) + \frac{C}{3k_BT} + \frac{k_1}{T}\left[\frac{\exp(-J/k_BT)}{1+3\exp(-J/k_BT)}\right]^2 \\ + \frac{Ca_d}{3k_BT}\left[3+\exp\left(-\frac{2J}{k_BT}\right)\right]^{-1} + C(1-a_d)\left\{\frac{J}{3k_BT} + \ln\left[3+\exp\left(-\frac{2J}{k_BT}\right)\right]\right\} \\ + k_2\sqrt{\frac{E_a}{k_BT}}\exp\left(1-\frac{E_a}{k_BT}\right)\end{aligned} \tag{9.4}$$

where N_A is the Avogadro's number, $n(\varepsilon_F)$ is the density of states per unit energy (in eV) for both spin orientations per monomer unit at ε_F, $\mu_{eff} = \mu_B g\sqrt{S(S+1)}$ is the effective magneton, S is a spin normally equal to ½ for PC in organic

polymers, $C = N\mu_B^2 g^2 S(S+1)$ is the Curie constant per mole-C/mole-monomer, k_1 and k_2 are constants, J is the exchange coupling constant, and a_d is a fraction of spin pairs interacting in disordered polymer regions. The contributions of these terms to the total paramagnetic susceptibility depend on various factors, for example, on the nature and mobility of charge carriers that can vary at the system modification. A small value of J corresponds to spin localization in a strongly disordered matrix and increases at overlapping of wave functions of interacting spins in more ordered regions.

In most polymer semiconductors, polarons are formed as very stable quasiparticles as a result of their doping and/or treatment by, for example, annealing or irradiation. Such charge carriers can also be excited on polymer chains quite reversibly, and this effect is used for conversion of solar light [5,8]. The treatment of polymer semiconductors modified by some electron acceptor normally leads to the transfer of electrons from their chains to the acceptor that is accompanied by the formation of polarons on polymer chains and anion radicals on acceptors. PC charged positively and negatively recombine after an irradiation down. Therefore, an effective spin susceptibility of such a system is the sum of these two alternating processes [53].

In polymer:fullerene composites, both initiated charges diffusing to the opposite electrodes must reach them prior to recombination. If these chargers after their transfer are still bound by the Coulomb potential, which is typical for the compounds with low-mobile charge carriers described here, they cannot escape from each other's attraction and will finally recombine. When the carrier dissipation distance is longer than the Coulomb radius, the excitons initiated by, for example, light in their heterojunctions can be split into positive and negative charge carriers. To fulfill this condition, the Coulomb field must be shielded or charge carrier-hopping distance must exceed the Coulomb radius. In this case, charges are transferred to the electrodes either by the diffusion of appropriate carriers or by the drift induced by the electric field. In order to excite a radical pair by each photon, charge carrier transit time t_{tr} should be considerably shorter than the lifetime of a radical pair τ, that is, $t_{tr} \ll \tau$. The former value is determined by charge carrier mobility μ, sample thickness d, and electric field E inside the film, $t_{tr} = d/\mu E$. If photocurrent is governed by the carrier drift in the applied electric field, the drift distance $l_{dr} = \mu\tau E$. If this current is governed by carrier diffusion, the diffusion distance $l_{diff} = (D\tau)^{1/2} = (\mu\tau k_B T/e)^{1/2}$, where D is the diffusion coefficient, and e is the elemental electron charge. Thus, the $\mu\tau$ product governs the average distance passed by the charge carrier before recombination and, therefore, is an important parameter determining whether the efficiency of solar cells is limited by charge transport and recombination. The latter, generally is described as a thermally activated bimolecular recombination [56] which consists of temperature-independent fast and exponentially temperature-dependent slow steps [55].

Let a polaron possessing a positive charge multihops along a polymer chain from one initial site i to other available site j close to a position occupied by a negatively charged fullerene globule. A charge hops easier between fullerenes

than from polaron and fullerene, and an effective charge recombination is still limited by the transport of polarons towards fullerene molecules. The recombination is mainly stipulated by sequential charge transfer by polaron along a polymer chain and its transfer from polymer chain to a site occupied by a fullerene. Polaronic dynamics in undoped and slightly doped conjugated polymers is highly anisotropic [77]. Therefore, the probability of a charge transfer along a polymer chain exceeds considerably that of its transfer between polymer macromolecules.

According to the tunneling model [87], positive charge on a polaron can tunnel from this carrier toward a fullerene and recombine with its negative charge during the time:

$$\tau(R_{ij}^{|}) = \frac{\ln X}{\nu_{\mathrm{pn}}} \exp\left(\frac{2R_{ij}^{|}}{a_0}\right), \tag{9.5}$$

where $R_{ij}^{|}$ is the spatial separation of sites i and j, a_0 is the effective localization (Bohr) radius, X is a random number between 0 and 1, and ν_{pn} is the attempt to jump frequency for positive charge tunneling from polymer chain to fullerene. The charge can also be transferred by the polaron thermally assisted multistep tunneling through energy barrier $\Delta E_{ij} = E_j - E_i$, so then:

$$\chi(R_{ij}, E_{ij}) = \chi_0 \frac{\ln X}{\nu_{\mathrm{pp}}} \exp\left(\frac{2R_{ij}}{a_0}\right) \exp\left(\frac{\Delta E_{ij}}{k_{\mathrm{B}}T}\right), \tag{9.6}$$

where ν_{pp} is the attempt frequency for a hole tunneling between the polymer chains. The values in the couples ν_{pn}, ν_{pp}, and $R_{ij}^{|}$, R_{ij} may be different due, for instance, to the different electronic orbits.

If one switches off light excitation of the polymer:fullerene system, the concentration of spin pairs excited in its BHJ starts to decrease. This leads to instantaneous collapse of radical pairs or their splitting into noninteracting charge carriers due to polaron diffusion. The rate of recombination of charge carriers with effective localization radius a separated by a distance R_0 can be written as [88]:

$$\nu(R) = \nu_0 \exp\left(-\frac{2R_0}{a}\right), \tag{9.7}$$

where ν_0 is an attempt to recombine frequency. Undoubtedly, both charge carriers have different localization radii. The localization radius for a negatively charged carrier should be on the order of the radius of the fullerene globule. The distance R_0 should depend, for example, on the length of a side alkyl chain substitute in a polymer:fullerene matrix [89]. Polaron stabilized in conjugated polymers normally covers near to five monomer units [55,90]. The nearest-neighbor distance of spin pair with the typical radiative lifetime τ_0 changes with time t as:

$$R_0(t) = \frac{a}{2} \ln\left(\frac{t}{\tau_0}\right). \tag{9.8}$$

Assuming that photoexcitation is turned off at some initial time $t_0 = 0$ at a charge carrier concentration n_0 and taking into account a time period of geminate recombination $t_1 - t_0$, one can determine for concentration of charge carriers with:

$$n(R) = \frac{n}{1 + \frac{4\pi}{3} n_1 (R_0^3 - R_1^3)}, \tag{9.9}$$

where R_0 is specified by Eqn (9.8), $R_1 = R(t_1)$ describes the distance between the nearest-neighbor charge carriers at time t_1, after which solely nongeminate recombination is assumed, and n_1 is the charge carrier concentration at time t_1. It follows from Eqn (9.9) that the time dependence of residual carrier concentration does not follow a simple exponential decay but shows a more logarithmic time behavior. After very long times, that is, at large R_0, one obtains $n(R_0) = (3/4\pi)R_0^{-3}$ which is independent of the initial carrier density n_1 and also n_0. It follows from Eqn (9.7) that photoexcited charge carriers have comparable long lifetimes which are solely ascribed to the large distances between the remaining trapped charge carriers. The excited carrier concentration n_1 follows directly from LEPR measurements, whereas the a and τ_0 values can be guessed in a physically reasonable range. Finally, the concentration of spin pairs should follow the relation [88]:

$$\frac{n(t)}{n_0} = \frac{\frac{n_1}{n_0}}{1 + \left(\frac{n_1}{n_0}\right) \frac{\pi}{6} n_0 a^3 \left[\ln^3\left(\frac{t}{\tau_0}\right) - \ln^3\left(\frac{t_1}{\tau_0}\right)\right]}. \tag{9.10}$$

The analysis showed that the spin concentration initially photoexcited at $t = 0$ is governed by certain factors. One factor is the number and distribution of spin traps inversely formed in a polymer matrix under irradiation. A number and a depth of such traps depend on the photon energy $h\nu_{ph}$ [42,91]. At the latter step, a polaronic charge carrier can either be retrapped by a vacant trap site or recombine with an electron on a fullerene anion radical. Trapping and retrapping of a polaron reduces its energy, which results in its localization into deeper trap and in the increase in number of localized polarons with time. So, the decay curves presented can be interpreted in terms of bulk recombination between holes and electrons during their repeated trapping into and detrapping from trap sites with different depths in an energetically disordered semiconductor [92]. Analyzing LEPR spectra, it becomes possible to separate the decay of mobile and pinned spin charge carriers excited in the composite. The traps in such a system should be characterized by different energy depths and energy distribution E_0. Polarons translative diffuse quickly along a polymer backbone, and fullerene anion radicals can be considered to be immobilized between polymer chains. This approach predicts the following law for decay of charge carriers [92]:

$$\frac{n(t)}{n_0} = \frac{\pi\alpha\delta(1+\alpha)\nu_d}{\sin(\pi\alpha)} t^{-\alpha}, \tag{9.11}$$

where n_0 is the initial number of polarons at $t = 0$, δ is the gamma function, $\alpha = k_B T/E_0$, ν_d is the attempt jump frequency for polaron detrapping.

Positive charge on a polaron is not required to be recombined with the first negative charge on the subsequent acceptor. Thus, the probability of annihilation of charges can differ from the unit. Q1D hopping of a positively charged polaron from site i to site j with the frequency ω_{hop} may collide with the acceptor located near the polymer matrix. While the polaron is mobile, the molecule of the acceptor can be considered as a translative fixed, but librating near its own main molecular axis. In this case, the spin flip-flop probability p_{ff} during a collision should depend on the amplitude of exchange and ω_{hop} value as shown by [93,94]:

$$p_{ff} = \frac{1}{2} \cdot \frac{\alpha^2}{1+\alpha^2} \tag{9.12}$$

where $\alpha = (3/2)\ 2\pi J_{ex}/\hbar\omega_{hop}$ and J_{ex} is the constant of exchange interaction of spins in a radical pair. In the polymer composites weak and strong exchange limits can be realized when the increase of ω_{hop} may result in decrease or increase in exchange frequency, respectively. If the ratio $J_{ex}/\hbar$ exceeds the frequency of collision of both types of spins, the condition of strong interaction is realized in the system leading to the direct relation of spin−spin interaction and polaron diffusion frequencies, so then $\lim(p) = 1/2$. In the opposite case $\lim(p) = 9/2\ (\pi/\hbar)^2(J_{ex}/\omega_{hop})^2$. It is evident that the longer both the above tunneling times and/or the lesser the probability p_{ff}, the smaller the number of ion-radical pairs possible to recombine and, therefore, higher spin susceptibility should be reached. A combination of the two previous equations gives:

$$\chi_p = \chi_{pn} + \chi_P^0 \frac{\hbar}{J_{ex}} \left(\alpha + \frac{1}{\alpha}\right). \tag{9.13}$$

Assuming the above-introduced activation character for polaron multistep hopping with the frequency $\omega_{hop} = \omega_{hop}^0 \exp(-\Delta E_r/k_B T)$ and the absence of dipole−dipole interaction between fullerene anion radicals, one can determine ΔE_r from temperature dependences of paramagnetic susceptibility.

9.2.3 LINE SHAPE AND WIDTH

In contrast with a solitary and isolated spin characterized by δ-function absorption spectrum, the spin interaction with a particle's own environment in a real system leads typically to the change in line shape and increase of line width. Analyzing the shape and intensity of the experimental spectrum it is possible to obtain direct information on electronic processes in polymer systems. An electron spin is affected by local magnetic fields, induced by another nuclear and electron n r_{ij}-distanced spins [95]:

$$B_{loc}^2 = \frac{1}{4n}\gamma_e^2\hbar^2 S(S+1)\sum_{i,j}\frac{(1-3\cos^2\theta_{ij})}{r_{ij}^6} = \frac{M_2}{3\gamma_e^2}, \tag{9.14}$$

where M_2 is the second moment of a spectral line. If a line broadening is stipulated by a local magnetic field fluctuating faster than the rate of interaction of a spin with the nearest environment, the first derivative of the Lorentzian resonant line with a distance between positive and negative peaks ΔB_{pp}^{L} and maximum intensity between these peaks $I_L^{'(0)}$ is registered at resonance frequency $\omega_e^{(0)}$ [96,97]

$$I'_L = \frac{16}{9} I_L^{'(0)} \frac{(B - B_0)}{\Delta B_{pp}^{L}} \left[1 + \frac{4}{3} \frac{(B-B_0)^2}{(\Delta B_{pp}^{L})^2}\right]^{-2} \tag{9.15}$$

whereas at slower fluctuation of an additional local magnetic field, the spectrum is defined by Gaussian function of distribution of spin packets:

$$I'_G = \sqrt{e} I_G^{'(0)} \frac{(B - B_0)}{\Delta B_{pp}^{G}} \exp\left[-\frac{2(B-B_0)^2}{(\Delta B_{pp}^{G})^2}\right]. \tag{9.16}$$

The EPR line shape due to dipole or hyperfine broadening is normally Gaussian. An exchange interaction between the spins in real system may result in the appearance of a more complicated line shape, described by a convolution of Lorentzian and Gaussian distribution function. This takes a possibility from the analysis of such a line shape to define the distribution, composition, and local concentrations of spins in such a system. For example, if equivalent PC with concentration n are arranged chaotically or regularly in the system their line shape is described by the Lorentzian and Gaussian distribution function, respectively, with the width $\Delta B_{pp}^{L} = \Delta B_{pp}^{G} = 4\gamma_e \hbar n$ [98]. In the mixed cases, the line shape transforms to Lorentzian at a distance from the center $\delta B \leq 4\gamma_e \hbar / r^3$ (here, r is a distance between magnetic dipoles) with the width $\Delta B_{pp}^{L} = 4\gamma_e \hbar n$ in the center and becomes Gaussian type on the tails at $\delta B \geq \gamma_e \hbar / r^3$ with the width $\Delta B_{pp}^{G} = \gamma_e \hbar \sqrt{n / r^3}$.

Line width is mainly determined by transverse (spin−spin) relaxation time T_2. However, there are several relaxation processes in a polymer composite which cause the shortening of T_2 and hence the broadening of the EPR line. One of them is spin longitudinal (spin−lattice) relaxation on the lattice phonons with time T_1, which shortens the lifetime of a spin state and therefore broadens the line. Representing all other possible relaxation processes by the time $T_2^{|}$, one can determine for effective peak-to-peak line width ΔB_{pp} as [99]:

$$\Delta B_{pp} = \Delta B_{pp}^{0} + \frac{2}{\sqrt{3}\gamma_e} \cdot \frac{1}{T_2} = \Delta B_{pp}^{0} + \frac{2}{\sqrt{3}\gamma_e} \cdot \left(\frac{1}{T_2^{|}} + \frac{1}{2T_1}\right), \tag{9.17}$$

where ΔB_{pp}^{0} is the line width at the absence of spin dynamics and interaction. The collision of these PC should broaden the EPR spectrum by [93,94]:

$$\delta(\Delta B_{pp}) = p_{ff} \omega_{hop} n_g = k_1 \omega_{hop} n_g \left(\frac{\alpha^2}{1 + \alpha^2}\right), \tag{9.18}$$

where p_{ff} is the flip−flip probability inserted above, n_g is the number of guest PC per each polymer unit, k_1 is constant equal to ½ and 16/27 for $S = ½$ and $S = 1$, respectively. In this case the guest spin acts as a nanoscopic probe of the polaron dynamics. Note, that the n_g parameter is temperature dependent that should be taken into account when calculating the effective line width. According to the spin exchange fundamental concepts [93], if exchange interaction changes between weak and strong exchange limits (see above), an appropriate $\delta(\Delta\omega)(T)$ dependency may demonstrate extremal dependence with characteristic temperature T_c. This should evidence the realization of high and low of spin−spin interaction at $T \leq T_c$ and $T \geq T_c$, respectively, realized, for example, in highly doped polyaniline samples [94,100−102].

The rate of charge hopping between two adjacent polymer units can be estimated to a good approximation using a semiclassical Marcus theory adopted for conjugated polymers [103,104]

$$\omega_{hop} = \frac{4\pi^2}{\hbar}\frac{t_{1D}^2}{\sqrt{4\pi E_r k_B T}}\exp\left(-\frac{E_r}{4k_B T}\right) \tag{9.19}$$

where t_{1D} is electronic coupling between initial and final states (intrachain transfer integral) and E_r is both the inner- and outer-sphere reorganization energy of charge carriers due to their interaction with the lattice phonons. The t_{1D} value decreases slightly with temperature, whereas its distribution broadens a line due to thermal motion of polymer units [105], similar to that which happens in organic crystals [106,107]. Note that the n_g parameter is temperature dependent and should be included in the finalized equation. Combination of Eqns (9.18) and (9.19) yields:

$$\delta(\Delta\omega) = \frac{\pi t_{1D}^2 n_g(T)}{\hbar\sqrt{\frac{E_r k_B T}{\pi}}}\cdot\frac{\exp\left(-\frac{E_r}{4k_B T}\right)}{1+\left[\frac{3J_{ex}}{2t_{1D}^2}\sqrt{\frac{E_r k_B T}{\pi}}\exp\left(\frac{E_r}{4k_B T}\right)\right]^{-2}}. \tag{9.20}$$

Excluding fast electron spin diffusion, the EPR line can also be broadened by the acceleration of molecular dynamics processes, for example, oscillations or slow torsion librations of the polymer macromolecules. The approach of random walk treatment [108] provides that such Q1D, Q2D, and Q3D spin diffusion with respective diffusion coefficients D_{1D}, D_{2D}, and D_{3D} in the motionally narrowed regime changes the respective line width of a spin-packet as [109]:

$$\Delta B_{pp} \approx \frac{\gamma_e^{1/3}(\Delta B_{pp}^0)^{4/3}}{D_{1D}^{1/3}}, \tag{9.21}$$

$$\Delta B_{pp} \approx \frac{\gamma_e(\Delta B_{pp}^0)^2}{\sqrt{D_{1D}D_{3D}}}, \tag{9.22}$$

$$\Delta B_{pp} \approx \frac{\gamma_e(\Delta B_{pp}^0)^2}{D_{3D}}. \tag{9.23}$$

This theory postulates that at the transition from Q1D to Q2D and then to Q3D spin motion the shape of the EPR line should transform from Gaussian to Lorentzian. This approach allows the evaluation of an effective dimension of the system under study, say from an analysis of temperature dependence of its EPR spectrum line width. For spin Q3D motion or exchange, the line shape becomes close to Lorentzian shape, corresponding to an exponential decay of transverse magnetization with time t, proportional to $\exp(-\eta t)$; for a Q1D spin motion, this value is proportional to $\exp(-\rho t)$ (here η and ρ are constants) [110]. In order to determine the type of spin dynamics in a Q1D system appropriate anamorphoses $I_0^{|}/I(B)$ versus $[(B-B_0)/\Delta B_{1/2}]^2$, and $I_0^{|}/I(B)$ versus $[(B-B_0)/\Delta B_{pp}]^2$ (here $\Delta B_{1/2}$ is the half-width of an integral line) [110] should be analyzed.

9.2.4 DYSONIAN SPECTRAL CONTRIBUTION

The EPR line of PC in conducting composites can be complicated by the fact that the magnetic term B_1 of the microwave field used to excite resonance sets up eddy currents in the material bulk. These currents effectively confine the magnetic flux to a surface layer of thickness of order of the "skin depth." This phenomenon affects the absorption of microwave energy incident upon a sample and results in less intensity of electron absorption per unit volume of material for large particles than for small ones. This also leads to the appearance of asymmetric Dyson-like contribution [111] in EPR spectra of some composites containing ordered domains embedded into an amorphous polymer matrix [43,102], as in the case of metal-like organic polymers [76,112,113]. Such an effect appears when the skin-layer thickness δ becomes comparable or thinner than a characteristic size of a sample, for example, due to the increase of conductivity. In this case the time of charge carrier diffusion through the skin-layer becomes essentially less than a spin relaxation time and the Dysonian line with characteristic asymmetry factor A/B (the ratio of intensities of the spectral positive peak to the negative one) is registered. Such line shape distortion is accompanied by the line shift into higher magnetic fields and the drop in sensitivity of EPR technique.

Generally, the Dysonian line consists of dispersion $\chi^{|}$ and absorption $\chi^{||}$ terms, therefore one can write for its first derivative the following equation:

$$\frac{d\chi}{dB} = A\frac{2x}{(1+x^2)^2} + D\frac{1-x^2}{(1+x^2)^2}, \tag{9.24}$$

where $x = 2(B - B_0)/\sqrt{3}\Delta B_{pp}^{L}$. The line asymmetry parameter A/B is correlated with the above coefficients A and D simply as $A/B = 1 + 1.5\ D/A$ independently on the EPR line width. Organic polymers are usually studied as powder and film. Appropriate coefficients of absorption A and dispersion D in Eqn (9.24)

for skin-layer on the surface of a spherical powder particle with radius R and intrinsic ac conductivity σ_{ac} can be calculated from equations [114]:

$$\frac{4A}{9}=\frac{8}{p^4}-\frac{8(\sinh p+\sin p)}{p^3(\cosh p-\cos p)}+\frac{8\sinh p\sin p}{p^2(\cosh p-\cos p)^2}+\frac{(\sinh p-\sin p)}{p(\cosh p-\cos p)}-\frac{(\sinh^2 p-\sin^2 p)}{(\cosh p-\cos p)^2}+1, \tag{9.25}$$

$$\frac{4D}{9}=\frac{8(\sinh p-\sin p)}{p^3(\cosh p-\cos p)}-\frac{4(\sinh^2 p-\sin^2 p)}{p^2(\cosh p-\cos p)^2}+\frac{(\sinh p+\sin p)}{p(\cosh p-\cos p)}-\frac{2\sinh p\sin p}{(\cosh p-\cos p)^2}, \tag{9.26}$$

where $p=2R/\delta$, $\delta=\sqrt{2/\mu_0\omega_e\sigma_{ac}}$, and μ_0 is the magnetic permeability for a vacuum. In case of the formation of skin-layer on the flat plate with a thickness of $2d$ the above coefficients can be determined from relations [114]:

$$A=\frac{\sinh p+\sin p}{2p(\cosh p+\cos p)}+\frac{1+\cosh p\cos p}{(\cosh p+\cos p)^2}, \tag{9.27}$$

$$D=\frac{\sinh p-\sin p}{2p(\cosh p+\cos p)}+\frac{\sinh p\sin p}{(\cosh p+\cos p)^2}, \tag{9.28}$$

where $p=2d/\delta$. The analysis of multifrequency EPR spectra with Dysonian term allows for the direct determination of the ac conductivity of conducting domains embedded into polymer matrix [76–78].

9.2.5 ELECTRON RELAXATION AND SPIN DYNAMICS

As the magnetic term B_1 of the steady-state microwave field increases, the line width ΔB_{pp} of a LEPR spectrum broadens and its intensity I_L first increases linearly, plateaus starting from some B_1 value, and then decreases. This occurs due to manifestation of the microwave steady-state saturation effect in the LEPR spectrum of the composite. Polaron and fullerene anion radicals are noninteracting and, therefore, independent of one another. This allows us to use such effects for separate estimation of their spin–lattice T_1 and spin–spin T_2 relaxation times from relations [115]

$$\Delta B_{pp}=\Delta B_{pp}^{(0)}\sqrt{1+\gamma_e^2B_1^2T_1T_2} \tag{9.29}$$

and

$$I_L=I_L^{(0)}B_1(1+\gamma_e^2B_1^2T_1T_2)^{-3/2}, \tag{9.30}$$

where $I_L^{(0)}$ is intensity of nonsaturated spectrum and $T_2=2/\sqrt{3}\gamma_e\Delta B_{pp}^{(0)}$. Normally, the inflection point characteristic for polarons' saturation curve is distinct from that obtained for fullerene anion radicals. This is evidence of different relaxation parameters of these PC and also confirms their mutual independence.

The mechanism and the rate of electron relaxation depend on the structure and conformation of an initial and modified polymer:fullerene composites in which radical pairs are photoinduced in differently ordered domains with respective

band gaps. Various spin-assisted dynamic processes occur in polymer:fullerene composites, for example, polaron diffusion along and between polymer chains with coefficients D_{1D} and D_{3D}, respectively, and librative rotational motion of fullerene anion radicals near their own main molecular axis with coefficient D_{rot}. These processes induce additional magnetic fields in the whereabouts of electron and nuclear spins which, in turn, accelerates relaxation of both spin ensembles. Relaxation of the whole spin reservoir in organic conjugated polymers is defined mainly by dipole−dipole interaction between electron spins [116], so then these coefficients can be determined from the following equations [117]:

$$T_1^{-1}(\omega_e) = \langle\omega^2\rangle[2J(\omega_e) + 8J(2\omega_e)], \tag{9.31}$$

$$T_2^{-1}(\omega_e) = \langle\omega^2\rangle[3J(0) + 5J(\omega_e) + 2J(2\omega_e)], \tag{9.32}$$

where $\langle\omega^2\rangle = 1/10\gamma_e^4\hbar^2 S(S+1)n\sum_{ij}$ is the constant of dipole−dipole interaction for powder, n is a number of polarons per each monomer, Σ_{ij} is the lattice sum for a powder-like sample, $J(\omega_e = (2D_{1D}^{|}\omega_e)^{-1/2})$ (at $D_{1D}^{|} \gg \omega_e \gg D_{3D}$), $J(0) = (2D_{1D}^{|}D_{3D})^{-1/2}$ (at $D_{3D} \gg \omega_e$) are the spectral density functions for polaron longitudinal diffusion, and $J(\omega_e) = \tau_c/(1 + \tau_c^2\omega_e^2)$ is the spectral density function for fullerene rotational libration with correlation time τ_c, $D_{1D}^{|} = 4D_{1D}/L^2$, and L is a factor of spin delocalization over a polaron equal approximately to five monomer units in P3AT [55,90].

9.2.6 MECHANISM OF CHARGE TRANSPORT IN POLYMERS

To account for the LEPR mobility data obtained, different theoretical models can be used. Polaron dynamics in some nanomodified polymer composites can be characterized by strong temperature dependence. This can probably be due to the scattering of polarons on the lattice phonons of crystalline domains embedded into an amorphous matrix. According to the model proposed for charge dynamics in crystalline domains of doped conjugated polymers, such scattering should affect polaron intrachain diffusion with an appropriate coefficient [118,119]:

$$D_{3D}(T) = \frac{\pi^2 M t_0^2 k_B^2 T^2}{h^3 \alpha_{eph}^2} \cdot \left[\sinh\left(\frac{E_{ph}}{k_B T}\right) - 1\right] = D_{3D}^{(0)} T^2 \cdot \left[\sinh\left(\frac{E_{ph}}{k_B T}\right) - 1\right] \tag{9.33}$$

where M is the mass of a polymer unit, t_0 is the transfer integral equal for π-electron to $\sim$2.5−3 eV, α_{eph} is a constant of electron−phonon interaction, and E_{ph} is phonon energy.

Spin dynamics in a less-ordered polymer matrix of composites can be realized in the frames of the Elliot model based on spin hopping over energetic barrier E_b [120]. This model predicts the following temperature dependencies for diffusion coefficients of a charge carrier at direct and alternating currents:

$$D_{dc}(T) = D_{dc}^0 T \exp\left(\frac{E_b}{k_B T}\right) \tag{9.34}$$

$$D_{ac}(\omega, T) = D_{ac}^{0} T^{2} \omega_{e}^{s} \exp\left(\frac{E_b}{k_B T}\right) \tag{9.35}$$

where the exponent $s = 1 - \alpha k_B T/E_b$ reflects system dimensionality and α is a constant. Comparison of spin dynamic parameters obtained at direct current and at different spin precession frequencies ω_e allows one to determine more precise details of charge transfer in organic polymer systems [76–78].

If spin traps are initiated in a polymer matrix, the dynamics of spin charge carriers can be explained in terms of the Hoesterey-Letson formalism modified for amorphous low-dimensional systems containing spin traps with concentration n_t and depth E_t [121]. Combining Eqns (9.18) and (9.25) in Ref. [121] and using from the modified Einstein relation of the trap-controlled interchain mobility μ_t and diffusion coefficient D_t of a charge carrier $\mu_t = eD_t d^2/k_B T$, one can obtain in the case of low trap concentration limit:

$$D_t(T) = \nu_0 \left(\frac{R_{ij}}{d}\right)^2 \exp\left(-\frac{2R_{ij}}{r}\right) \exp\left(\frac{E_t}{2k_B T_{cr}}\right) \exp\left[-\frac{E_t}{2k_B T}\left(\frac{\sigma_0}{k_B T}\right)^2\right] \tag{9.36}$$

where ν_0 is hopping attempt frequency, d is the lattice constant, $T_{cr} = E_t/2k_B \ln(n_t)$ is critical temperature at which the transition from trap-controlled to trap-to-trap hopping transport regimes occurs, and σ_0 is the width of intrinsic energetic distributions of hopping states in the absence of traps.

9.3 MAGNETIC RESONANCE PARAMETERS OF SPIN CHARGE CARRIERS IN POLYMER:FULLERENE COMPOSITES

Once excitons are conversed into polarons and ion radicals in the polymer:fullerene BHJ, respective positive and negative charge carriers appear in the system. Both charge carriers possess spin, so then they are characterized by different magnetic resonance parameters. In addition, the energies of reorientation transition of these spins are affected by their local environment. Thus, EPR spectra can yield information about the type, number, state, etc., of spin charge carriers and also about their local environment in a sample.

Figure 9.2a shows schematic structures of the regioregular P3AT with hexyl ($m = 6$, P3HT), oktyl ($m = 8$, P3OT), dodecyl ($m = 12$, P3DDT) side groups, PCDTBT, poly[2,5-dimethoxy-1,4-phenylene-1,2-ethenylene-2-methoxy-5-(2-ethylhexyloxy)-(1,4-phenylene-1,2-ethenylene)] (M3EH − PPV), poly[2-methoxy-5-(3′,7′-dimethyloctyloxy)-1,4-phenylenevinylene] (MDMO-PPV), and the emeraldine salt form of polyaniline (PANI-ES) heavely doped by paratoluenesulfonic acid (PANI:TSA) used as polymer matrices, whereas the [6,6]-phenyl-C_{61}-R [$PC_{61}R$ where R≡—$(CH_2)_2C(O)OCH_2Ph$ ($PC_{61}R_1$), —$(CH_2)_2C(O)O$—CH_3 ($PC_{61}R_2$), —$(CH_2)_2C(O)OCH_2CH_3$ ($PC_{61}R_3$), —$(CH_2)_3C(O)OCH_3$ ($PC_{61}R_4$), —$(CH_2)_2C(O)O(CH_2)_2CH_3$ ($PC_{61}R_5$)], $PC_{61}BM$, *bis*-$PC_{62}BM$, 2-(azahomo[60]

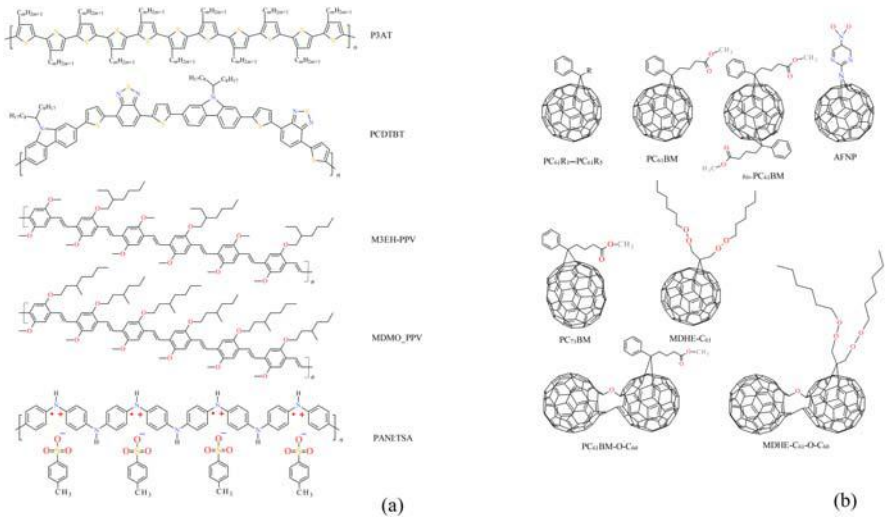

FIGURE 9.2

Schematic structures of the regioregular P3AT with hexyl ($m = 6$, P3HT), oktyl ($m = 8$, P3OT), dodecyl ($m = 12$, P3DDT) side groups, PCDTBT, M3EH – PPV, MDMO-PPV, and PANI:TSA (a) as well as fullerene derivatives $m\mathrm{F}_{1\text{-}5}$, $\mathrm{PC}_{61}\mathrm{BM}$, *bis*-$\mathrm{PC}_{62}\mathrm{BM}$, AFNP, $\mathrm{PC}_{71}\mathrm{BM}$, $\mathrm{PC}_{61}\mathrm{BM\text{-}O\text{-}C}_{60}$, MDHE-$\mathrm{C}_{61}$, and MDHE-$\mathrm{C}_{61}$-O-$\mathrm{C}_{60}$ (b) used in polymer composites.

fullereno)-5-nitropyrimidine (AFNP), $\mathrm{PC}_{71}\mathrm{BM}$, $\mathrm{PC}_{61}\mathrm{BM\text{-}O\text{-}C}_{60}$, [6,6]-malonedihexyle-fullerene ester (MDHE-C_{61}), and MDHE-C_{61}-O-C_{60}-fullerene derivatives embedded as electron acceptors into polymer composites are shown schematically in Fig. 9.2b. These materials and their composites were studied by multifrequency, X-, K-, W-, and D-bands EPR spectroscopy when spin precession frequency $\omega_e/2\pi$ and resonant magnetic field B_0 lie near 9.7 GHz and 3.4 kG, 24 GHZ and 8.6 kG, 85 GHz and 33 kG, 140 GHz and 49 kG, respectively.

9.3.1 LINE SHAPE AND G-FACTOR

No EPR signal has been found in pure fullerene derivatives at 3-cm wave band in whole temperature range. Some initial P3AT samples, for example, P3HT demonstrates at 3-cm wave band EPR Lorentzian exchange-narrowed nearly symmetrical line with effective $g_{\mathrm{eff}} = 2.0029$ (Fig. 9.3). As in the cases of other regioregular P3AT with longer side chains, this fact was interpreted as stabilization in the polymer of mobile polarons during synthesis and/or its treating by oxygen of air [40,41]. As the sample is modified by methanofullerenes $m\mathrm{F}_1 - m\mathrm{F}_5$ two additional lateral lines appear in its spectrum (Fig. 9.3). This fact evidences the localization of part of polarons probably at cross-bonds and/or at ends of polymer chains during such a modification. The intensity of these components decreases in the series

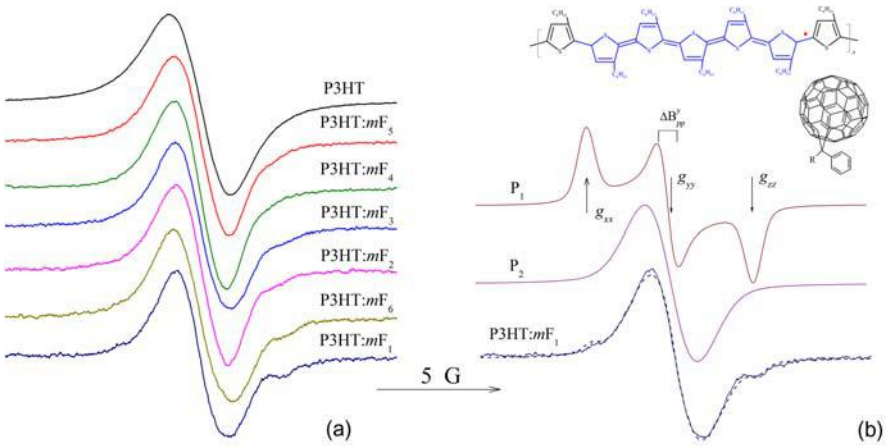

FIGURE 9.3

(a) Room temperature EPR spectra of the initial P3HT and P3HT:mF$_1$÷P3HT:mF$_6$ composites. (b) Experimental EPR spectrum of the sample P3HT:mF1 (solid line) compared with sum theoretical spectrum (dashed line) of localized $P_1^{\bullet}$ and mobile $P_2^{\bullet}$ polarons with relative concentration ratio $[P_1^{\bullet}]/[P_2^{\bullet}] = 0.089$ and $I_L^0/I_G^0 = 0.3$ and 0.2, respectively. The formation of polaron in P3HT is shown schematically. The magnetic resonance parameters measured are shown as well.

P3HT:mF$_1$ → P3HT:mF$_6$ → P3HT:mF$_2$ → P3HT:mF$_3$ → P3HT:mF$_4$ → P3HT:mF$_5$. A high-field/frequency EPR study shown [122–124] that the interaction of an unpaired electron of $P^{+\bullet}$ with sulfur heteroatoms involving into the P3AT backbone leads to anisotropy of its magnetic resonance parameters.

Computer simulation and deconvolution of EPR spectra of P3HT:mF$_i$ showed that two types of PC are stabilized in the samples, namely, polarons localized at cross-bonds and/or on the short π-conjugated polymer chains $P_1^{+\bullet}$ with $g_{xx} = 2.0049$, $g_{yy} = 2.0030$, $g_{zz} = 2.0010$, and line width $\Delta B_{pp} = 0.66$ G, and a polaron moving along the main π-conjugated polymer chain $P_2^{+\bullet}$ with $g_{xx} = g_{yy} = g_{zz} = 2.0029$, and $\Delta B_{pp} = 2.15$ G. The principal x-axis is chosen parallel to the longest molecular c-axis, the y-axis lies in the thiophene rings plane, and the z-axis is perpendicular to the x- and y-axes. The best fit of the $P_1^{+\bullet}$ signal was achieved using a nearly Gaussian line shape, which means that the transitions are inhomogeneously broadened mainly due to unresolved hyperfine interaction of unpaired spin with protons. Simulated spectra of $P_1^{+\bullet}$ and $P_2^{+\bullet}$ are also shown in Fig. 9.3. The isotropic g-factor of polarons $P_1^{+\bullet}$ lies near to that of the $P_2^{+\bullet}$ ones. This fact supports the supposition made previously about the nature of PC. Spin concentration ratio $[P_1^{+\bullet}]/[P_2^{+\bullet}]$ lies near 0.089 for P3HT:mF$_1$ and decreases for other compounds (see Fig. 9.3a). Note that the existence of such polarons with different relaxation and dynamics was also determined in other conjugated polymers [77] and polymer composites [91].

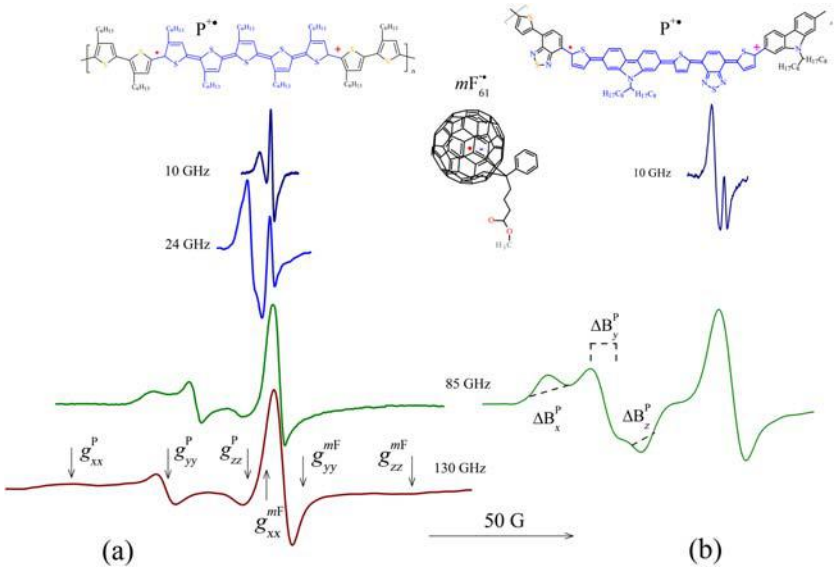

FIGURE 9.4

LEPR spectra of the P3HT:$PC_{61}BM$ (a) and PCDTBT:$PC_{61}BM$ (b) composites irradiated by laser registered at different spin precession frequencies ω_e and low temperature. The appearance of a polaron $P^{+\bullet}$ on polymer chain and methanofullerene ion radical $mF_{61}^{-\bullet}$ embedded between polymer chains are shown. The main values of **g**-tensors of these PC are shown as well.

As a polymer with embedded fullerene derivative is irradiated at $T \leq 200$ K by visible light directly in the cavity of the EPR spectrometer, in LEPR spectra two overlapping contributions appear, whose shape, relative intensity, and position depend on spin precession frequencies ω_e. Figure 9.4 shows as an example the LEPR spectra of the P3HT:$PC_{61}BM$ and PCDTBT:$PC_{61}BM$ composites background irradiated by laser light at different ω_e values [42,43,68,127,128]. Subsequent LEPR measurement cycles of heating up to the room temperature, cooling down to $T \leq 200$ K, illumination with light, switching light off and heating up again yield identical data. The spectra registered in low and high fields can be attributed to positively charged polarons $P^{+\bullet}$ and negatively charged methanofullerene $mF_{61}^{-\bullet}$ photoinduced in BHJ of the composites, respectively. These PC are characterized by anisotropic magnetic resonance parameters more evidently manifesting at higher ω_e as it follows from Eqn (9.1). These parameters measured at different ω_e are also summarized in Table 9.1. The g-factor of the fullerene ion radicals lies near that of other fullerene anion radicals [133]. As in case of the initial C_{60} molecule [134], the deviation of the $C_{61}^{-\bullet}$ g-factor from that of free electron, $g_e = 2.00232$, is due to the fact that the orbital angular moment is not completely quenched. Due to the dynamical Jahn-Teller effect

Table 9.1 The Main Magnetic Resonance Parameters Obtained for Polymer Composites by the Light-Induced EPR Method at Different Wave Bands and Low (20–80 K) Temperatures When All Spin Motions Are Considered Frozen

Sample	g_{xx}	g_{yy}	g_{zz}	g_{iso}	ΔB^{x}_{pp}, G	ΔB^{y}_{pp}, G	ΔB^{z}_{pp}, G	ΔB^{iso}_{pp}, G	Wave band[a]	References
P3HT	2.0049	2.0030	2.0010	2.0030	6.6	6.6	6.6	6.6	X	[40]
P3HT	2.0030	2.0021	2.0011	2.0021	1.6	1.5	1.6	1.6	K	[125]
P3HT	2.0028	2.0019	2.0009	2.0019	10.7	5.3	6.4	7.5	W	[68]
P3HT	2.00380	2.00230	2.00110	2.00240					D	[126]
P3OT	2.00409	2.00332	2.00232	2.00324	8.2	7.8	8.8	8.3	D	[124]
P3DDT	2.0026	2.0017	2.0006	2.0016	2.5	1.4	1.5	1.8	X	[42]
PCDTBT	2.0031	2.0026	2.0010	2.0022	–	–	–	1.4	X	[127]
PCDTBT	2.00320	2.00240	2.00180	2.00247	–	–	–	–	D	[128]
M3EH-PPV	2.0034	2.0025	2.0024	2.0028	2.2	2.7	2.8	2.5	K	[125]
M3EH – PPV	2.00377	2.00275	2.00220	2.00291	4.0	4.0	4.0	4.0	W	[43]
(MDMO-PPV)	2.00341	2.00341	2.00241	2.00308	8.0	5.0	5.0	6.0	W	[129]
(MDMO-PPV)	2.0033	2.0022	2.0022	2.0026	9.6	8.2	8.2	8.7	W	[68]
bis-$PC_{62}BM$	–	–	–	2.0007	–	–	–	1.3	X	[130]
$PC_{61}BM$	2.0005	2.0004	1.9988	1.9999	1.2	1.1	2.9	1.7	K	[125]
$PC_{61}BM$	2.00031	2.00011	1.99821	1.99954	2.3	1.3	8.8	4.1	W	[129]
$PC_{61}BM$	2.00021	2.00000	1.99860	1.99960	5.0	4.0	17	8.7	W	[43]
$PC_{61}BM$	2.00058	2.00045	1.99845	1.99983	–	–	–	–	D	[126]
$PC_{71}BM$	2.0062	2.0031	2.0027	2.0040	–	–	–	1.4	X	[131]
$PC_{71}BM$	2.0056	2.0023	2.0022	2.0034	–	–	–	–	X	[132]
$PC_{71}BM$	2.00592	2.00277	2.00211	2.00360	–	–	–	–	D	[126]
$PC_{61}BM$-O-C_{60}	2.0004	2.0002	1.9984	1.9997	3.6	3.6	4.4	3.9	K	[125]
$PC_{61}BM$-O-C_{60}	2.00045	2.00004	1.99860	1.99970	5.7	5.8	16	9.2	W	[43]
MDHE-C_{61}	2.00016	2.00000	1.99940	1.99985	2.1	1.9	10	4.7	W	[43]
MDHE-C_{61}-O-C_{60}	2.00050	2.00023	1.99910	1.99994	2.1	23	9.0	11.4	W	[43]

[a]*The spin precession frequency* $\omega_e/2\pi$ *and resonant magnetic field* B_0 *at the X, K, W, and D wave bands are 9.7 GHz and 3.4 kG, 24 GHZ and 8.6 kG, 85 GHz and 33 kG, and 140 GHz and 49 kG, respectively.*

accompanying the structural molecular deformation, the isotropic nature of the icosahedral C_{60} molecule is distorted after formation of the $F_{61}^{-\bullet}$ anion radical, resulting in an axial or even lower symmetry [135]. This is also realized in case of the $F_{61}^{-\bullet}$ anion radical [129], where the high symmetry of the molecule is already decreased by the bond to the phenyl side chain prior to electron accepting. Asymmetrical distribution of spin density in polaron and fullerene anion radical leads also to tensor character of their line widths [123,129]. This should be taken into account in order to calculate more precisely an effective LEPR spectrum of the P3AT:$PC_{61}BM$ system.

If one includes Coulomb interactions, this should affect the activation energy for either defrosting or thermally assisted tunneling by an amount $U_c = e^2/4\pi\varepsilon\varepsilon_0 r$, where e is elemental charge, ε is a dielectric constant, and r is charge pair separation. Assuming, for example, $\varepsilon = 3.4$ for P3HT [136], minimum separation of charge carriers is equal to the radius of π electrons on the C atoms a which are two times longer than the Bohr radius, that is, 0.106 nm, r equal to interchain separation, 0.38 nm [137]. One obtains the decrease in U_c from $\sim$0.4 eV down to 0.02 eV during dissociation of an initial radical pair. Therefore, both the photoinduced polaron and the anion radical indeed should be considered noninteracting, which prolongs their life.

Electronic properties of plastic solar cell can also be improved, for example, by the increase of its light absorption coefficient. Photoluminescence and atomic force microscopy studies showed [138–140] that wider and stronger light absorption is reached in polymer:$PC_{71}BM$ composites. Since optical absorption is closely related to crystallinity of such systems, it was inferred that, for example, a P3HT:$PC_{71}BM$ composite is more crystalline than a P3HT:$PC_{61}BM$ one and, therefore, demonstrates higher (by $\sim$33%) current density and power-conversion efficiency. Thus, the understanding of the elementary processes of exciton initiation, charge separation, stabilization, and recombination should be as a prerequisite for improving the efficiency of such photovoltaic systems. Indeed, the formation of C_{70} anion radicals initiates a subgap photoinduced absorption band at 0.92 eV [141], hidden in the spectra of polymer:$PC_{71}BM$ composites, which allows more exact studies of charge-separated states in such systems. On the other hand, comparative multifrequency EPR investigation of various polymer:fullerene composites have demonstrated [126,128] significant difference in deconvoluted LEPR spectra of both charge carriers. Indeed, the isotropic g-factor of the $m\mathrm{F}_{61}^{-\bullet}$ and $m\mathrm{F}_{71}^{-\bullet}$ methanofullerene anion radicals was obtained as equal to 1.99983 and 2.00360, respectively. Taking into account that isotropic (effective) g-factor, $g_{iso} = (g_{xx} + g_{yy} + g_{zz})/3$ of polarons lies near 2.003, this should mean the decrease in spectral resolution at the $PC_{61}BM$ replacing by $PC_{71}BM$ counter ions. So, the effective g-factor of different $F_{61}^{-\bullet}$ anion radicals is normally less than the g-factor of free electrons [42,126,129,130,142], and the g_{iso} value of the $m\mathrm{F}_{71}^{-\bullet}$ anion radical exceeds g_e [126,132]. This is in agreement with the study of respective anion radicals in crystalline ($g_{iso} = 2.0047$) [143,144] and dissolved [144–147] C_{70}. Such an effect is supposed [148] to appear due to different Jahn-Teller dynamics

of C_{60} and C_{70} molecules, which might contribute to different signs of the *g*-value shifts. According to the classical Stone theory of *g*-factors [149], negative deviation of the *g*-factor from g_e is due to spin − orbit coupling with empty *p*- or *d*-orbitals, while spin-orbit coupling with occupied orbitals leads to positive *g*-factor deviation. The latter case is typical for most organic radicals. Thus, a difference in *g*-values of $mF_{61}^{\bullet -}$ and $mF_{71}^{\bullet -}$ anion radicals indicates the different electronic structure of their molecular orbitals. Positive shift of the *g*-factors in solution for $mF_{61}^{\bullet -}$ relative $mF_{71}^{\bullet -}$ can be explained in the framework of the static Jahn-Teller effect [148,150]. Jahn-Teller dynamics in the solid phase seems to be quite different for C_{60} and C_{70} globes, which might contribute to different signs of their *g*-value shifts [148]. However, there is not yet a unified theory that can explain **g**-tensors of both $mF_{61}^{\bullet -}$ and $mF_{71}^{\bullet -}$ radicals.

Nevertheless, the contribution of the $mF_{71}^{\bullet -}$ charge carriers can be obtained by using the "light on-light off" method accompanied with the deconvolution of sum LEPR spectrum of both charge carriers into two individual spectra which can then be compared with those obtained at millimeter wave band EPR. Figure 9.5 shows X-band LEPR spectra of the P3HT:PC_{71}BM and PCDTBT:PC_{71}BM composites irradiated at $T = 77$ K [127,151]. Assuming that each optical photon initiates a positively and a negatively charged carriers, the $mF_{71}^{\bullet -}$ spectrum may simply be obtained by the extraction of the $P^{\bullet +}$ spectrum from the initial LEPR one shown in Fig. 9.5.

In order to analyze all magnetic resonance parameters in detail as a function of different effects, sum LEPR spectra were deconvoluted by using numerical simulations as it was done in the case of other polymer:fullerene systems [42,126,131,142]. Such an algorithm in combination with the "light on-light off" method allowed for determining appropriate parameters of both charge carriers photoinduced in the P3HT:PC_{71}BM composite (see Table 9.1). These values lie near those determined at higher spectral resolution [68,126]. This was used also for separate determination of all main magnetic resonance parameters of charge carriers stabilized and photoinitiated in other analogous BHJ at wide regions of the temperature, photon energy, and registration frequency. The best fit of such LEPR spectra was achieved using a convolution of Gaussian and Lorentzian line shapes, which means that electron excitation leads to inhomogeneous and homogeneous line broadening, respectively, due to unresolved hyperfine interaction of unpaired spin with neighboring protons and also to its different mobility.

It was demonstrated [76−78] that the main parameters of spin charge carriers stabilized in conjugated polymers are governed by their structure as well as by different adducts embedded into the polymer matrix [91,113,152]. A similar effect should be probably reached by varying the number of electrons trapped by each acceptor of a polymer:fullerene composite. In order to test this assumption, the charge carriers photoinitiated in some BHJ formed by the M3EH-PPV macromolecules with different mono- and di-C_{60}-fullerene derivatives were studied at W-band EPR [43]. Figure 9.6 shows W-band LEPR spectra of the M3EH-PPV:PC_{61}BM, M3EH-PPV:PC_{61}BM-O-C_{60}, M3EH-PPV:MDHE-C_{61}, and

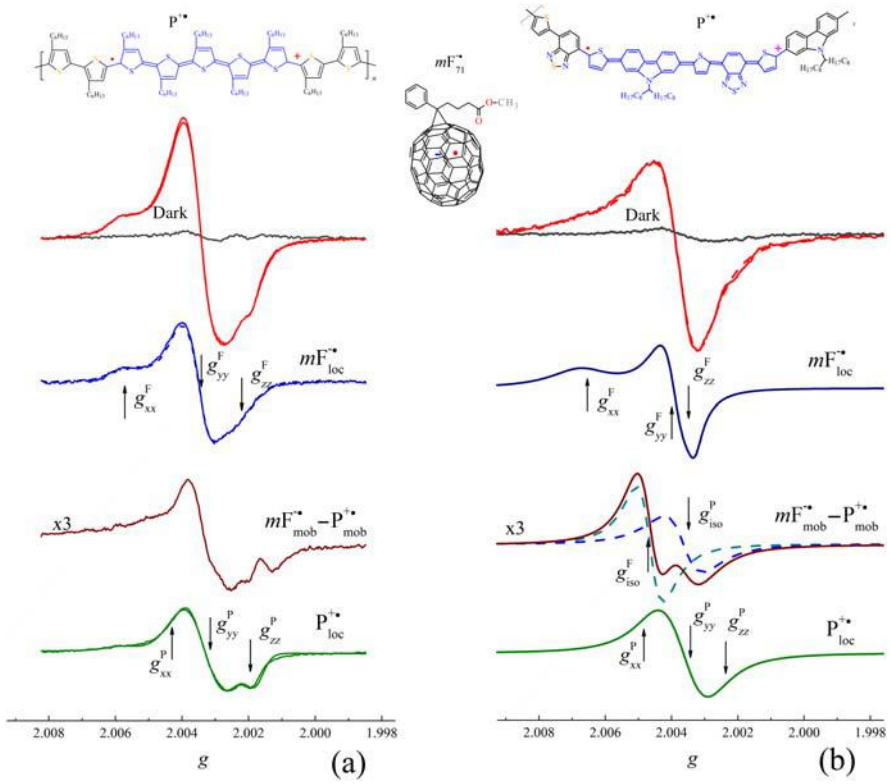

FIGURE 9.5

X-band LEPR spectra of the P3HT:$PC_{71}BM$ (a) and PCDTBT:$PC_{71}BM$ (b) composites and their contributions due to mobile quasipairs $mF^{-\bullet}_{mob} - P^{+\bullet}_{mob}$ and localized polarons $P^{+\bullet}_{loc}$ and methanofullerene anion radicals $mF^{-\bullet}_{loc}$ background photoinduced by photons with $h\nu_{ph} = 2.10$ eV at $T = 77$ K. Dashed lines show the spectra calculated using the terms of appropriate terms of their g-tensor, as presented in Table 9.1. Photoinitiation of a polaron on a polymer chain accompanied by electron transfer to a methanofullerene globe is schematically shown. The positions of photoinduced radicals and terms of their g-tensors are shown as well.

M3EH-PPV:MDHE-C_{61}-O-C_{60} composites. The main magnetic resonance parameters determined for both charge carriers in these systems are summarized in Table 9.1. It was shown that the increase of a number of elemental negative charge on fullerene molecules leads to the appearance of dispersion term in LEPR spectra of respective ion radicals (see Fig. 9.6). This effect was interpreted as the formation of highly ordered fullerene domains (conductive crystallites) in the amorphous phase of M3EH-PPV matrix. Interaction of conduction electrons with microwave field originates the appearance on the surface on the sample of skin

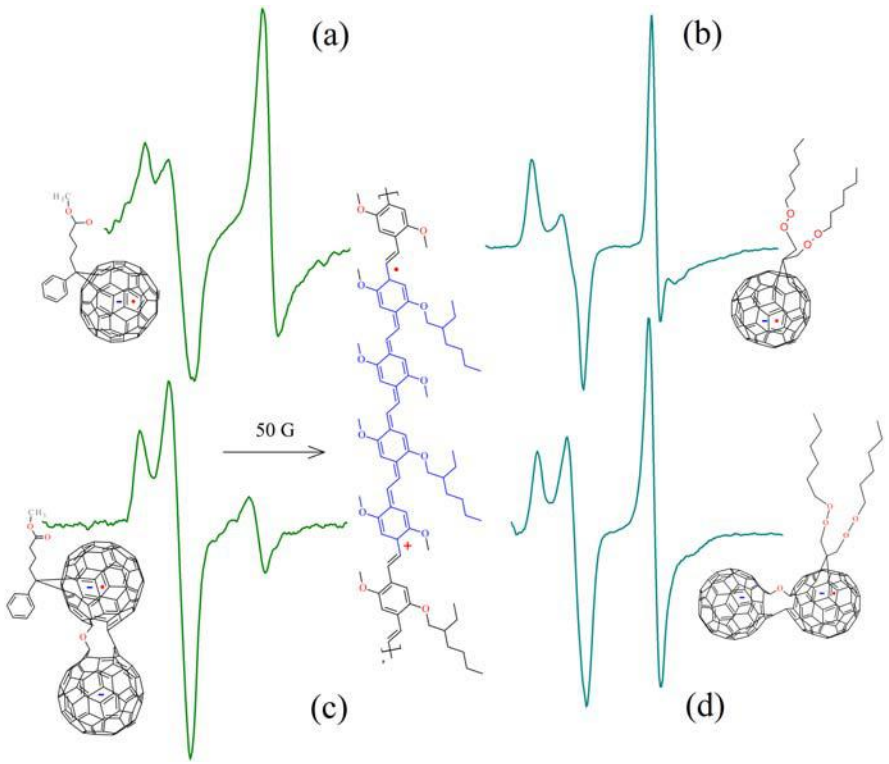

FIGURE 9.6

W-band LEPR spectra of charge carriers photoinitiated in BHJ formed by M3EH-PPV macromolecules with $PC_{61}BM$ (a), MDHE-C_{61} (b), $PC_{61}BM$-O-C_{60} (c), and MDHE-C_{61}-O-C_{60} (d) irradiated by laser photons with the energy of 2.3 eV (wavelength $\lambda_{ph} = 530$ nm) at low temperature when molecular motion is frozen. The polaron formed on the polymer after transfer a charge from its chain to a fullerene molecule is shown schematically.

depth δ and, therefore, Dysonian contribution in its LEPR spectrum described previously. Figure 9.7 shows that the data obtained for M3EH-PPV modified with both di-fullerene derivatives are well fitted by the dependence calculated from Eqns (9.24), (9.27), and (9.28). The conclusion made above is also confirmed by scanning electron microscopy [43]. This allowed a more complete investigation of magnetic, relaxation, and dynamic parameters of spin charge carriers depending on different properties of polymer composites and their ingredients. The skin-layer depth δ was estimated for di-C_{62}-fullerene to be near 10 μm at $\omega_e/2\pi = 95$ GHz. This allows the evaluation of the ac conductivity of the di-C_{60}-fullerene domains.

Main resonance parameters of both charge carriers are governed by the energy of excitation photons $h\nu_{ph}$. Figure 9.8 demonstrates how this parameter affects

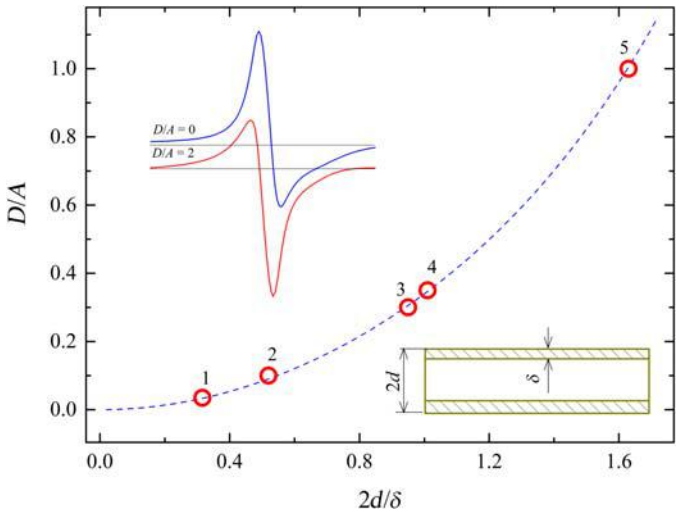

FIGURE 9.7

Dependence $D/A(2d/\delta)$ calculated from Eqns (9.24), (9.27), and (9.28) (solid line) and obtained experimentally for the M3EH-PPV:PC_{61}BM-O-C_{60} (open points 2, 3, and 5) and M3EH-PPV:MDHE-C_{61}-O-C_{60} (open points 1 and 4) composites at their different plane thickness $2d$ and spin precession frequencies $\omega_e \sim \delta^{-2}$. The inserts show X-band LEPR spectra and parameters of the samples.

the LEPR spectrum of the P3DDT:PC_{61}BM composite at $T \leq 200$ K. As in the case of other polymer:fullerene composites, sum spectra were attributed to radical quasipairs of polarons $P^{+\bullet}$ with $g_{iso} = 2.0023$, and negatively charged anion radicals $mF_{61}^{-\bullet}$ with $g_{iso} = 2.0001$ [42,59,153–159]. The sum spectra calculated with the fitting magnetic parameters presented in Table 9.1 are also shown in Fig. 9.8.

In order to analyze the conjoint effect of the structure of fullerene derivative and the energy of initiating photons on electronic properties of a polymer:fullerene composite, P3HT:PC_{61}BM and P3HT:*bis*-PC_{62}BM composites were studied at X-band LEPR [130,142,160]. Their detached ingredients are characterized by the absence of both "dark" and photoinduced LEPR signals over the entire temperature range (77–340 K). As they form polymer:fullerene BHJ and irradiated by visible light directly in a cavity of the EPR spectrometer, two overlapping LEPR lines appear at $T \leq 200$ K (Fig. 9.9). As in case of other polymer:fullerene systems, low- and high-field lines photoinduced in the P3HT:PC_{61}BM composite consist of two Lorentzian contributions of mobile polarons, $P_{mob}^{+\bullet}$, and methanofullerene anion radicals, $mF_{mob}^{-\bullet}$ (shown in Fig. 9.9 as radical quasipairs 2, $P_{mob}^{+\bullet} - mF_{mob}^{-\bullet}$) as well as two Gaussian contributions of localized polarons, $P_{loc}^{+\bullet}$, and methanofullerene anion radicals, $mF_{loc}^{-\bullet}$, pinned in polymer traps. Analogous localized polarons $P_{loc}^{+\bullet}$ with $g_{iso}^{P} = 2.0023$ and quasipairs with $g_{iso}^{F} = 2.0007$ also contribute to the LEPR spectra of the P3HT:*bis*-PC_{62}BM composite, however, the

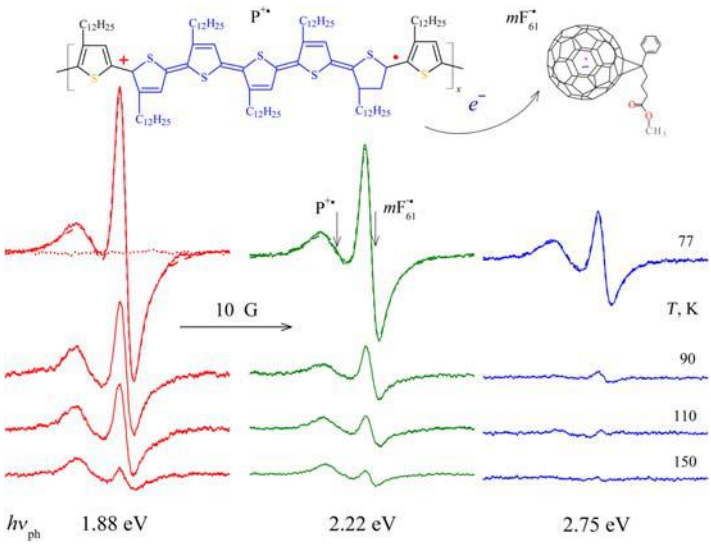

FIGURE 9.8

X-band LEPR spectra of the radical quasipairs photoinduced in the P3DDT:$PC_{61}BM$ system shown in the above insert by steady-state laser irradiation with different photon energy $h\nu_{ph}$ and as function of temperature. By the left dotted line is shown the "dark" spectrum obtained before laser irradiation. Dashed lines show sum LEPR spectra calculated using magnetic resonance parameters presented in Table 9.1.

contribution of pinned *bis*-methanofullerene radicals, $bmF^{+\bullet}_{loc}$ is absent (Fig. 9.9). These values differ slightly from those obtained for P3HT:$PC_{61}BM$, but are close to appropriate parameters determined for polarons stabilized in other fullerene-modified conjugated polymers [91,154,155,161,162] and fullerene anion radicals [133]. The absence of localized anion radicals in the P3HT:*bis*-$PC_{62}BM$ composite implies that the number of deep traps able to capture is sufficiently lower than that in the P3HT:$PC_{61}BM$ one due to the better ordinary of the former, however, their depth depends on the energy of photons.

PCDTBT, in contrast with P3AT, is characterized by the "dark" EPR spectrum typical for localized PC which changed slightly under its irradiation by visible light over a wide temperature range. Figure 9.10 shows LEPR spectra of charge carriers stabilized and reversibly photoinitiated in the PCDTBT:$PC_{61}BM$ sample under its background irradiation in a microwave cavity of the EPR spectrometer by light with a photon energy of $1.32 - 2.73$ eV in comparison with its IR−vis absorption spectrum [127]. In the latter, the low energy, broad, and featureless absorption band with a peak at $h\nu_{ph} = 2.23$ eV ($\lambda_{ph} = 560$ nm) corresponds to the intramolecular charge transfer transition, whereas meanwhile the pronounced absorption lines in the higher energy region $h\nu_{ph} = 3.09$, 3.72, and 4.70 eV ($\lambda_{ph} = 400$, 333, and 264 nm) (the two latter lines are not shown) are attributed to

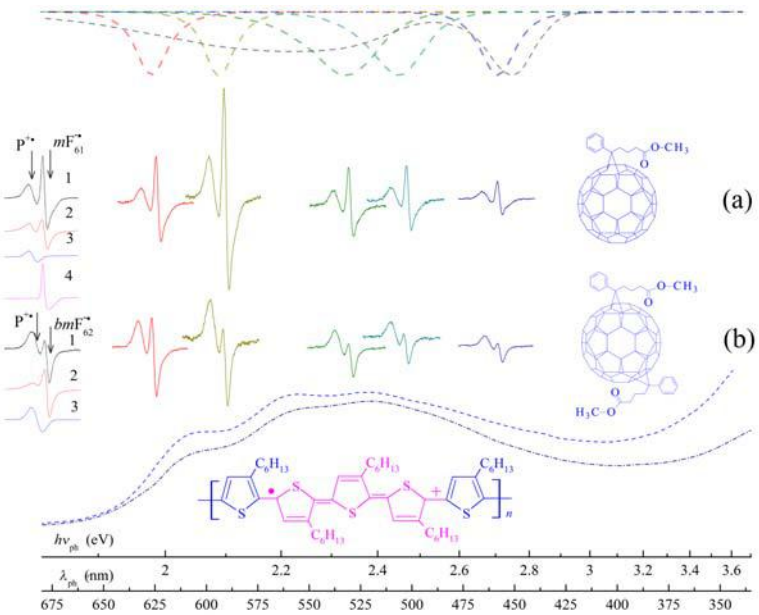

FIGURE 9.9

Normalized LEPR spectra of charge carriers background photoinduced at 77 K in BHJ formed by macromolecules of regioregular P3HT with globes of $PC_{61}BM$ and (a) *bis*-$PC_{62}BM$ (b) as a function of the photon energy $h\nu_{ph}$ (wavelength λ_{ph}). From left to right: the spectra obtained at irradiation of the samples by the white light and by the light with photon energy of 1.98, 2.10, 2.33, 2.45, 2.72 eV are shown. Above are shown irradiation spectra of the light sources. Below UV–vis absorption spectra of the P3HT:$PC_{61}BM$ and P3HT:*bis*-$PC_{62}BM$ composites are shown by dashed and dash-dotted lines, respectively. At the left are also shown theoretical sum spectra (1) and their Lorentzian contribution of mobile radical quasipairs, $P^{+\bullet}_{mob} - bmF^{-\bullet}_{mob}$ (2), Gaussian contributions caused by localized polarons $P^{+\bullet}_{loc}$ (3), and methanofullerene $mF^{-\bullet}_{loc}$ (4), calculated using respective magnetic resonance parameters presented in Table 9.1 and concentration ratios $[P^{+\bullet}_{loc}]:[P^{+\bullet}_{mob} - bmF^{-\bullet}_{mob}]:[mF^{-\bullet}_{loc}]$ of 6:57:1 for P3HT:$PC_{61}BM$ and 15:87 for P3HT:*bis*-$PC_{62}BM$. The polaron formed on the P3HT chain after transfer of its charge to the methanofullerene is shown schematically. The positions of LEPR spectra of polarons, $P^{+\bullet}$, and methanofullerene anion radicals, $bmF^{-\bullet}_{mob}$, are shown as well.

the fullerene units. This leads to an increase in the intensity of the initial EPR spectrum and the appearance of the second line at higher magnetic fields (see Fig. 9.10). Following previous studies, these low- and high-field signals can be also assigned to $P^{+\bullet}_{mob} - mF^{-\bullet}_{mob}$ quasipairs.

There were some unusual effects recorded which should be emphasized. The main one is that the LEPR signal of the sample appears under its irradiation even in the near infrared region, $h\nu_{ph} = 1.32$ eV ($\lambda_{ph} = 940$ nm), where the optical

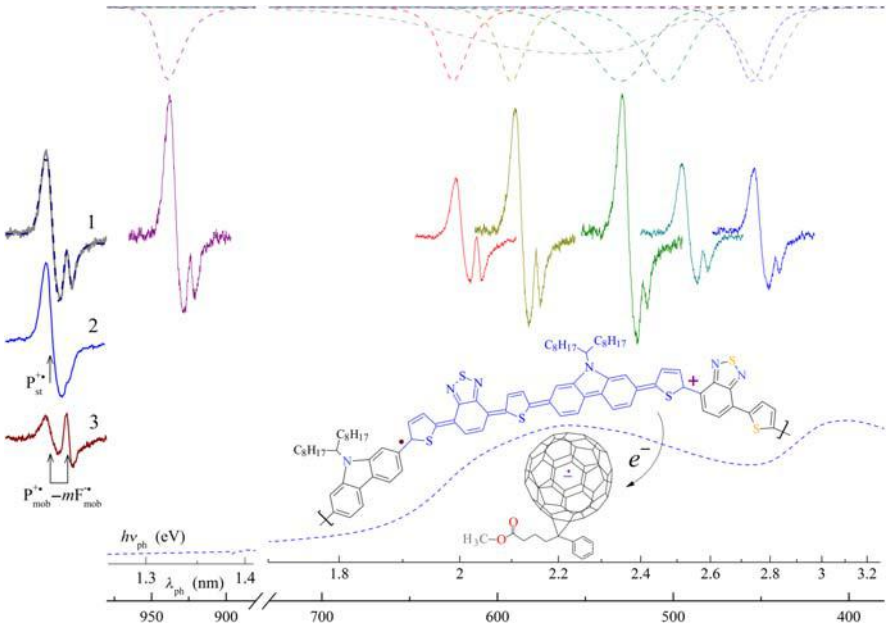

FIGURE 9.10

LEPR spectra of charge carriers background photoinduced at $T = 77$ K in BHJ formed by macromolecules of PCDTBT with globes of $PC_{61}BM$ as function of the photon energy $h\nu_{ph}$ (line width λ_{ph}) normalized to the intensity of light sources. From left to right are shown the spectra obtained at irradiation of the samples by the white light and by the light with photon energy $h\nu_{ph} = 1.32$, 1.98, 2.10, 2.34, 2.46, and 2.73 eV. On the left are shown theoretical sum spectra (1, dashed lines) and their Lorentzian contributions caused by stabilized polarons $P^{+\bullet}_{st}$ (2) and highly mobilized pair radicals, $P^{+\bullet}_{mob}$ and $mF^{-\bullet}_{mob}$ (3) numerically calculated using $\Delta B^{P}_{pp} = 1.37$ G, $\Delta B^{mF}_{pp} = 1.13$ G and a concentration ratio $[P^{+\bullet}_{st}]:[P^{+\bullet}_{mob} - mF^{-\bullet}_{mob}] = 1:14$. Above, dashed lines show irradiation spectra of the light sources and below dashed line shows IR–vis absorption spectrum of the PCDTBT:$PC_{61}BM$ composite. The charge transfer from PCDTBT to the methanofullerene accompanied by the formation on the polymer chain positively charged polaron $P^{+\bullet}$ and negatively charged ion radical $mF^{-\bullet}_{61}$ both with spin $S = ½$ is shown schematically. The positions of LEPR spectra of all charge carriers are also shown.

absorption band is nearly nulled (Fig. 9.10). The intensity of this signal is comparable to that obtained at higher photon frequencies. This fact can be originated, for example, by a nonlinear optical effect in the bulk of the PCDTBT:$PC_{61}BM$ composite converting the photon frequency/energy into the higher value, however, such a supposition was not supported under second harmonic illumination of the composite. Thus, it can be assumed that the formation of spin quasipairs indeed occurs in the sample BHJ under their excitation by infrared quanta. Besides, the comparison of an intensity of all LEPR and optical spectra presented shows that

the intensity of the former definitely does not correlate neither with the number of optical quanta reaching the sample surface nor with those absorbed by the sample. This does not confirm the conclusion made by Tong et al. [163] that the efficiency of carrier generation in the PCDTBT:fullerene BHJ should be essentially independent of the excitation wavelength. Various hypotheses can be supposed for explanation of these effects. One of them could be the interaction of charge carriers with a microwave field. Indeed, only for those relatively isolated excitons there is a reasonably high probability that a metastable PC will result from the optical production of an electron-hole pair by means of the trapping of one carrier and the hopping away of the other [164]. Thus, the separation and, therefore, lifetime of photoinitiated radical quasipairs $P^{+\bullet}_{mob} - mF^{-\bullet}_{mob}$ will generally increase with electron spin precession frequency ω_e. One, therefore, can take into account a combination of different processes affecting electronic transport through PCDTBT:PC_{61}BM BHJ.

The best fit was achieved by supposing stabilization in a polymer backbone of polarons $P^{+\bullet}_{loc}$, characterized by the anisotropic Lorentzian spectrum 2 in the left of Fig. 9.10 with the main magnetic resonance parameters presented in Table 9.1. The anisotropic nature of the $P^{+\bullet}_{loc}$ spectrum is *prima facie* evidence for its perceptible spin-orbit interaction with the nucleus of nitrogen and sulfur heteroatoms in the polymer network, as well as slow mobility. Under light irradiation of the composite, the number of such polarons somewhat increases and additionally highly mobile radical quasipairs $P^{+\bullet}_{mob} - mF^{-\bullet}_{mob}$ with $g^{P}_{iso} = 2.0022$ and $g^{mF}_{iso} = 2.0006$ (contribution 3 in the left of Fig. 9.10) appear. The latter value lies close to that obtained for other fullerene anion radicals [126,128,133,165,166], however, it slightly exceeds that obtained for PC_{61}BM embedded into P3AT matrices [42,91,157,161,162]. The absence of a Gaussian contribution in LEPR spectra of these charge carriers argues, as in case of the P3HT:*bis*-PC_{62}BM composite, in favor of a smaller number of spin traps, as well as their faster dynamics in this sample. Two main differences of this composite from the known systems should be emphasized. Hyperfine polaron interaction with neighboring hydrogen and heteroatoms should broaden its spectrum and cause its Gaussian shape. Such a line shape is also characteristic of spins captured by energetically deep traps. This leads to the appearance of appropriate Gaussian contributions in LEPR spectra of P3HT:PC_{61}BM and analogous composites. Both charge carriers stabilized and photoinitiated in the PCDTBT:PC_{61}BM composite, however, are characterized by Lorentzian line shapes. This fact was not previously detected in LEPR study of various polymer:fullerene composites and should likely indicate a lower number of spin traps and higher spin dynamics in the PCDTBT:PC_{61}BM system.

Methanofullerene anion radicals photoinduced, for example, in the P3HT:*bis*-PC_{62}BM, P3HT:PC_{61}BM, and PCDTBT:PC_{61}BM systems demonstrate nearly temperature independent g^{F}_{iso}. On the other hand, this parameter of polaronic charge carriers, g^{P}_{iso}, was determined to be a function of temperature and, to a lesser extent, of photon energy $h\nu_{ph}$ (see Figs 9.9 and 9.10). Figure 9.11 illustrates

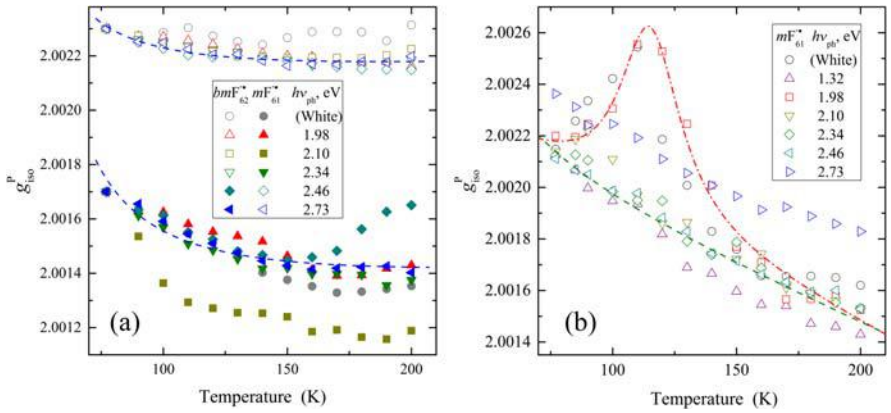

FIGURE 9.11

The value of g_{iso}^{P} for polarons photoinduced in the P3HT:*bis*-$PC_{62}BM$, P3HT:$PC_{61}BM$ (a) and PCDTBT:$PC_{61}BM$ (b) BHJ as a function of photon energy $h\nu_{ph}$ and temperature. The dashed line shows the dependences calculated from Eqn (9.3) with E_i equal to 9.5 meV (a, above line), 8 meV (a, below line), and 8 meV (b). The dash-dotted line (b) is drawn arbitrarily only for illustration to guide the eye.

that the temperature increase leads to the decrease in g_{iso}^{P}, especially in the two latter composites. It can be noted that as $PC_{61}BM$ counter ions are replaced by *bis*-$PC_{62}BM$ ones, the scattering in $g_{iso}^{P}(T)$ dependences decreases, possibly due to the ordering of the polymer:fullerene composite. In other words, this parameter is strongly governed by the structure and conformation of conjugated π-electron system. Indeed, the HOMO energy level depends on the overlap of adjacent thiophene molecular orbits and, therefore, is expected to shift with ring angle [167] similarly to the valence band involved in the $\pi-\pi^*$ transition. The band gap, LUMO−HOMO, slightly depends on both temperature [105] and torsion angle θ [168], being near 30° in regioregular P3HT [169]. A decrease in g_{iso}^{P} occurs at electron excitation from the unoccupied shell to the antibonding orbit, $\pi \rightarrow \sigma^*$ [170]. Comparing the data obtained, one may conclude that the energy of antibonding orbits decreases as *bis*-$PC_{62}BM$ is embedded into the P3HT matrix instead of $PC_{61}BM$. This increases g_{iso}^{P} of the P3HT:*bis*-$PC_{62}BM$ composite and decreases the slope of its temperature dependency characteristic of more ordered system. Indeed, the changes in total energy with the torsion angle θ appear as effective steric potential energy. The angular dependence of this energy is nonharmonic, with larger angles becoming more probable with the temperature increase. In this case the decrease of molecular regioregularity or a greater distortion of the thiophene rings out of coplanarity reduces charge mobility along the polymer chains [104]. This is usually attributed to a decrease in the effective conjugation lengths of the chain segments. The intrachain transfer integral t_{1D} is primarily

governed by the degree of overlap between the p_z atomic orbitals of the carbon atoms forming polymer units and, therefore, should evolve a square-cosine function of the torsion angle θ between the planes of the neighboring thiophene rings [103]. This allows one to evaluate the decrease in the θ value by nearly 12° at the replacement of the PCBM by *bis*-PCBM in appropriate polymer:fullerene system. Therefore, this indicates a more planar and ordered polymer matrix in the P3HT:*bis*-$PC_{62}BM$ composite than in the P3HT:$PC_{61}BM$ one. Peculiar extreme g_{iso}^{P} (T) dependences obtained for polarons photoinitiated in PCDTBT:$PC_{61}BM$ BHJ by wideband white and monochromic light with photon energy $h\nu_{ph} = 1.98$ eV was explained by competitive impact of the change in the energy transition of a spin from the unoccupied shell to the antibonding orbit $\pi \rightarrow \sigma^*$ [170]. This effect can be explained by the change in effective dimensionality of the polymer matrix [38] and is additional evidence for the better ordering of PCDTBT:$PC_{61}BM$ BHJ in comparison with analogous P3AT composites.

Monotonic temperature dependences presented in Fig. 9.11, can be explained *inter alia* by joint harmonic librations of polymer units and chains together with localized polarons which change the backbone dimensionality [38], modulate charge transfer integrals [79], lift symmetry restrictions, and enable intrachain and interchain spin relaxation to cause broader polaron line width due to the relation $\Delta B_{pp}^{P} \propto (\Delta g_{iso}^{P})^2$ [171]. Figure 9.11 indicates that the dependences calculated from Eqn (9.3) with respective E_l summarized in Table 9.2 are well fitted in the main experimental data. Such libration dynamics in the P3HT:*bis*-$PC_{61}BM$ and PCDTBT:$PC_{61}BM$ composites occurs mainly with the lower activation energy than in the P3HT:$PC_{61}BM$ one (see Table 9.2). Temperature sensitivity of the polaron g-factor decreases at $T \geq 200$ K. The concentration of both types of charge carriers decreases dramatically at this temperature region anf limits significantly the precision of determination for their main magnetic resonance parameters. Such effects can be attributed to fluctuations in local symmetry of side groups relative to the main polymer axis. These groups begin to move at the glass transition of the polymer matrix at $T \approx 200$ K [172], their local relaxation contributes to the topological disorder in the polymer structure and leads to an increase in energy barriers for charge transport. The temperature dependence of g-factors is argued to be due to a coupling of the holes to local vibrations of the chains or/and side groups along a backbone of the polymer matrix. This means that photoinitiated spins act as a nanoscopic probe of molecular and polaron dynamics in polymer:fullerene composites. More detailed information can be obtained at higher spin precession frequencies ω_e that are at higher spectral resolution. Thus, the absence in the LEPR spectra of Gaussian signals of localized charge carriers can evidence for higher ordering of PCDTBT layers and also for low number of energetically deep spin traps that facilitates charge transfer from the polymer chain to the methanofullerene cage. This is similar to cation radical single crystals with alternating organic and inorganic layers possessing a Lorentzian EPR spectra of their charge carriers, characteristic of free electrons [171].

Table 9.2 The n_p, n_f Values Determined for Polarons and Fullerene Ion Radicals, Energies E_I Determined from Eqn (9.3), ΔE_{ij} Determined from Eqn (9.13), E_0 Determined from Eqn (9.11), E_r Determined from Eqn (9.20), E_{ph} Determined from Eqn (9.33), E_b Determined from Eqn (9.35), σ_0 and E_t Determined from Eqn (9.36) (all in eV) for the P3HT:$PC_{61}BM$, P3HT:*bis*-$PC_{62}BM$, and PCDTBT:$PC_{61}BM$ Composites Irradiated by Polychromatic White and Monochromatic Light with Different Photon Energy/Lineidth $h\nu_{ph}/\lambda_{ph}$ (in eV nm^{-1})

	$h\nu_{ph}/\lambda_{ph}$						
Parameter	**White**	**1.32/940**	**1.98/625**	**2.10/590**	**2.34/530**	**2.46/505**	**2.73/455**
P3HT:$PC_{61}BM$							
n_p	4.9×10^{-5}	–	3.9×10^{-5}	9.7×10^{-5}	4.2×10^{-5}	4.3×10^{-5}	2.4×10^{-5}
n_f	4.2×10^{-5}	–	2.5×10^{-5}	7.7×10^{-5}	3.1×10^{-5}	3.4×10^{-5}	2.1×10^{-5}
E_I	0.0098	–	0.0100	0.0097	0.0099	0.0056	0.0095
ΔE_{ij}[a]	0.0092	–	0.0054	0.0028	0.0017	0.0048	0.0066
ΔE_{ij}[b]	0.0607	–	0.0307	0.0476	0.0663	0.0793	0.0744
ΔE_{ij}[c]	0.0304	–	0.0258	0.0438	0.0540	0.0558	0.0569
E_0[a]	0.0134	–	0.0519	0.0430	0.0088	0.0082	0.0318
E_0[b]	0.0103	–	0.0181	0.0208	0.0113	0.0075	0.0163
E_0[c]	0.0210	–	0.0236	0.0296	0.0307	0.0186	0.0169
E_r	0.0465	–	0.0460	0.0452	0.0351	0.0412	0.0473
E_{ph}	0.1132	-	0.1218	0.0822	0.1042	0.0709	0.0823
σ_0	0.0086	–	0.0144	0.0212	0.0109	0.0133	0.0183
E_t	0.1409	–	0.1441	0.1356	0.1335	0.1267	0.1404
E_b	0.0504	–	0.1024	0.0739	0.0551	0.0363	0.0454
P3HT:*bis*-$PC_{62}BM$							
n_p	9.7×10^{-5}	–	7.6×10^{-5}	1.6×10^{-4}	7.0×10^{-5}	6.5×10^{-5}	4.9×10^{-5}
n_f	7.2×10^{-5}	–	5.2×10^{-5}	7.7×10^{-5}	3.3×10^{-5}	3.2×10^{-5}	2.2×10^{-5}
E_I	0.0053	–	0.0093	0.0066	0.0097	0.0088	0.0081

ΔE_{ij}[a]	0.0027	–	0.0014	0.0288	0.0140	0.0162	0.0177
ΔE_{ij}[c]	0.0171	–	0.0239	0.0404	0.0350	0.0375	0.0413
E_0[a]	0.0309	–	0.0409	0.0272	0.0184	0.0144	0.0107
E_0[c]	0.0080	–	0.0202	0.0136	0.0198	0.0222	0.0227
E_r	0.0453	–	0.0479	0.0495	0.0468	0.0509	0.0503
E_{ph}	0.0615	–	0.0765	0.0751	0.0909	0.0875	0.0650
σ_0	0.0193	–	0.0167	0.0219	0.0174	0.0160	0.0206
E_t	0.1228	–	0.1283	0.1294	0.1275	0.1189	0.1250
E_b	0.0627	–	0.0770	0.0423	0.0786	0.0565	0.0588
PCDTB:$PC_{61}BM$							
E_l	0.006[d]	0.004	0.008[d]	0.003	0.002	0.004	0.004
ΔE_{ij}[a]	0.018	0.005	0.056	0.050	0.032	0.072	0.059
ΔE_{ij}[c]	0.048	0.051	0.068	0.060	0.076	0.065	0.058
E_r[a]	0.028	0.117	0.001	0.001	0.017	0.003	0.015
E_r[c]	0.013	0.013	0.014	0.019	0.020	0.018	0.018
E_{ph}	0.121	0.098	0.049	0.074	0.080	0.043	0.120
E_b	0.079	0.093	0.067	0.081	0.110	0.141	0.178

[a]*Determined for* $P^{+\bullet}_{loc}$.
[b]*Determined for* $mF^{-\bullet}_{loc}$.
[c]*Determined for* $mF^{-\bullet}_{mob}$.
[d]*Determined for monotonic part.*

9.3.2 PHOTOINITIATION AND RECOMBINATION OF CHARGE CARRIERS IN POLYMER:FULLERENE COMPOSITES

Another important parameter of a nanomodified polymer composite, proportional to the number of both charge carriers is its paramagnetic susceptibility χ.

In darkened P3HT:mF$_1$ BHJ, spin concentration ratio $[P_1^{\bullet}]/[P_2^{\bullet}]$ of coupled polarons lies near 0.089 (see Fig. 9.3a) [40,41] and decreases for other compounds. Under light illumination the number of spin charge carriers increases sharply in composites and tend to recombine. This means that by illuminating a polymer:fullerene BHJ one can register only the net PC as a difference of forward initiating (fast) and reversed recombination (slow) processes [53]. The number of such centers depends mainly on the maximum number of polarons able to be formed at the first photoinitiation stage and also on recombination coefficient of charge carriers. To determine the limiting number of polarons able to be stabilized in a polymer matrix and to compare magnetic resonance parameters of polarons reversibly and irreversibly initiated in a polymer matrix, its modification by, for example, iodine molecules [68,129] can be used. However, this allows one to only modify an initial polymer. Such a procedure was used to obtain the limiting number of both polarons n_p and methanofullerene anion radicals n_f simultaneously formed per each polymer unit of the P3HT:PC$_{61}$BM and P3HT:*bis*-PC$_{62}$BM composites [142]. The former parameter was obtained for these systems at $T = 77$ K to be 0.0028 and 0.0038, respectively. Note, that the n_P values obtained are considerably lower than those estimated for polarons excited, for example, in doped polyaniline, $n_p \approx 0.05$ [94]. Limiting paramagnetic susceptibility χ was determined for these systems to be 8.7×10^{-6} and 1.1×10^{-5} emu mol^{-1}, respectively, at $T = 310$ K. As the temperature decreases to 77 K, these values increase to 8.7×10^{-5} and 9.9×10^{-5} emu mol^{-1}, respectively. The analysis also showed that the cooling of the samples leads to the appearance of anisotropic Gaussian term in their sum EPR spectra attributed to strongly frozen polarons. The ratio of a number of mobile to frozen polarons at 77 K is near 8:1 for P3HT:PC$_{61}$BM and 7:1 for P3HT:*bis*-PC$_{62}$BM. Mobile polarons initiated in these systems by the I$_2$-doping at 310 K demonstrate single Lorentzian EPR spectra with line width ΔB_{pp} of 4.0 and 5.6 G, respectively, which are much broader than those obtained for polarons in other conjugated polymers [77]. The broadening of the EPR transitions becomes most likely due to interaction between neighboring charged polarons. The contribution to line width due to such interaction can be estimated as $\Delta B_{dd} = \mu_B R_0^{-3} = 4/3\pi\mu_B n_p$, where R_0 is a distance between polarons proportional to their concentration n_p on the polymer chain. At the transition from PC$_{61}$BM to *bis*-PC$_{62}$BM counter-anion, the ΔB_{pp} value of mobile and trapped polarons characterized by Lorentzian and Gaussian distribution of spin packets, respectively, changes at 77 K from 1.9 and 2.3 G down to 1.8 and 1.9 G. Assuming intrinsic line width of polarons $\Delta B_{pp}^0 = 1.5$ G in regioregular P3HT [173], one can obtain from the line broadening as a result of dipole−dipole interaction $R_0 \approx 1.6$ nm for P3HT:PC$_{61}$BM and

1.3 nm for P3HT:*bis*-$PC_{62}BM$. Intrinsic concentration of doping-initiated polarons relying only upon polymer fraction in these composites was determined to be 1.6×10^{19} and $2.2 \times 10^{19}\,cm^{-3}$, respectively, at 77 K. This value lies near $2 \times 10^{19}\,cm^{-3}$ obtained for concentration of acceptors in ZnO-treated P3HT [174], however, less sufficiently than $10^{21}\,cm^{-3}$ supposed for maximum polaron concentration in regioregular P3HT [55]. Effective concentration calculated for both polymer and fullerene phases in the P3HT:$PC_{61}BM$ and P3HT:*bis*-$PC_{62}BM$ composites is 1.8×10^{18} and $2.1 \times 10^{18}\,cm^{-3}$, respectively. This allows one to evaluate an effective number of both types of charge carriers per each polymer unit initiated in these polymer:fullerene composites by I_2-doping (described previously) and also by light irradiation. The values obtained for photoinitiated charge carriers are summarized in Table 9.2.

Figure 9.12 illustrates the changes in LEPR spectra of the P3HT:$PC_{61}BM$ and P3HT:*bis*-$PC_{62}BM$ composites with their heating and shows temperature dependences of all contributions into sum χ. Since concentration of main charge carriers decreases dramatically at $T > 200$ K, the precision of determination of their spin susceptibility falls significantly. The fitting of their double integrated sum LEPR spectra allowed us to separately obtain all terms of effective paramagnetic susceptibility χ. This value consists of the contributions of mobile and localized polarons χ_P and methanofullerene anion radicals χ_F. The contribution of localized fullerene anion radicals into χ of the P3HT:*bis*-$PC_{62}BM$ composite is absent within the whole temperature range used. Assuming the absence of a dipole−dipole interaction between fullerene anion radicals, one can evaluate energy ΔE_{ij} from Eqn (9.13) for all charge carriers from temperature dependences of their paramagnetic susceptibility as a function of the energy of photons $h\nu_{ph}$ (see Table 9.2). As is seen from Fig. 9.12, the net electronic processes in the composites can be described in terms of spin exchange with ΔE_{ij} presented in Table 9.2.

It is evident that the energy required for polaron trapping in the P3HT matrix is lower than that obtained for other charge carriers. ΔE_{ij} evaluated from $\chi(T)$ for mobile radicals increases considerably indicating that higher energy is required for their trapping in the system. This value becomes larger for methanofullerene after its pinning in bulk of the P3HT:$PC_{61}BM$ matrix. The data obtained again evidences that all spin-assisted processes are governed mainly by the structure of anion radicals, as well as by the nature and dynamics of charge carriers photoinduced in BHJ of a composite. The χ value of both charge carriers becomes distinctly higher at characteristic energy $h\nu_{ph} \approx 2.1$ eV lying near the band gap of P3AT [175]. Such a dependence of spin concentration on photon energy can be explained either by the formation of spin pairs with different properties in homogeneous (higher-ordered) composite fragments or by the excitation of identical charge carriers in heterogeneous (lower-ordered) domains of the system. Different spin pairs can be photoinduced as a result of the photon-assisted appearance of traps with different energy depths in a polymer matrix. However, the revealed difference in the parameters of radicals seems to be a result of their interaction with their microenvironment in domains inhomogeneously distributed in a polymer:

Table 9.3 The Spin–Lattice T_1 and Spin–Spin T_2 Relaxation Times (in s) of Polarons and Metanofullerene Anion Radicals Stabilized $P^{+\bullet}_{loc}$, $mF^{-\bullet}_{loc}$ and Mobile $P^{+\bullet}_{mob}$, $mF^{-\bullet}_{mob}$ Photoinduced in Some Polymer:Fullerene Composites at Different Photon Energy/Line Width $h\nu_{ph}/\lambda_{ph}$ (in eV nm^{-1})

		$h\nu_{ph}/\lambda_{ph}$						
Parameter		**White**	**1.32/940**	**1.98/625**	**2.10/590**	**2.34/530**	**2.46/505**	**2.73/455**
P3HT:$PC_{61}BM$								
$P^{+\bullet}_{loc}$	T_1	2.8×10^{-6}	–	2.6×10^{-6}	1.9×10^{-6}	2.3×10^{-6}	1.9×10^{-6}	1.4×10^{-6}
	T_2	5.6×10^{-8}	–	5.4×10^{-8}	5.5×10^{-8}	5.3×10^{-8}	5.4×10^{-8}	5.4×10^{-8}
$P^{+\bullet}_{mob}$	T_1	1.8×10^{-6}	–	1.2×10^{-6}	1.5×10^{-6}	1.7×10^{-6}	1.7×10^{-6}	2.6×10^{-6}
	T_2	2.6×10^{-8}	–	2.6×10^{-8}	2.5×10^{-8}	2.5×10^{-8}	2.5×10^{-8}	2.5×10^{-8}
$mF^{-\bullet}_{loc}$	T_1	1.5×10^{-6}	–	7.3×10^{-7}	9.4×10^{-7}	1.3×10^{-6}	1.2×10^{-6}	1.2×10^{-6}
	T_2	8.9×10^{-8}	–	8.9×10^{-8}	9.1×10^{-8}	8.9×10^{-8}	9.4×10^{-8}	8.9×10^{-8}
$mF^{-\bullet}_{mob}$	T_1	1.6×10^{-6}	–	1.3×10^{-6}	1.6×10^{-6}	1.4×10^{-6}	1.6×10^{-6}	1.5×10^{-6}
	T_2	4.1×10^{-8}	–	4.2×10^{-8}	4.2×10^{-8}	4.2×10^{-8}	4.3×10^{-8}	4.1×10^{-8}
P3HT:*bis*-$PC_{62}BM$								
$P^{+\bullet}_{loc}$	T_1	3.3×10^{-6}	–	2.8×10^{-6}	1.3×10^{-6}	1.8×10^{-6}	1.4×10^{-6}	1.3×10^{-6}
	T_2	5.6×10^{-8}	–	5.4×10^{-8}	4.9×10^{-8}	4.7×10^{-8}	4.8×10^{-8}	4.8×10^{-8}
$P^{+\bullet}_{mob}$	T_1	1.3×10^{-6}	–	3.8×10^{-6}	3.2×10^{-6}	2.4×10^{-6}	5.2×10^{-6}	1.2×10^{-6}
	T_2	2.6×10^{-8}	–	2.5×10^{-8}	2.3×10^{-8}	2.2×10^{-8}	2.2×10^{-8}	2.2×10^{-8}
$mF^{-\bullet}_{mob}$	T_1	1.2×10^{-6}	–	2.1×10^{-6}	1.4×10^{-6}	1.1×10^{-6}	1.3×10^{-6}	1.1×10^{-6}
	T_2	5.4×10^{-8}	–	5.3×10^{-8}	5.3×10^{-8}	5.4×10^{-8}	5.3×10^{-8}	5.0×10^{-8}
PCDTBT:$PC_{61}BM$								
$P^{+\bullet}_{loc}$	T_1	1.9×10^{-6}	2.1×10^{-6}	2.9×10^{-6}	2.1×10^{-6}	2.2×10^{-6}	1.6×10^{-6}	2.3×10^{-6}
	T_2	4.8×10^{-8}	4.4×10^{-8}	4.4×10^{-8}	4.3×10^{-8}	4.9×10^{-8}	4.7×10^{-8}	4.5×10^{-8}
$mF^{-\bullet}_{mob}$	T_1	1.1×10^{-6}	8.9×10^{-7}	1.4×10^{-6}	1.3×10^{-6}	1.3×10^{-6}	1.2×10^{-6}	9.7×10^{-7}
	T_2	5.8×10^{-8}	5.8×10^{-8}	5.6×10^{-8}	5.4×10^{-8}	5.3×10^{-8}	5.5×10^{-8}	5.9×10^{-8}

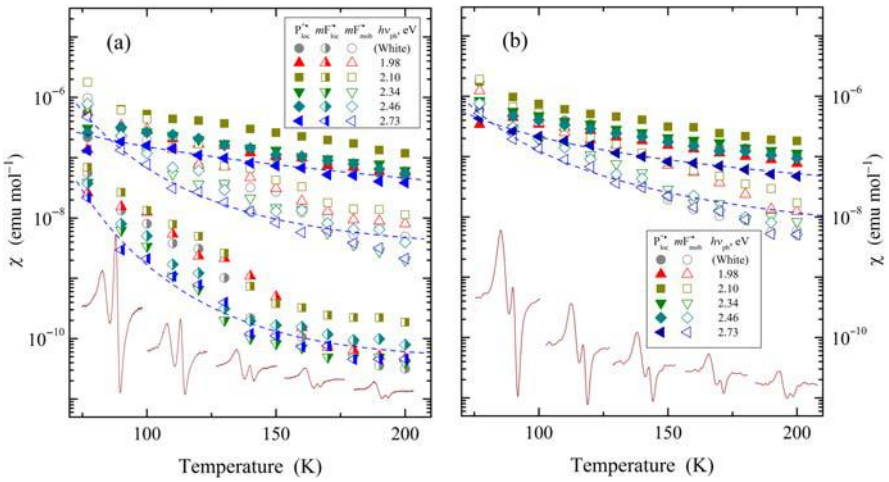

FIGURE 9.12

Temperature dependence of paramagnetic susceptibility of the $P^{+\bullet}_{loc}$, $mF^{-\bullet}_{loc}$, and $mF^{-\bullet}_{mob}$ charge carriers photoinduced in BHJ formed by P3HT chains with the $PC_{61}BM$ (a) and *bis*-$PC_{62}BM$ (b) methanofullerenes by photons with different energy $h\nu_{ph}$. Dashed lines show dependences calculated as an example for $h\nu_{ph} = 2.73$ eV from Eqn (9.13) with ΔE_{ji} summarized in Table 9.2. LEPR spectra of these heterojunctions registered at respective temperatures are shown at the bottom.

fullerene composite. Different ordering of these domains can be the reason for variation in their band gap energy which leads to their sensitivity to photons with definite but different energies. This can give rise to the change in the interaction of charge carriers with a lattice and other spins. Effective spin susceptibility of the P3HT:*bis*-$PC_{62}BM$ composite somewhat exceeds that obtained for the P3HT:$PC_{61}BM$ one. This effect and the absence of trapped anion radicals in the former support additionally higher ordering of BHJ in this system which interfere in the formation of traps in its matrix.

Figure 9.13 depicts appropriate contributions of charge carriers into an effective spin susceptibility of the PCDTBT:$PC_{61}BM$ composite as function of temperature and photon energy. The data presented can also be interpreted in terms of the exchange interaction of both charge carriers with the spin flip-flop probability p_{ff} previously introduced in Eqn (9.12). The figure illustrates that the spin−spin interaction processes in the composite can indeed be described by Eqns (9.6) and (9.13), so the energies ΔE_{ij} evaluated for both charge carriers from their dependences can be determined (Table 9.2). It is evident that polaron diffusion in the PCDTBT matrix requires lower energy ΔE_{ij} when compared with mobile methanofullerene anion radicals. It is also shows that the χ value of anion radicals becomes more temperature dependent when $h\nu_{ph} \approx 1.98$ and 2.73 eV. The former value lies near the band gap obtained for PCDTBT (1.88 eV) [29]. Such a

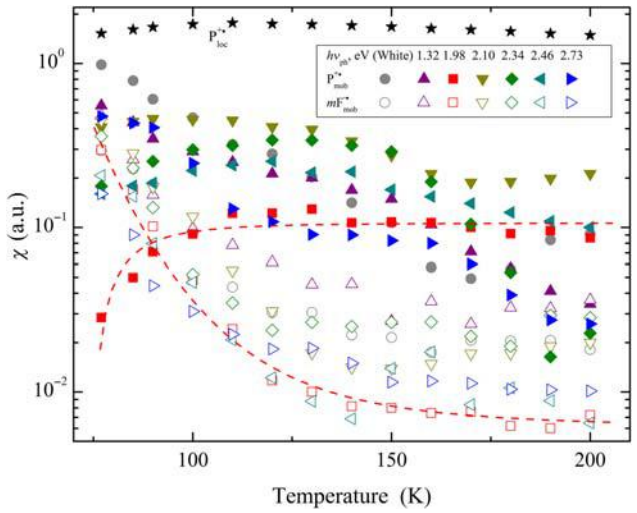

FIGURE 9.13

Temperature dependence of the paramagnetic susceptibility of polarons $P^{+\bullet}_{loc}$ and $P^{+\bullet}_{mob}$ (filled points) and methanofullerene anion radicals $mF^{-\bullet}_{mob}$ (open points) photoinduced in PCDTBT:$PC_{61}BM$ BHJ by photons with different energy $h\nu_{ph}$ normalized to illumination intensity of the light sources. The dashed lines show dependences calculated as an example for $h\nu_{ph} = 1.98$ eV from Eqn (9.6) with $\Delta E_{ji} = 0.056$ eV, and Eqn (9.13) with $\Delta E_{ji} = 0.068$ eV.

dependence of spin concentration on photon energy should indeed be a result of different interaction of charge carriers with their microenvironment in domains inhomogeneously distributed in the composite causing sensitivity to photon energy. Figure 9.13 shows that the illumination of the PCDTBT:$PC_{61}BM$ composite by photons with $h\nu_{ph}$=1.98 eV induces the minimum number of traps for polarons that leads to formation of a larger number of mobile spin quasipairs at low temperatures. Such photon frequency selectivity is governed by the polymer structure, effective dimensionality, and also by the properties of an acceptor involved in BHJ. It can be used, for example, in plastic sensoric photovoltaics, whereas the composites with low selectivity seem to be more suitable for higher efficient conversion of solar energy.

When initiating background illumination is switched off, photoinitiation of charge carriers in some polymer:fullerene BHJ stops and the concentration of spin charge carriers excited starts to decrease. This is demonstrated in the insert of Fig. 9.14, where the decay of spin charge carriers in the P3HT:$PC_{61}BM$, P3HT:*bis*-$PC_{62}BM$, and P3DDT:$PC_{61}BM$ systems is shown. Lifetime of charge carriers seems to be much longer than the $t \sim 0.1$ μs obtained by optical absorption spectroscopy for relevant recombination times of mobile photoexcitations in organic solar cells [176,177]. Thus, the data obtained are mainly pertinent to carriers time-dependent separated or trapped in a polymer matrix [42,130,142,157,178,179].

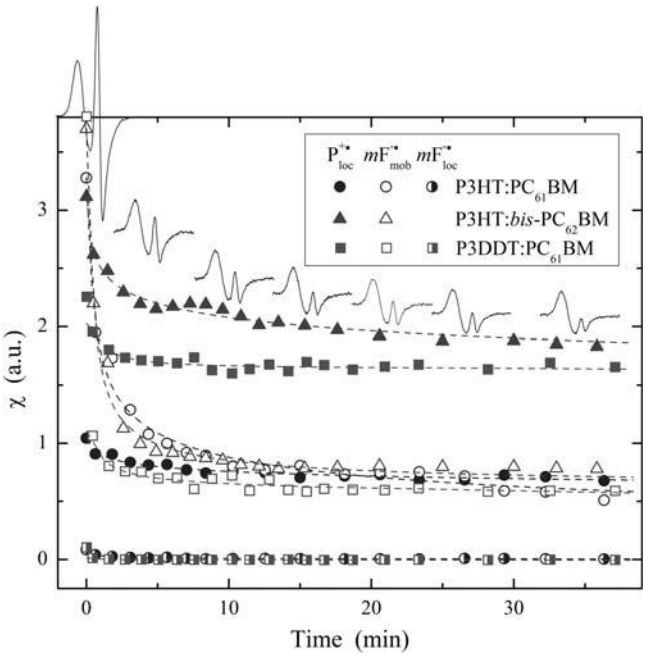

FIGURE 9.14

Decay of spin susceptibility of pinned polarons $P^{+\bullet}_{loc}$ (filled points) as well as pseudorotating ($mF^{-\bullet}_{mob}$, open points) and pinned ($mF^{-\bullet}_{loc}$, semi-filled points) methanofullerenes photoinduced in the BHJ of P3HT:PC_{61}BM (circles), P3HT:*bis*-PC_{62}BM (triangles), and P3DDT:PC_{61}BM (squares) systems at 77 K. Dashed lines show the dependences calculated for these carriers in the latter sample from Eqn (9.10) with $n_0a^3 = 2.1 \times 10^{-5}$ and $\tau_0 = 0.27$ min, $n_0a^3 = 1.4 \times 10^{-7}$ and $\tau_0 = 7.2 \times 10^{-5}$ min, and $n_0a^3 = 6.4 \times 10^{-6}$ and $\tau_0 = 2.2 \times 10^{-5}$ min, respectively, as well as from Eqn (9.11) with ΔE_0 summarized in Table 9.2. Typical changes in the LEPR spectrum of a polymer:fullerene composite at appropriate time t is shown as well.

The decay of spin susceptibility of the P3DDT:PC_{61}BM composite shown in Fig. 9.14 was interpreted [42] in terms of the above described approach of recombination of charge carriers with different effective localization radii, $n_p = 1.2 \times 10^{-4}$, $n_f = 6.3 \times 10^{-5}$ and separated by a time-dependent distance R_0 [88]. Figure 9.14 evidences that the dependences calculated from Eqn (9.10) with respective n_0a^3 products and τ_0 values fit the experimental data obtained well. Therefore, the decay of long-living spin quasipairs photoinduced in the P3DDT:PC_{61}BM composite can indeed be described in terms of this model, in which the low-temperature recombination rate is particularly strongly dependent on the spatial distance between photoinduced polarons and methanofullerene ion radicals. The long lifetimes are solely ascribed to the large spatial distances that buildup among the remaining photoinduced charge carriers, which did not recombine at a

shorter time. The product n_0a^3 decreases considerably as the methanofullerene acceptor is replaced by, for example, the azagomofullerene one [42]. This can be due to the higher probability of excitation of mobile polarons in the P3DDT:$PC_{61}BM$ system characterizing with prolonged radiative lifetime of spin quasi-pairs τ_0 that also corresponds to the lower constant of bimolecular recombination in this system.

The other data presented in Fig. 9.14 can be described in frameworks of the Tachiya concept [92] of bulk recombination of charge carriers during their repeated trapping into and detrapping from trap sites with different depths. The dependences calculated with E_0 presented in Table 9.2 for charge carriers photoinduced in the BHJ studied are also shown in Fig. 9.14. It is shown that Eqn (9.11) fits the experimental data presented in the Fig. 9.14 well. Therefore, the decay of long-lived charge carriers originated from initial spin pairs photoinduced in the polymer:fullerene composite can successfully be described in terms of the above model in which the low-temperature recombination rate is strongly governed by temperature and the width of energy distribution of trap sites. The analysis of the experimental data allows one to support the crucial role of the photon energy on the formation and energetic properties of the traps in BHJ of such disordered systems. This parameter obtained for the sites occupied by both localized polarons and fullerene anion radicals in P3HT:$PC_{61}BM$ changes extremely, with $h\nu_{ph}$ attaining the minimum at $h\nu_{ph} \sim 2.4$ eV. The width of energy distribution of the traps in the P3HT:*bis*-$PC_{62}BM$ system decreases with growing $h\nu_{ph}$. On the other hand, mobile charge carriers are characterized by extremal $E_0(h\nu_{ph})$ dependences with a maximum at $h\nu_{ph} \sim 2.3$ eV for P3HT:$PC_{61}BM$ and a minimum at $h\nu_{ph} \sim 2.1$ eV for P3HT:*bis*-$PC_{62}BM$ (Table 9.2). This indicates that the local structure and ordering govern the depth of spin traps and their distribution in these composites.

It should be noted that the other polymer:fullerene composites are characterized by much shorter-lived centers, making it impossible to register them just after their light excitation due to the higher ordering of such systems.

9.3.3 LEPR LINE WIDTH

Temperature dependences of effective LEPR line width $\Delta B_{pp}^{(0)}$ of charge carriers photoinduced in different polymer:fullerene composites by light photons is presented in Figs 9.15 and 9.16. It should be noted that the value obtained for polarons photoinduced in the composites lies near 1.5−1.8 G, and is evaluated for respective charge carriers stabilized in different P3AT matrices [81]. However, this value is considerably lower than that determined for undoped polythiophene [81,180], which is evidence of weaker spin interaction with the P3AT lattice. The LEPR line width should reflect different processes occurring in a polymer:fullerene composite. One of them is the association of mobile polarons with the counter charges. Another process realized in the system is exchange interaction between mobile and trapped polarons and fullerenes that broadens the line by

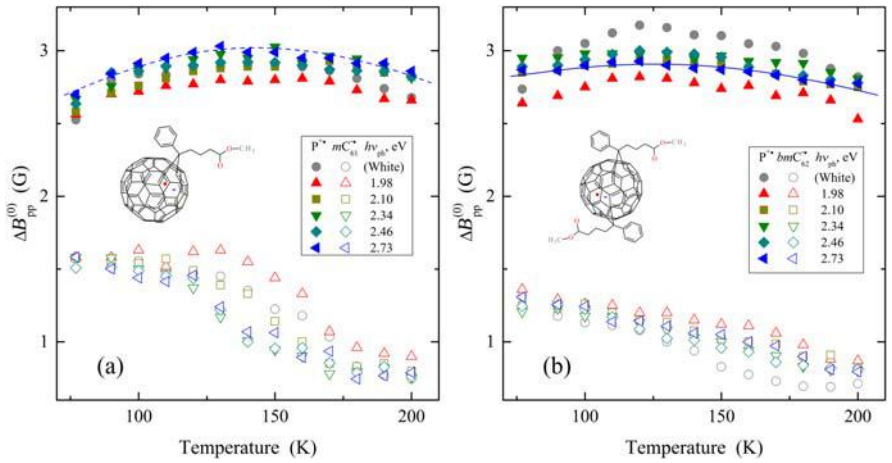

FIGURE 9.15

Line width of charge carriers photoinduced in the P3HT:$PC_{61}BM$ (a) and P3HT:*bis*-$PC_{62}BM$ (b) composites as a function of temperature and photon energy $h\nu_{ph}$. As an example, dashed lines show the dependences calculated from Eqn (9.20) with $E_r = 0.047$ (a) and 0.050 eV (b). The symbol (0) in $\Delta B_{pp}^{(0)}$ implies that the LEPR spectra were measured far from microwave saturation, when $B_1 \to 0$.

$\delta\Delta B_{ex} = \mu_B/R_0^3 = 4/3\pi\mu_B n_P$, where R_0 is the distance between dipoles proportional to polaron concentration n_P on the polymer chain. Assuming anisotropic character of the main magnetic resonance parameters of polarons discussed above, one can evaluate $R_0 \approx 2.3-2.5$ nm for a distance between dipoles in the P3AT:$PC_{61}BM$ systems.

Figure 9.15 shows that the line width obtained for polarons in the P3HT:$PC_{61}BM$ and P3HT:*bis*-$PC_{62}BM$ systems is characterized by $\cap$-like temperature dependence with the extremes lying near 140 and 130 K, respectively, and remains almost unchanged at the exchange of the fullerene derivatives. Line width of the methanofullerene anion radicals demonstrates more monotonic temperature dependence and decreases with the system heating (Fig. 9.15).

The data presented were interpreted in terms of the exchange interaction of spins with different mobility in a polymer matrix. The dependences calculated from Eqn (9.20) with and $t_{1D} = 1.18$ eV [105] and E_r summarized in Table 9.2 are also presented in Fig. 9.15. The fitting is evidence of the applicability of these approaches for interpretation of electronic processes realized in these polymer composites. The energy E_r obtained for P3HT:$PC_{61}BM$ and P3HT:*bis*-$PC_{62}BM$ lies close to that evaluated for regioregular P3HT from its ac conductometric (0.080 eV) [181] and ^{13}C NMR (0.067−0.085 eV at $T < 250$ K) [172] data. Figure 9.15 shows that line width of the $PC_{61}BM$ anion radicals decreases with the system heating. This value decreases with the replacement of the $PC_{61}BM$

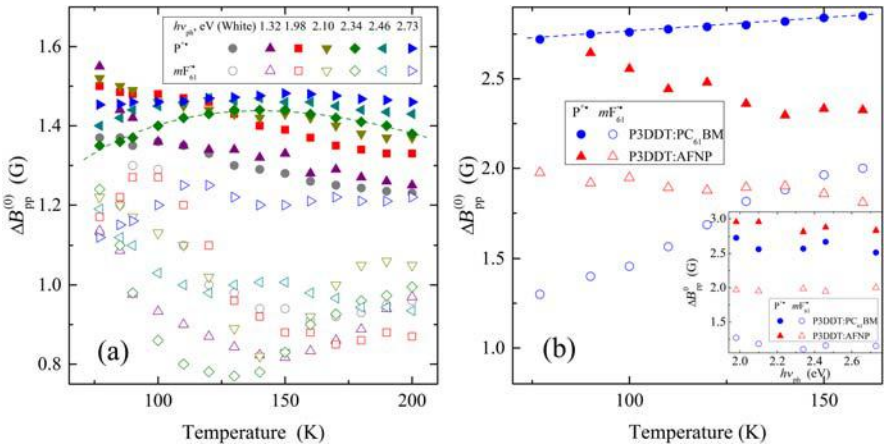

FIGURE 9.16

Line width of stabilized and mobile charge carriers photoinduced in the PCDTBT:$PC_{61}BM$ (a), P3DDT:$PC_{61}BM$ and P3DDT:AFNP (b) composites as a function of temperature and photon energy $h\nu_{ph}$. Dashed lines show the dependences calculated as an example from Eqn (9.20), with E_a equal to 0.017 (a) and 0.001 eV (b), respectively. The symbol (0) in $\Delta B_{pp}^{(0)}$ implies that the LEPR spectra were measured far from microwave saturation, when $B_1 \rightarrow 0$.

acceptor by *bis*-$PC_{62}BM$ in such polymer:fullerene composites. The latter fact additionally indicates a more ordered structure of the P3HT:*bis*-$PC_{62}BM$ composite as compared with P3HT:$PC_{61}BM$ one.

Figure 9.16a shows the line widths of both charge carriers photoinitiated in the PCDTBT:$PC_{61}BM$ composite and those normalized to the unit concentration n_i as a function of temperature and photon energy $h\nu_{ph}$. One of the dependences calculated from Eqn (9.20) and fitting appropriate data are also presented in Fig. 9.16. This is also evidence of the applicability of the approach proposed above for interpretation of electronic processes realized in organic composites. It is seen from the figure that the line width of polarons and methanofullerene anion radicals differently depends not only on the temperature, but also on the energy of the initiated photons. These charge carriers also demonstrate a different sign of own temperature dependence. This can be due to their different nature and dynamics mechanism in domains inhomogeneously distributed in the composite. Such inhomogeneity seems to be more characteristic for methanofullerene domains than for polaronic phase, possibly because of more ordered, layer morphology of PCDTBT matrix. The energy necessary for activation of both the charge carriers change slightly as $h\nu_{ph}$ excesses the polymer band gap.

Respective dependences obtained for the P3DDT:$PC_{61}BM$ and P3DDT:AFNP composites are presented in Fig. 9.16b. The figure shows that the line width of polarons in the P3DDT:$PC_{61}BM$ composite broadens with the temperature,

however, this value oppositely depends on the temperature as P3DDT is modified by AFNP nanoadduct. The data obtained were also interpreted in terms of the previously mentioned approach of the collision of localized and mobile spins. Indeed, the dependences calculated from Eqn (9.20) with E_r summarized in Table 9.2 fits the experimental data presented well.

One can conclude that the energy required for initiation of polaron diffusion in the P3HT:$PC_{61}BM$ composite exceeds E_r obtained for both the PCDTBT:$PC_{61}BM$ and P3DDT:$PC_{61}BM$ ones. This parameter additionally decreases as $PC_{61}BM$ globes in P3DDT matrix are replaced by AFNP nanoadducts.

The data presented are additional evidence that relaxation and dynamics processes realized in the composites are governed mainly by the structure of polymer matrix and fullerene derivative, as well as by the nature and dynamics of charge carriers photoinduced in appropriate BHJ. As in the case of feature of spin susceptibility, variation in $\Delta B_{pp}^{(0)}(h\nu_{ph})$ registered for charge carriers can also be attributed to inhomogeneous distribution of domains with different ordering (and, hence, band gap energies) in the polymer:fullerene BHJ. The photon-energy-correlation obtained for the main magnetic resonance parameters of the polymer:fullerene BHJ can be used in creation of organic molecular devices with spin-assisted (spintronic) properties.

9.3.4 ELECTRON RELAXATION AND DYNAMICS OF SPIN CHARGE CARRIERS

With the increase of the magnetic term B_1 of microwave irradiation in a polymer:fullerene BHJ, the width and intensity of the LEPR spectra of both polarons and fullerene anion radicals shown in Figs 9.3–9.10 change according to Eqns (9.29) and (9.30), respectively. The slope of these dependences is evidently governed by the nature, electron relaxation, and mobility of these spin charge carriers. The insert of Fig. 9.17 shows changes at different B_1 values, for example, the intensity of both the charge carriers photoinitiated in the P3HT:$PC_{61}BM$ composite [42]. These data are well described by Eqn (9.30). Since polarons and fullerene anion radicals carrying a charge through BHJ are found to be independent, this allows the separate determining of both their T_1 and T_2 relaxation times. One should only take into account the different distribution of spin packets in the LEPR spectra of mobile and localized charge carriers. Figure 9.17 shows as an example these parameters determined for charge carriers stabilized and photoinitiated in the P3HT:$PC_{61}BM$ and P3DDT:$PC_{61}BM$ composites in a wide temperature region. Both the T_1 and T_2 values of charge carriers photoinitiated in some polymer:fullerene composites at $T = 77$ K are summarized in Table 9.3.

The analysis of the data presented shows that the interaction of most charge carriers with the lattice is characterized by monotonic temperature dependences, whereas T_1 of fullerene anion radicals trapped by the P3DDT matrix demonstrates sharper temperature dependence. Spin–spin interaction is nearly temperature

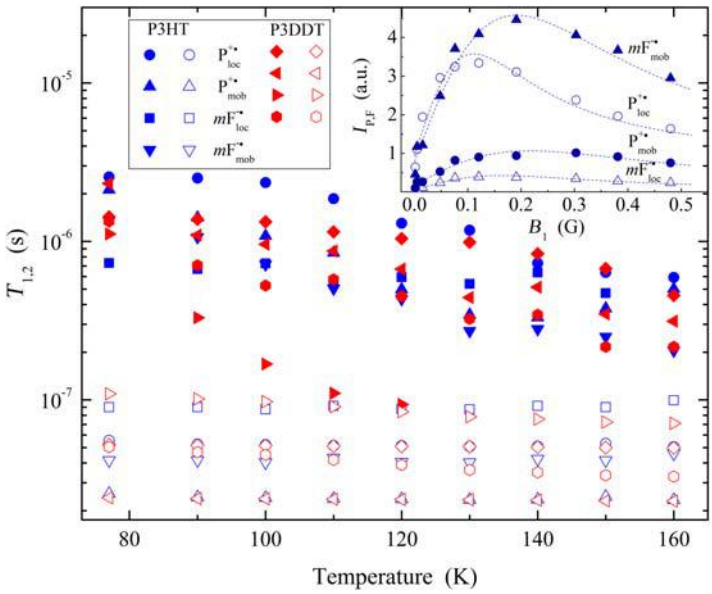

FIGURE 9.17

Temperature dependence of spin–lattice (T_1, filled points) and spin–spin (T_2, open points) relaxation times of charge carriers $P^{+\bullet}_{loc}$ and $mF^{-\bullet}_{loc}$, as well as $P^{+\bullet}_{mob}$ and $mF^{-\bullet}_{mob}$ photoinduced in the P3HT:PC_{61}BM and P3DDT:PC_{61}BM composites by light with $h\nu_{ph} = 1.98$ eV. The insert shows the changes in intensity of their contributions to the effective LEPR spectrum initiated in the P3HT:PC_{61}BM BHJ by light with $h\nu_{ph} = 1.98$ eV at 90 K as a function of the magnetic term B_1 of microwave field as well as the dependences shown by dashed lines and calculated from Eqn (9.30) with $T_1 = 2.5 \times 10^{-6}$ and $T_2 = 5.3 \times 10^{-8}$ s, $T_1 = 1.4 \times 10^{-6}$ and $T_2 = 2.4 \times 10^{-8}$ s, $T_1 = 1.1 \times 10^{-6}$ and $T_2 = 4.2 \times 10^{-8}$ s, $T_1 = 6.7 \times 10^{-7}$ and $T_2 = 9.0 \times 10^{-8}$ s, respectively.

independent. However, it is governed by structural properties of a polymer:fullerene composite (Fig. 9.17).

Diffusion coefficients calculated from Eqns (9.31) and (9.32) for both types of charge carriers photoinduced in the P3HT:PC_{61}BM and P3HT:*bis*-PC_{62}BM composites using the relaxation and susceptibility data as well as the appropriate spectral density functions are presented in Fig. 9.18 as a function of temperature and $h\nu_{ph}$. Figure 9.18 shows that the coefficient of polaron intrachain diffusion D_{1D} is governed sufficiently by the energy of initiated photons $h\nu_{ph}$. The replacement of PC_{61}BM by *bis*-PC_{62}BM suppresses this effect. Such a replacement increases anisotropy of polaron diffusion D_{1D}/D_{3D} in the P3HT matrix. This fact additionally justifies better planarity of the matrix with *bis*-PC_{62}BM molecules embedded. This is due to the fact that these more side-ramified methanofullerenes restrict the number of possible conformations able to be formed by two adjacent thiophene rings rotating about their shared C–C bond. As seen from the data presented,

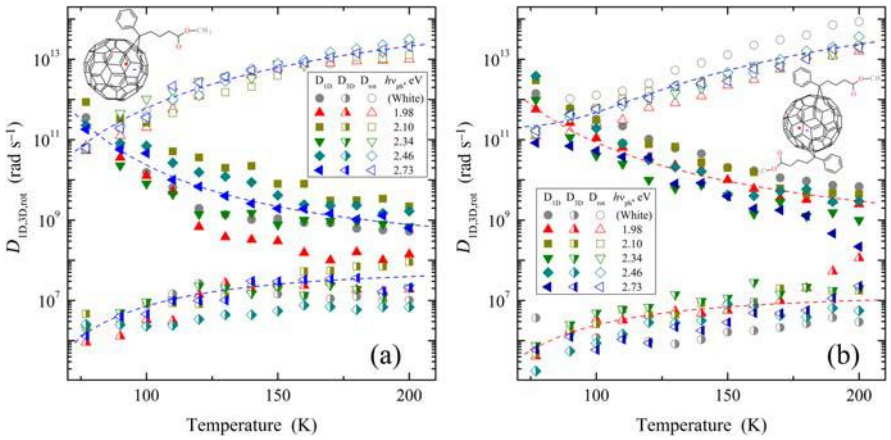

FIGURE 9.18

Temperature dependence of intrachain (D_{1D}, filled points), interchain (D_{3D}, semi-filled points), and rotational diffusion (D_{rot}, open points) coefficients of mobile charge carriers $P^{+\bullet}_{mob}$ and $mF^{-\bullet}_{mob}$ (left and right lines of the quasipairs 2 in Fig. 9.9, respectively) photoinduced in the P3HT:$PC_{61}BM$ (a) and P3HT:*bis*-$PC_{62}BM$ (b) composites by the polychromatic white and monochromatic light with different photon energy $h\nu_{ph}$. Dashed lines show the dependences calculated from Eqn (9.35) with $E_b = 0.045$ eV, Eqn (9.33) with $E_{ph} = 0.082$ eV, Eqn (9.36) with $E_t = 0.140$ eV, $\sigma_0 = 0.018$ eV (a) and from Eqn (9.35) with $E_b = 0.059$ eV, Eqn (9.33) with $E_{ph} = 0.077$ eV, Eqn (9.36) with $E_t = 0.128$ eV, $\sigma_0 = 0.017$ eV (*b*).

both fullerene anion radicals pseudorotate between the P3HT chains with approximately the same rate in the whole temperature range used (except charge carriers photoinduced in the P3HT:*bis*-$PC_{62}BM$ system by white light, see Fig. 9.18).

To account for the LEPR mobility data obtained, different theoretical models can be used. Intrachain polaron dynamics in the samples is characterized by strong temperature dependence (Fig. 9.18). Such a behavior can be associated, for example, with the scattering of polarons on the lattice phonons of crystalline domains embedded into an amorphous matrix. Figure 9.18 evidences that the D_{1D} obtained for a polaron from Eqn (9.31) follows well Eqn (9.33) with the phonon energy summarized in Table 9.2. This value lies near the energy of lattice phonons, 0.09−0.32 eV determined for other conjugated polymers [77]. E_{ph} obtained for the P3HT:*bis*-$PC_{62}BM$ composite appears to be sensitive to the energy of illuminated photons attaining a maximum at $h\nu_{ph} = 2.46$ eV.

The interchain spin hopping dynamics can be analyzed in terms of the previously discussed Hoesterey-Letson formalism of trap-controlled spin mobility. Figure 9.18 also shows exemplary temperature dependences calculated from Eqn (9.36) with $T_{cr} = 111-126$ K (P3HT:$PC_{61}BM$), $T_{cr} = 127-140$ K (P3HT:*bis*-$PC_{62}BM$), σ_0 and E_t summarized in Table 9.2. The figure evidences

that interchain polaron dynamics can indeed be described in the frame of the previously mentioned theory. The E_t values obtained for P3HT:$PC_{61}BM$ prevail for those characteristics of P3HT:*bis*-$PC_{62}BM$ (Table 9.2), which is additional evidence of deeper traps reversible formed in the former polymer matrix. Moreover, the replacement of the $PC_{61}BM$ by the *bis*-$PC_{62}BM$ counter-ions somewhat increases T_{cr} of a polymer:fullerene system. This fact probably indicates the decrease in trap concentration due the increase in effective crystallinity (ordering) of the polymer matrix. The data presented show that the photon energy governs simultaneously both the T_{ct} and E_t parameters, which attain the maximal and the minimal values, respectively, at $h\nu_{ph} \approx 2.5$ eV. Assuming all the electron wave functions exponentially decay, the interchain transfer integral, $t_\perp = 2e^2r/3\varepsilon a^2 \exp(-r/a)$ [182], was roughly estimated for P3HT to be equal to 0.12 eV. Comparing the data presented, one can note rather extremal $E_t(h\nu_{ph})$ dependences with a minimum at $h\nu_{ph} \approx 2.3-2.4$ eV.

The fullerene pseudorotational mobility data can be analyzed in the framework of Elliot's charge carrier-hopping model described previously. The energies, E_b, necessary to activate methanofullerene pseudorotational diffusion in the polymer:fullerene composites obtained from the fitting of experimental data by Eqn (9.35) are summarized in Table 9.2. Figure 9.18 illustrates the temperature dependences of dynamic parameters calculated from Eqn (9.35), with E_b determined approximately to fit the experimental data. These values depend on photon energy (see Table 9.2) and lie near those obtained, for example, from molecular dynamics in polycrystalline fullerene [183] and a triphenylamine fullerene complex [184].

Spin diffusion coefficients of both types of charge carriers photoinduced in the PCDTBT:$PC_{61}BM$ composite in wide temperature region and photon energy $h\nu_{ph}$ calculated from Eqns (9.31) and Eqn (9.32) are presented in Fig. 9.19. The figure shows that the values and frequency dispersion of all diffusion coefficients are characterized by weak dependence on the $h\nu_{ph}$ value, as in case of the P3HT/*bis*-$PC_{62}BM$ composite which appeared to become more ordered than P3HT/$PC_{61}BM$ and other known polymer:fullerene systems [142].

The anisotropy of polaron dynamics, $A = D_{1D}/D_{3D}$, in the PCDTBT:$PC_{61}BM$ composite is significantly lower than that obtained for analogous P3DDT:$PC_{61}BM$ and P3HT:*bis*-$PC_{62}BM$ (see above) that is typical for more ordered systems. This value determined at $T = 77$ K is characterized by a U-like dependence on the photon energy $h\nu_{ph}$ (see inset of Fig. 9.19). This can probably evidence the better ordering of the composite at intermediate $h\nu_{ph}$ and A values. One can only note an unusual feature of this dependence, namely the evident increase of an anisotropy of the polaron diffusion at $h\nu_{ph} = 2.10$ eV lying near the polymer band gap. This effect can probably be explained by stronger interaction of the polymer matrix with light photons. Indeed, the layer ordering of the polymer matrix allows longer polaron diffusion and formation of well-ordered $PC_{61}BM$ pools located between these layers [34,36]. This can, in principle, lead to resonant electronic response on photon energy. If the latter becomes comparable with the polymer band gap, the stronger polaron interaction with the lattice phonons can initiate the

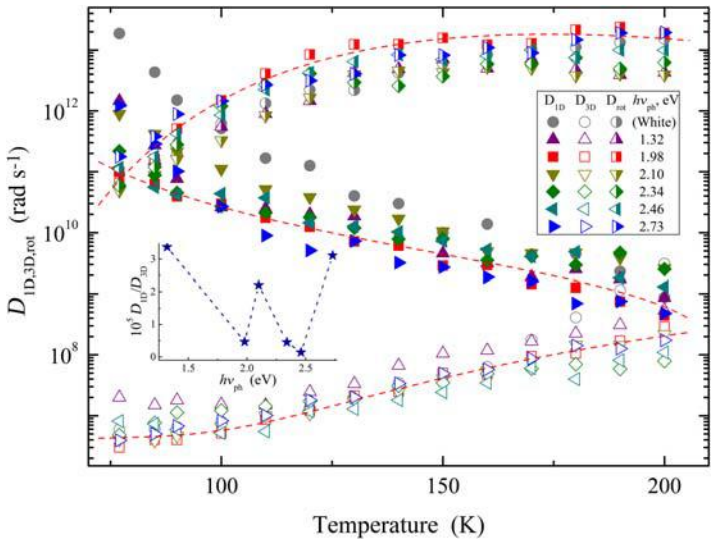

FIGURE 9.19

Temperature dependence of intrachain (D_{1D}, filled points), interchain (D_{3D}, open points), and rotational diffusion (D_{rot}, semi-filled points) coefficients of mobile charge carriers $P^{+\bullet}_{mob}$ and $mF^{-\bullet}_{mob}$ photoinduced in the PCDTBT:$PC_{61}BM$ composite by the polychromatic white and monochromatic light with different photon energy $h\nu_{ph}$ determined at their appropriate unit concentration n_i. Top-to-bottom dashed lines show the dependences calculated from Eqn (9.19) with $E_r = 0.102$ eV, Eqn (9.33) with $E_{ph} = 0.049$ eV, and Eqn (9.35) with $E_b = 0.067$ eV as well. The insert shows the anisotropy of polaron motion, $A = D_{1D}/D_{3D}$ as function of $h\nu_{ph}$. The dash-dotted line shortly connects experimental points only for illustration to guide the eye.

observed change in its g-factor and diffusion anisotropy. An analogous decrease by two orders of magnitude in the anisotropy of polaron dynamics was detected under microwave-treatment of the P3HT:$PC_{61}BM$ composite [160]. This effect was explained by the increase of well-ordered polymer and methanofullerene clusters under such system modification that facilitates polaron diffusion, inhibits fullerene reorientation, and decreases interaction of charge carriers in photoinduced radical pairs. The formation of appropriate crystallites in an amorphous polymer matrix leads to the longer diffusion of charge carriers and higher light conversion efficiency. Thus, one can conclude better matrix planarity of the PCDTBT:$PC_{61}BM$ composite at illumination by such phonons that accelerate charge transport.

Intrachain polaron dynamics in the PCDTBT:$PC_{61}BM$ BHJ, as in the case of other polymer:fullerene composites, is characterized by a strong temperature dependence. Thus, the data presented in Fig. 9.19 can also be described in terms of polaron scattering on the phonons of crystalline lattice domains embedded into

an amorphous polymer matrix. E_{ph} obtained for polaron diffusion in the PCDTBT:$PC_{61}BM$ composite at different photon energy $h\nu_{ph}$ is also summarized in Table 9.2. Figure 9.19 evidences that the D_{1D} obtained for polarons initiated by photons with, for example, $h\nu_{ph} = 1.98$ eV follows Eqn (9.33) well, with $E_{ph} = 0.049$ eV. This value lies near the energy of lattice phonons determined for various conjugated polymers (0.09−0.32 eV) [77] and plastic solar cells [91].

Interchain spin dynamics can also be analyzed in terms of the Hoesterey-Letson concept [121] of the trap-controlled charge hopping between polymer layers. The analysis of the data obtained, however, have showed that such an approach cannot be used for the interpretation of the $D_{3D}(T)$ dependences presented in Fig. 9.19. These values, as well as methanofullerene reorientational diffusion coefficients $D_{rot}(T)$, can be explained in the frame of the Pike [185] and Elliott [186] models based on the carrier hopping over the energetic barrier E_b [187]. This may be due to a suggestion that the PC produced by the influence of light might be expected to have a large effect on the ac mobility of charge carriers [164]. The respective energies E_b required to activate polaron transverse diffusion in the PCDTBT:$PC_{61}BM$ composite are also summarized in Table 9.2.

Reorientational mobility of the methanofullerene cages can be described in the framework of the Marcus mechanism. Reorganization energies, E_r, obtained from Eqn (9.19) with $t_r = 1.18$ eV [105] for charge carriers photoinitiated in the PCDTBT:$PC_{61}BM$ composite are also summarized in Table 9.2. The E_r values obtained exceed the energy required for activation of reorientation of $C_{60}^{-\bullet}$ anions in polymethylmethacrylate (0.026 eV) and C_{70} globes in cyclohexane [188], however, and lie near those determined for a motion of fullerene derivatives in conjugated polymer matrices [42,142]. It should be noted that the E_r value obtained for methnofullerene photoinitiated by achromatic (white) and monochromic (with the photon energy of 1.98 and 2.73 eV) light becomes compatible to that (0.224 eV) required for activating fullerene reorientational hopping or rotation in pure C_{60} matrix [189]. The data described considers the dynamics of solitary polarons and fullerene. Undoubtedly, the interaction of these charge carriers with the nearest spins, lattice phonons, etc., may also affect their relaxation and, therefore, should also be taken into account when interpreting the results.

9.4 UTILIZATION OF POLYMER COMPOSITES IN SPIN-ASSISTED MOLECULAR ELECTRONICS

Conjugated polymers and their composites can successfully be used as a base for organic elements of molecular electronics and spintronics [4,8], including sensors for solution and gas components [190,191]. In order to construct such elements, the correlations of their electronic properties, selectivity, sensitivity, etc., with magnetic, relaxation, and dynamics properties of spin charge carriers should be analyzed.

Lubentsov et al. [192] found that PANI doped with sulfuric acid becomes sensitive to water molecules. The EPR data gave additional independent support for the conclusions presented above. X-band EPR spectrum of polarons in PANI sample is characterized by a symmetric Lorentzian solitary line with $g_{iso} = 2.0031$.

The saturation of the emeraldine base form of PANI with water vapor broadens its spectrum from 2.5 up to 9.0 G, however, its doping with the H_2SO_4 molecules narrows the line down to 1.5 G; the saturation of the doped sample broadens its signal up to 5.2 G. At D-band EPR, its spectrum becomes Gaussian and the anisotropy of polaron's g-factor becomes more evident. At this wave band, the initial and modified samples reveal typical spectra of polarons with axially symmetrical distribution of unpaired electrons, which have effective relaxation times near 3×10^{-7} s. The saturation of the initial PANI sample with the water vapor causes the broadening of individual EPR lines from 4.6 up to 5.9 G, sustaining unchanged the **g**-tensor components, $g_{\perp} = (g_{xx} + g_{yy})/2 = 2.00301$ and $g_{\parallel} = g_{zz} = 2.00249$. The doping of this sample with sulfuric acid is not found to lead to a noticeable change in its magnetic parameters. However, the exposure of doped PANI samples to a wet atmosphere resulted in the narrowing of the individual EPR components from 4.1 down to 3.2 G and, moreover, in a change of the spectrum shape when its **g**-tensor components shift to $g_{\perp} = 2.00288$ and $g_{\parallel} = 2.00271$. This change in the spectrum shape indicates a significant rearrangement of the microenvironment of unpaired electrons localized on chains caused by the diffusion of water molecules into the polymer matrix bulk. Since the energy of the excited configuration of macromolecular systems is inversely proportional to the g-factor shift, $\Delta E \propto (g_{\perp} - g_{\parallel})^{-1}$ [193,194], the above-mentioned change in the EPR spectrum shape may be explained by the growth of the ordering of the doped and water-vapor-saturated PANI, in accordance with the analogous conclusion made from the analysis of its X-ray phase data [192].

A highly sensitive and selective polymer sensor for water molecules with polyvinyl chloride matrix treated by fuming sulfuric acid was also constructed and studied by both the EPR and conductometry methods [195]. This material exhibited a Lorentzian weak EPR singlet with $\Delta B_{pp} = 5.4$ G and $g = 2.0031$ at room temperature, characteristic of π-electron systems. This is accompanied by the increase in the film conductivity, especially under its contact with the water molecules. The line width and signal intensity changed weakly while the temperature decreased down to $T = 77$ K. Magnetic parameters of this material appeared to be close to those of solitons formed in a small amount of *trans*-polyacetylene, usually presented in *cis*-polyacetylene [112]. Thus, the change in electronic and paramagnetic properties of the film can be explained by dehydrochlorination during its oleum treatment with the formation of *trans*-polyacetylene regions with unpaired electrons in neutral solitons, $[-CHCl-CH_2-]_m \rightarrow [-CHCl-CH_2-]_m - [CH=CH=CH=CH-]_k$. Due to their status as weak electron acceptors, water molecules can partially accept the electron density from the solitary charge carriers [112], on the surface or in the bulk of the film, thus providing p-type conductivity of the sample. When the water molecules diffuse into the polymer bulk, they form bridge-type hydrogen bonds between the

conjugated chains. As a result, the solitons acquire a positive charge in the *trans*-polyacetylene fragments. Moreover, solitons which may occur in the spreading water associate [196] may also participate in charge transfer between polymer chains. Thus, the macroconductivity of the sample contacting water vapor increases considerably as a result of both intra- and interchain charge transfer. Other molecules are not able to form such associations which determines the selectivity of the sensor to water molecules only.

There were other utilizations of conducting polymers as an active matrix of organic sensors [190,197–199], Schottky diodes [200–202], etc. Since charge carriers in conjugated polymers and their composites possess spin, this feature can be used for creation of spintronic devices with spin-assisted electronic properties [4]. It was previously demonstrated that since both the charge carriers exchangeable spin-flip, their further recombination becomes dependent on their dynamics, number, polarization, and mutual separation. For large separations, when thermal energy exceeds the interaction potential, the charges are considered as noninteracting. Once the carriers become nearer than the inverted Coulombic interaction potential, their wave functions overlap and exchange interactions become non-negligible. This can originate a formation of singlet or triplet excitons in organic semiconductors. Such excited states can be detected in organic systems using optical (fluorescence and phosphorescence) and/or magnetic resonance [203] methods. However, other absorbing species are generally present in such systems, namely polaronic charge carriers, which themselves introduce efficient subgap optical transitions. Thus, a clear assignment to triplet excitations is not always possible.

The EPR method was proved [203] to be the most effective direct tool able to reveal the underlying nature of spin carriers excited in such systems. This method allows one to study various materials with weak spin-orbit coupling, where the differences in lifetime between the three excited-state triplet sublevels give rise to a spin-dependent buildup of macroscopic polarization [204], including spin charge carriers stabilized in conjugated polymers [77,81] and photoinduced in their fullerene-based compositions for photovoltaic applications [8,91]. The interaction between polarons and excitons increases under paramagnetic resonance [205]. Thus, singlet excitons are quenched to promote nonradiative decay to the ground state. The study of exchange effects in composites of two or more spin subsystems and their ingredients are expected to provide a good framework for understanding the underlying nature of exchange interactions among spins in such systems with different polaron lattices. However, there is no simple picture which would clarify spin resonance-assisted processes in organic semiconductors governed by spin-dependent exciton–charge interactions and consistent with the spin-dependent polaron pair recombination model [206]. The previously presented data prove that such processes are also governed by the energy of initiating photons due mainly to inhomogeneous distribution of polymer and fullerene domains in BHJ. It should also be noted that only very few data are published on molecular magnetic resonance spectroscopy related to actual problems in organic electronics.

The interaction between spin charge carriers affects electronic properties of organic polymers with spin charge carriers. In order to study exchange interaction in a multispin composite, P3DDT (previously used as an effective polymer matrix of organic solar cells) [42,154,155,157,158] was selected as one of a model spin reservoir [102]. PANI-ES was chosen to be a second suitable spin subsystem for the study of spin-assisted charge transfer in its composite with nanomodified P3DDT. The existence of two types of PC, namely polarons trapped on chains in amorphous polymer phase and polarons diffusing along and between chains of crystalline polymer clots was found [77,113] to be in typical PANI-ES. Polarons diffusing along polymer chains in such regions appeared to be accessible for triplet excitations injected into the polymer bulk. It was shown above that spin exchange interaction in polymer:fullerene composites leads to collision of domestic and guest spins, dramatically changing their magnetic, relaxation, and electronic dynamics parameters. This effect was not registered in main PANI-ES samples [77,113] except PANI:TSA, due to more accessibility of its spin ensemble for guest spins [100,101,207]. Unlike other PANI-ES, the latter system becomes Fermi glass with high density of states near the Fermi energy level ε_F [208,209] and its dc conductivity follows the 3D Mott's variable range hopping model [210]. This is why PANI:TSA demonstrates better material quality and therefore more metallic behavior with extended states near ε_F.

This section considers the results of a detailed LEPR study of main magnetic resonance parameters of polarons stabilized in highly doped PANI:TSA, as well as polarons and fullerene anion radicals background photoinduced in the PANI:TSA/P3DDT:$PC_{61}BM$ composite in a wide temperature range. Such study was expected to schedule the strategy of spin handling in organic complex nanocomposites for the further construction of novel molecular devices with spin-assisted electronic transport.

Initial PANI:TSA samples exhibit single X-band EPR spectrum (central spectrum shown in Fig. 9.20) attributed to polarons $P_1^{\bullet+}$ with $g_{iso} = 2.0028$ stabilized in its backbone. This value remains almost unchanged within a wide temperature range typical for crystalline high-conductive solids [77,211,212]. The P3DDT:$PC_{61}BM$ subcomposite does not demonstrate any EPR spectrum without light irradiation. When illuminated by visible light, it exhibits superposed lines attributed to positively charged diffusing polarons $P_2^{\bullet+}$ with $g_{iso} = 2.0018$ and negatively charged anion radicals $mF_{61}^{-\bullet}$ with $g_{iso} = 1.9997$ rotating around its own main axis (lower spectrum in Fig. 9.20). When combined, these systems form the PANI:TSA/P3DDT:$PC_{61}BM$ composite, of which the dark EPR spectrum mainly demonstrates contribution of polarons $P_1^{\bullet+}$ (upper spectrum in Fig. 9.20). Under light illumination its shape and intensity change, as shown in Fig. 9.20. Such transformation was interpreted as the result of the appearance of photoinduced quasipair $P_2^{\bullet+} - mF_{61}^{\bullet-}$ in its latter subsystem. In this case, two spin subsystems appear in the PANI:TSA/P3DDT:$PC_{61}BM$ composite, containing $P_1^{\bullet+}$ and $P_2^{\bullet+} - mF_{61}^{\bullet-}$ spin ensembles. As illumination is turned off, the spectra originated from the polarons $P_1^{\bullet+}$ stabilized in PANI:TSA composite and polarons $P_2^{\bullet+}$

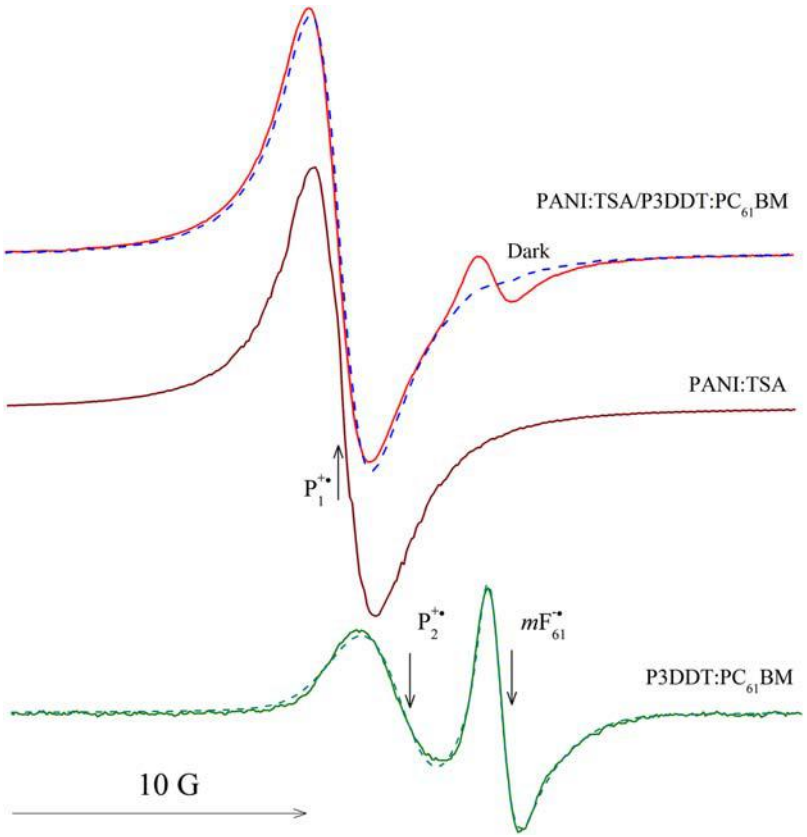

FIGURE 9.20

X-band LEPR spectra of the PANI:TSA/P3DDT:$PC_{61}BM$ composite illuminated by white light at $T = 90$ K (above) as well as its contributions due to polarons $P_1^{\bullet+}$ stabilized in PANI:TSA (center) and radical quasipairs $P_2^{\bullet+} - mF_{61}^{\bullet-}$ (below). The above and below dashed lines show EPR spectra obtained in the absence of illumination and were calculated using $\Delta B_{pp}^{P} = 2.67$ G, $\Delta B_{pp}^{mF} = 1.17$ G, and $[P_2^{\bullet+}]/[mF_{61}^{\bullet-}] = 2.0$, respectively. The positions of PC are also shown.

pinned in P3DDT:$PC_{61}BM$ system are only detected. In order to study charge-separated states and spin−spin interactions in this composite, its sum spectrum was tentatively deconvoluted [102]. As in case of other organic systems [42,126,131,142,213,214], this allowed the obtaining of separate magnetic resonance parameters for all PC stabilizing in initial polymers, and their appropriate composites for analyzing of these parameters in PANI:TSA/P3DDT:$PC_{61}BM$ BHJ.

Figure 9.21a shows temperature dependences of the line width ΔB_{pp} of polarons $P_1^{\bullet+}$ stabilized in the PANI:TSA, $P_2^{\bullet+}$ photoinitiated in P3DDT:$PC_{61}BM$ BHJ, and those values obtained for the darkened and illuminated PANI:TSA/P3DDT:$PC_{61}BM$

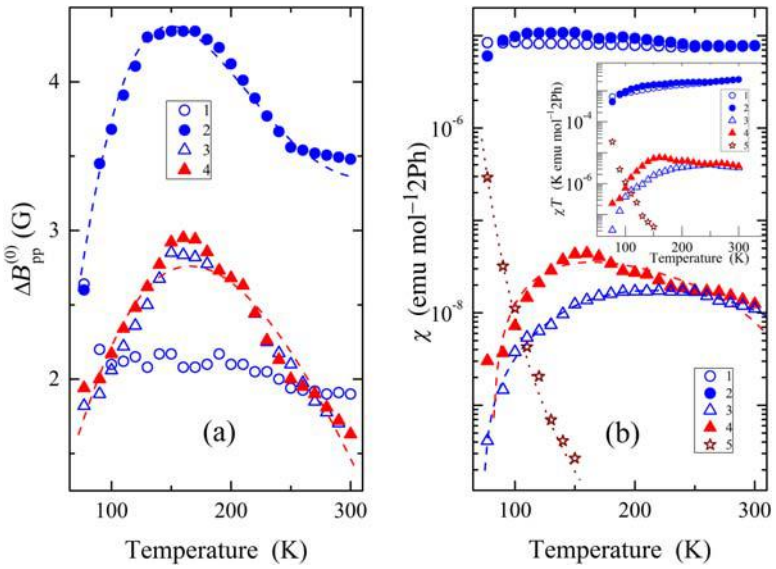

FIGURE 9.21

Temperature dependence of peak-to-peak line width $\Delta B_{pp}^{(0)}$ (a), spin susceptibility χ and χT product (inserts) (b) determined for domestic polarons $P_1^{\bullet+}$ stabilized in the initial PANI:TSA backbone (1), PANI:TSA/P3DDT:PC_{61}BM composite (2), polarons $P_2^{\bullet+}$ stabilized in the darkened (3) and irradiated by white light (4) PANI:TSA/P3DDT:PC_{61}BM composite, as well as methanofullerene radical anions $mC_{61}^{\bullet-}$ (5) photoinitiated in the composite. The upper (0) symbol in $\Delta B_{pp}^{(0)}$ implies that this parameter is to be measured far from the spectrum microwave saturation. Dashed lines in (a) show the dependences calculated from Eqn (9.18) with $\omega_{hop}^0 = 1.2 \times 10^9$ s^{-1}, $E_r = 0.006$ eV (above line), $\omega_{hop}^0 = 1.3 \times 10^9$ s^{-1}, $E_r = 0.012$ eV (below line), $J_{ex} = 0.110$ eV, and $n_P = 1.2 \times 10^{-4}$. Above and below dashed lines in (b) show the dependences χ_{ECP} calculated from Eqn (9.4) with $C = 1.0 \times 10^{-8}$ emu mol^{-1} 2Ph, $a_d = 0.98$, $J = 0.015$ eV and $C = 9.8 \times 10^{-7}$ emu mol^{-1} 2Ph, $a_d = 0.98$, $J = 0.010$ eV, respectively. The dotted line shows the dependences calculated from Eqn (9.13) with $E_r = 0.050$ eV.

composite. The EPR line width for both polarons stabilized in these systems depends on the structure of polymer matrix. Indeed, the heating of the initial PANI-ES sample is accompanied by a monotonic decrease in ΔB_{pp} of polarons $P_1^{\bullet+}$ stabilized on its chains. However, this parameter for polarons $P_2^{\bullet+}$ photoinitiated in the P3DDT:PC_{61}BM BHJ shows an opposite temperature dependence when compared with that for polarons $P_1^{\bullet+}$ (Fig. 9.21). This effect can be explained by different interaction of these polarons with appropriate polymer lattice. The formation of the PANI:TSA/P3DDT:PC_{61}BM composite does not noticeably changes the line width for PC $P_1^{\bullet+}$. However, this originates the change in the temperature dependence of $P_2^{\bullet+}$ charge carriers photoinitiated in the P3DDT matrix.

Spin properties of both polaronic reservoirs in this composite are strongly governed by the morphology of PANI chains which determines their main electronic properties [215]. Figure 9.21 shows that once both polymers form a composite, their polarons $P_1^{\bullet+}$ and $P_2^{\bullet+}$ start to demonstrate extreme temperature-dependent line widths characterized by appropriate critical point $T_{ex} \approx 150$ K. A similar effect was observed in the EPR study of exchange interaction for polarons with guest oxygen biradicals $^{\bullet}O - O^{\bullet}$ in highly doped PANI:HCl [94] and PANI:TSA [100,101]. This effect was identified [102] as exchange interaction in quasipairs formed by the guest spins with domestic polarons hopping across energy barrier E_b. Thus, the data, presented in Fig. 9.3b can be described in terms of the polaron exchange interaction hopping in the closely located solitary polymer chains.

The collision of both type spins should additionally broaden the absorption term of the EPR line expressed by Eqn (9.18). Indeed, this equation fits well the line width of both the polarons $P_1^{\bullet+}$ and $P_2^{\bullet+}$ at $n_P = 1.2 \times 10^{-4}$ obtained for P3DDT:PC_{61}BM BHJ [42] and $E_r = 0.006$ and 0.012 eV, respectively (see Fig. 9.21a).

Figure 9.21b shows the temperature dependence of spin susceptibility χ with contributions by polarons $P_1^{\bullet+}$, $P_2^{\bullet+}$, and methanofullerene radical anions $mF_{61}^{\bullet-}$ forming spin quasipairs in the P3DDT:PC_{61}BM and PANI:TSA/P3DDT:PC_{61}BM BHJ. The analysis of the above data was performed in the framework of the above-mentioned ECP model for an ensemble of $N_s/2$ interacting spin pairs with an uniform distribution of intrapair exchange characterized by coefficient J. $\chi_{ECP}(T)$ dependences calculated from Eqn (9.4) with appropriate C, a_d, and J values, which are presented in Fig. 9.21b. The model used provides an excellent fit to all the experimental data sets within all temperature ranges used.

Spin susceptibility determined for polarons $P_1^{\bullet+}$ is close to that obtained for PANI highly doped by sulfonic [208] and hydrochloric [216] acids. The appropriate term of Eqn (9.4) is normally a function of distance. When polymer chains vibrate, J for polarons diffusing along neighboring chains would oscillate and should be described by a stochastic process [217]. However, such effect appears at low temperatures, when $k_B T < J$. Thus, it can be neglected within all temperature ranges used. Nevertheless, this constant increases as polarons $P_1^{\bullet+}$ start to interact with polarons $P_2^{\bullet+}$ in the composite. This is additional evidence of the strong interaction of polarons stabilized in both PANI:TSA and P3DDT matrices. When the Fermi energy ε_F is close to the mobility edge, the temperature dependence of spin susceptibility gradually changes from Curie-law behavior $\chi_C \propto 1/T$ to temperature-independent Pauli-type behavior with increasing temperature. Corresponding density of states $n(\varepsilon_F)$ for both spin directions per monomer unit at ε_F can be determined from the analysis of the $\chi(T)T$ dependence for all polarons stabilized in both polymers (see insert in Fig. 9.21b). Krinichnyi et al. [100,101] showed that the transition-state approach (TSA)-treated system is characterized by higher $n(\varepsilon_F)$ compared with other PANI-ES. This can be explained by the difference in their metallic properties and also by onsite electron−electron interaction [218].

Spin susceptibility obtained for methanofullerene radical anions $mF_{61}^{\bullet -}$ photoinduced in the composite demonstrates sharper temperature dependence (Fig. 9.21b). This can be explained by the fast recombination of $P_2^{\bullet +} - mF_{61}^{\bullet -}$ quasipairs. Effective paramagnetic susceptibility of this charge carrier should inversely depend on the probability of their recombination, which in turn is governed by polaron Q1D hopping between polymer units [219]. In this case, the χ value should follow Eqn (9.13). The dependence calculated from Eqn (9.13) with $E_r = 0.050$ eV is also presented in Fig. 9.21b. Therefore, the decay of long-lived charge carriers originated from initial spin pairs photoinduced in the PANI:TSA/P3DDT:$PC_{61}BM$ composite can indeed be described in terms of the above model. This process is also determined by the structure and morphology of a radical anion and its environment in a polymer backbone. The use, for example, of PCDTBT instead of P3DDT and $PC_{71}BM$ instead of $PC_{61}BM$ should facilitate the excitation to reach the polymer:fullerene interface for charge separation before it becomes spatially self-localized and bound within an exciton [36]. Therefore, the main properties of an exciton are irrelevant to ultrafast charge transfer and do not limit effective charge transfer in such composites.

Figure 9.21b shows that the spin susceptibility of polarons $P_1^{\bullet +}$ stabilized in the initial PANI:TSA sample is characterized by weak temperature dependence without any anomaly. Interaction between neighboring polarons provokes extremal χ versus T dependence obtained for both polarons $P_1^{\bullet +}$ and $P_2^{\bullet +}$ (see Fig. 9.21b). Such interaction increases the overlapping of their wave functions and the energy barrier which overcomes the polaron crossing BHJ. This affects the polaron intrachain mobility and, therefore, the probability of its recombination with a fullerene anion.

There are several relaxation and dynamic processes, for example, dipole−dipole, hyperfine, exchange interactions between PC of different spin-packets, etc., which cause the shortening of spin relaxation times and, hence, the change of the shape of an EPR line. Thus, the study of spin relaxation can supply us with important information about spin-assisted electronic processes carried out in the PANI:TSA/P3DDT:$PC_{61}BM$ composite. As previously demonstrated, the initial EPR line width is oppositely proportional to the spin−spin relaxation time in accordance with Eqn (9.17). Spin−lattice relaxation also shortens the lifetime of a spin state and broadens the line. Electron relaxation of spin charge carriers stabilized in, for example, PANI-SA [212,220], PANI:TSA [100,101,207], and P3DDT [42,154,155,157,158] was shown to be strongly defined by the structural, conformational, and electronic properties of their microenvironment. Thus, it would be important to analyze also how spin exchange affects spin−lattice relaxation of polarons in polymer matrix.

Figure 9.22 exhibits temperature dependencies of T_1 and T_2 values for polarons $P_1^{\bullet +}$ stabilized in the PANI:TSA and PANI:TSA/P3DDT:$PC_{61}BM$ samples. Spin−spin relaxation was shown to be governed by the spin−spin exchange interaction. Spin−lattice relaxation time of the samples was measured at room temperature to be 0.45×10^{-7} and 0.33×10^{-7} s, respectively. These values are

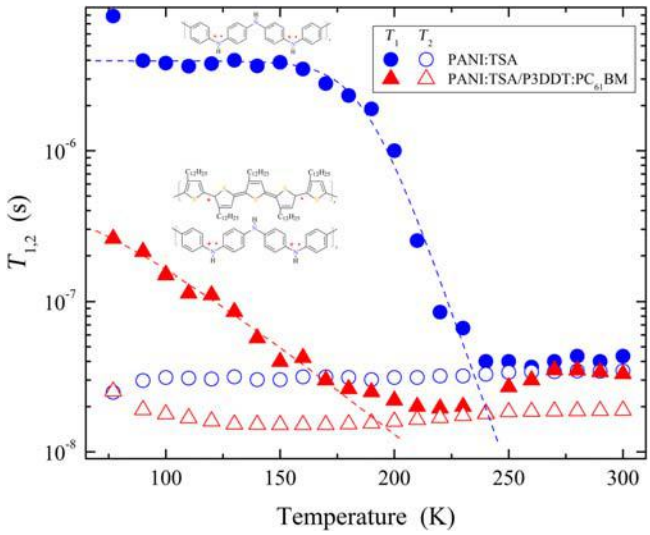

FIGURE 9.22

Temperature dependence of spin–lattice, T_1, and spin–spin, T_2, relaxation times determined for polarons $P_1^{\bullet+}$ stabilized in the PANI:TSA backbone and respective PANI:TSA/P3DDT:$PC_{61}BM$ composite without light illumination.

in good agreement with $T_1 = 0.98 \times 10^{-7}$ s obtained by Wang et al. [221] for highly doped PANI:HCl. It is seen that spin–lattice relaxation of $P_1^{\bullet+}$ stabilized in the initial PANI:TSA changes weakly as the temperature increases to $T \sim 180$ K, which is typical for organic ordered systems. This process accelerates suddenly near $T \sim 210$ K, possibly due to a phase transition, and then plateaus at higher temperatures. As $P_1^{\bullet+}$ start to interact with $P_2^{\bullet+}$ in the PANI:TSA/P3DDT:$PC_{61}BM$ composite, their spin–lattice relaxation strongly accelerates and becomes more temperature-dependent (Fig. 9.22). This is more evidence of the exchange between polarons stabilized in different neighboring polymer chains. Figure 9.22 demonstrates that T_1 tends to T_2 at high temperatures. This is typical for organic systems of lower dimensionality and can be explained by the defrosting of macromolecular dynamics.

Therefore, light excitation of P3DDT:$PC_{61}BM$ BHJ in the PANI:TSA/P3DDT:$PC_{61}BM$ composite leads to charge separation and transfer from a P3DDT chain to methanofullerene globes. This is accompanied by the appearance of polarons $P_2^{\bullet+}$ on the P3DDT backbone and anion radicals $mF_{61}^{\bullet-}$ located between polymer chains. Polarons $P_2^{\bullet+}$ moving in P3DDT solitary chains interact with $P_1^{\bullet+}$ stabilized on neighboring PANI:TSA chains due to overlapping of their wave functions. Such interaction is governed mainly by nanomorphology of the conducting form of PANI:TSA subdomains. Exchange interaction and polaron relaxation are governed by Q1D activation hopping of $P_2^{\bullet+}$ along domestic polymer chains.

Paramagnetic susceptibility of both polarons is described in frames of the model of exchange-coupled spin pairs differently distributed in appropriate polymer matrices. This deepens the overlapping of wave functions for these charge carriers and leads to an increase in the energy barrier which overcomes the polaron under its crossing through a BHJ. It is evident that EPR investigation of spin properties of domestic and photoexcited PC in a complex polymer:dopant/polymer:fullerene composite and its ingredients allows for control of its texture and other structural properties. This can open new opportunities in the creation of flexible and scalable organic molecular devices with spin-assisted electronic properties. They suggest an important role played by interchain coupling of different spin charge carriers on a handling of charge transfer through BHJ of the PANI:TSA/P3DDT:$PC_{61}BM$ and analogous multispin composites. Photoinitiation of additional spins allows the making such handling more delicate, which is a critical strategy in creating systems with spin-assisted charge transfer. The correlations established between dynamics, electronic, and structural parameters of these systems can be used for controllable synthesis of various organic spintronic devices with optimal properties.

9.5 SUMMARY

Light excitation of BHJ formed by organic polymer macromolecules with fullerene globes leads to fast formation of two long-living noninteracting PC with rhombic symmetry, namely the positively charged polaron $P^{+\bullet}$ (hole) on the polymer backbone and the negatively charged fullerene anion radical $F^{-\bullet}$ located between polymer chains. The main magnetic resonance, relaxation, and dynamic parameters of these charge carriers are governed by the structure, morphology, and ordering of BHJ, as well as by the energy of excited photons. Weak interaction of these charge carriers originated from the former radical quasipairs, stipulating a difference in their dynamics, interaction with their own microenvironment, and, hence, in their magnetic resonance parameters. Spatial separation due to charge distribution over the full fullerene globule additionally reduces the recombination rate of these charge carriers. This allows one to separately determine all their parameters.

LEPR spectroscopy was proved to be the powerful direct tool for detailed study of spin charge carriers and the processes that occurred with their participation. It is characterized, as other physical methods, by advantages and limitations. This is why the LEPR data should be discussed in comparison with those determined by other methods. The method becomes more informative at millimeter wave bands EPR. Therefore, complex organic composites should be investigated with the multifrequency EPR method. Polarons and fullerene anion radicals photoinitiated tend to recombine, and the probability of such a process depends on the rate of polaron diffusion, the energy of initiating photons, and properties of

their microenvironment. Illumination initiates the appearance in a polymer matrix of spin traps, whose number and energy depth are governed by the photon energy. Such selectivity can be used, for example, in plastic photovoltaic sensors. A part of charge carriers can be captured by such traps that decreases the conversion efficiency of a composite. The data obtained suggest the impact of the polymer ring-torsion and layer motions on the charge initiation, separation, and diffusion in disordered organic composites.

Optimization of the structure of polymer matrix and nanoadditives allows the improvement of the electronic properties of appropriate composite. The substitution, for example, $PC_{61}BM$ by *bis*-$PC_{62}BM$ increases the planarity and ordering of the P3HT matrix. It also decreases the number of traps, facilitates local molecular vibrations, and, therefore, accelerates charge transfer through a BHJ. On the other hand, the replacement of P3AT matrix by PCDTBT also increases the planarity and crystallinity of the polymer matrix, suppresses the appearance of spin traps, facilitates local site molecular vibrations that accelerates charge transfer through BHJ, minimizes the energy loss, and, therefore, increases the power-conversion efficiency. The illumination of this sample by photons with energy lying near the polymer band gap also decreases the number of such traps. This significantly reduces the anisotropy of polaron dynamics in such layer-ordered Q2D matrix due to collective interaction of charge carriers. This more noticeably affects the splitting of the polarons' σ, π, and σ^* levels, increases the number of initial spin quasipairs, broadens the LEPR spectrum, slightly reduces spin interaction with the polymer network, and increases diffusion anisotropy in the polymer network.

A polaron diffusing along a polymer chain interacts with the spin of a counter anion radical which acts as a nanoscopic probe of such dynamics. This causes a variety of mechanisms of charge transport in appropriate polymer:fullerene composite. Charge transfer is governed by polaron scattering on the lattice phonons of crystalline domains embedded into an amorphous polymer matrix and its activation hopping between polymer layers. Fullerene cages reorientate between polymer units according to the Marcus mechanism. These spin-assisted processes are governed mainly by the structure of ingredients of a composite as well as by the nature and dynamics of photoinduced charge carriers. The specific structure of the polymer matrix changes the energy levels of the appropriate composite and shifts the competition between excited states in its BHJ. It was proven that the charge transfer in the polymer/polymer:fullerene composite can be handled by the interaction of polarons stabilized in both polymer backbones with fullerene anion radicals.

The LEPR study described contributes to a better understanding of the correlations of polymer:fullerene and polymer/polymer:fullerene composites and appropriate ingredients with their structural, magnetic, and transport properties. Such direct correlations seem to be important for a further development and optimization of plastic photovoltaic devices. The results presented suggest an important role played by interchain coupling of different spin ensembles on a handling of

charge transfer in BHJ. Initiation of spins by different photons allows making such handling more delicate, which is a critical strategy in creating optimal systems with spin-assisted charge transfer. Solitary spin carriers trapped in bulk of darkened polymer matrix can, in principle, be used as elemental dots for quantum computing. Since coherent spin dynamics in such organic BHJ is anisotropic, our strategy seems to make it possible to obtain complex correlations of anisotropic electron transport and spin dynamics from multifrequency EPR study for the further design of progressive molecular electronics and spintronics.

ACKNOWLEDGMENTS

The author gratefully thanks Professor Dr H.-K. Roth and Dr E.I. Yudanova for the fruitful discussions, Dr B. Wessling for collaboration, Dr N.N. Denisov for the assistance in EPR experiments. The partial support by the Russian Foundation of Basic Researches, Grant No. 12-03-00148, and the Program of Fundamental Researches of Presidium of the Russian Academy of Sciences is also gratefully acknowledged.

REFERENCES

[1] Tjong SC, Mai Y-W, editors. Physical properties and applications of polymer nanocomposites. Cambridge: Woodhead Publishing; 2010.
[2] Tjong SC, editor. Polymer composites with carbonaceous nanofillers: properties and applications. Weinheim: Wiley-VCH Verlag; 2012.
[3] Zhang G, Manjooran N, editors. Nanofabrication and its application in renewable energy. Cambridge: The Royal Society of Chemistry; 2014.
[4] Xu Y, Awschalom DD, Nitta J, editors. Handbook of spintronics. Berlin: Springer-Verlag; 2015.
[5] Sun SS, Sariciftci NS, editors. Organic Photovoltaics: mechanisms, materials, and devices (Optical Engineering). Boca Raton, FL: CRC Press; 2005.
[6] Poortmans J, Arkhipov V, editors. Thin film solar cells: fabrication, characterization and applications. West Sussex: Wiley; 2006.
[7] Pagliaro M, Palmisano G, Ciriminna R. Flexible solar cells. Weinheim: Wiley-WCH; 2008.
[8] Brabec C, Scherf U, Dyakonov V, editors. Organic photovoltaics: materials, device physics, and manufacturing technologies, vol. 1. Weinheim: Wiley-VCH; 2014.
[9] Shaheen SE, Brabec CJ, Sariciftci NS, Padinger F, Fromherz T, Hummelen JC. 2.5% efficient organic plastic solar cells. Appl Phys Lett 2001;78:841–3.
[10] Hwang IW, Soci C, Moses D, Zhu ZG, Waller D, Gaudiana R, et al. Ultrafast electron transfer and decay dynamics in a small band gap bulk heterojunction material. Adv Mater 2007;19:2307–12.
[11] Kraabel B, McBranch D, Sariciftci NS, Moses D, Heeger AJ. Ultrafast spectroscopic studied of photoinduced electron-transfer from semiconducting polymers to C-60. Phys Rev B 1994;50:18543–52.

[12] Brabec CJ, Zerza G, Cerullo G, DeSilvestri S, Luzatti S, Hummelen JC, et al. Tracing photoinduced electron transfer process in conjugated polymer/fullerene bulk heterojunctions in real time. Chem Phys Lett 2001;340:232–6.
[13] Banerji N, Cowan S, Leclerc M, Vauthey E, Heeger AJ. Exciton formation, relaxation, and decay in PCDTBT. J Am Chem Soc 2010;132:17459–70.
[14] Pivrikas A, Sariciftci NS, Juska G, Osterbacka R. A review of charge transport and recombination in polymer/fullerene organic solar cells. Progress Photovoltaics 2007;15:677–96.
[15] Kubis P, Lucera L, Machui F, Spyropoulos G, Cordero J, Frey A, et al. High precision processing of flexible P3HT/PCBM modules with geometric fill factor over 95%. Org Electron 2014;15:2256–63.
[16] Green MA, Emery K, Hishikawa Y, Warta W, Dunlop ED. Solar cell efficiency tables (version 44). Progress Photovoltaics: Res Appl 2014;22:701–10.
[17] Halls JJM, Cornil J, Dos Santos DA, Silbey R, Hwang DH, Holmes AB, et al. Charge- and energy-transfer processes at polymer/polymer interfaces: a joint experimental and theoretical study. Phys Rev B 1999;60:5721–7.
[18] Brabec CJ, Winder C, Sariciftci NS, Hummelen JC, Dhanabalan A, van Hal PA, et al. A low-bandgap semiconducting polymer for photovoltaic devices and infrared emitting diodes. Adv Funct Mater 2002;12:709–12.
[19] Brabec CJ, Cravino A, Meissner D, Sariciftci NS, Fromherz T, Rispens MT, et al. Origin of the open circuit voltage of plastic solar cells. Adv Funct Mater 2001;11:374–80.
[20] Koster LJA, Mihailetchi VD, Ramaker R, Blom PWM. Light intensity dependence of open-circuit voltage of polymer:fullerene solar cells. Appl Phys Lett 2005;86:123509.
[21] Koster LJA, Mihailetchi VD, Blom PWM. Ultimate efficiency of polymer/fullerene bulk heterojunction solar cells. Appl Phys Lett 2006;88:093511–13.
[22] Wu P-T, Ren G, Jenekhe SA. Crystalline random conjugated copolymers with multiple side chains: tunable intermolecular interactions and enhanced charge transport and photovoltaic properties. Macromolecules 2010;43:3306–13.
[23] Lenes M, Wetzelaer GJAH, Kooistra FB, Veenstra SC, Hummelen JC, Blom PWM. Fullerene bisadducts for enhanced open-circuit voltages and efficiencies in polymer solar cells. Adv Mater 2008;20:2116–19.
[24] Li G, Shrotriya V, Huang J, Yao Y, Moriarty T, Emery K, et al. High-efficiency solution processable polymer photovoltaic cells by self-organization of polymer blends. Nat Mater 2005;4:864–8.
[25] Huang JH, Li KC, Chien FC, Hsiao YS, Kekuda D, Chen PL, et al. Correlation between exciton lifetime distribution and morphology of bulk heterojunction films after solvent annealing. J Phys Chem C 2010;114:9062–9.
[26] Jarzab D, Cordella F, Lenes M, Kooistra FB, Blom PWM, Hummelen JC, et al. Charge transfer dynamics in polymer-fullerene blends for efficient solar cells. J Phys Chem B 2009;113:16513–17.
[27] Dyer-Smith C, Reynolds LX, Bruno A, Bradley DDC, Haque SA, Nelson J. Triplet formation in fullerene multi-adduct blends for organic solar cells and its influence on device performance. Adv Funct Mater 2010;20:2701–8.
[28] Berton N, Ottone C, Labet V, de Bettignies R, Bailly S, Grand A, et al. New alternating copolymers of 3,6-carbazoles and dithienylbenzothiadiazoles: synthesis, characterization, and application in photovoltaics. Macromol Chem Phys 2011;212:2127–41.

[29] Kim J, Yun MH, Kim GH, Kim JY, Yang C. Replacing 2,1,3-benzothiadiazole with 2,1,3-naphthothiadiazole in PCDTBT: towards a low bandgap polymer with deep HOMO energy level. Polym Chem 2012;3:3276–81.
[30] Blouin N, Michaud A, Leclerc M. A low-bandgap poly(2,7-carbazole) derivative for use in high-performance solar cells. Adv Mater 2007;19:2295–300.
[31] Choy WCH, editor. Organic solar cells: materials and device physics. London: Springer; 2013.
[32] Ostroverkhova O, editor. Handbook of organic materials for optical and (Opto) Electronic devices: properties and applications, vol. 39. New York, NY: Elsevier; 2013.
[33] Huh YH, Park B. Interface-engineering additives of poly(oxyethylene tridecyl ether) for low-band gap polymer solar cells consisting of PCDTBT:PCBM70 bulk-heterojunction layers. Opt Express 2013;21:A146–56.
[34] Lu XH, Hlaing H, Germack DS, Peet J, Jo WH, Andrienko D, et al. Bilayer order in a polycarbazole-conjugated polymer. Nat Commun 2012;3. Available from: http://dx.doi.org/10.1038/ncomms1790.
[35] Park SH, Roy A, Beaupre S, Cho S, Coates N, Moon JS, et al. Bulk heterojunction solar cells with internal quantum efficiency approaching 100%. Nat Photon 2009;3:297–302.
[36] Moon JS, Jo J, Heeger AJ. Nanomorphology of PCDTBT:$PC_{70}BM$ bulk heterojunction solar cells. Adv Energy Mater 2012;2:304–8.
[37] Liu JG, Chen L, Gao BR, Cao XX, Han YC, Xie ZY, et al. Constructing the nanointerpenetrating structure of PCDTBT:PC70BM bulk heterojunction solar cells induced by aggregation of PC70BM via mixed-solvent vapor annealing. J Mater Chem A 2013;1:6216–25.
[38] Gutzler R, Perepichka DF. π-Electron conjugation in two dimensions. J Am Chem Soc 2013;135:16585–94.
[39] Bässler H. Charge transport in disordered organic photoconductors a Monte Carlo simulation study. Phys Status Solidi (B) 1993;175:15–56.
[40] Krinichnyi VI, Troshin PA, Denisov NN. The effect of fullerene derivative on polaronic charge transfer in poly(3-hexylthiophene)/fullerene compound. J Chem Phys 2008;128:164715/01–164715/07.
[41] Krinichnyi VI, Troshin PA, Denisov NN. Structural effect of fullerene derivative on polaron relaxation and charge transfer in poly(3-hexylthiophene)/fullerene composite. Acta Mater 2008;56:3982–9.
[42] Krinichnyi VI, Yudanova EI, Spitsina NG. Light-induced EPR study of poly(3-alkylthiophene)/fullerene composites. J Phys Chem C 2010;114:16756–66.
[43] Konkin A, Ritter U, Scharff P, Mamin G, Aganov A, Orlinskii S, et al. W-band ESR study on photo-induced ion radical formation in solid films of mono- and di-fullerenes embedded in conjugated polymers. Carbon 2014;77:11–17.
[44] Ginder JM, Epstein AJ, MacDiarmid AG. Ring-torsional polarons in polyaniline and polyparaphenylene sulfide. Synth Metals 1991;43:3431–6.
[45] Lee JM, Park JS, Lee SH, Kim H, Yoo S, Kim SO. Selective electron- or hole-transport enhancement in bulk-heterojunction organic solar cells with N- or B-doped carbon nanotubes. Adv Mater 2011;23:629–33.
[46] Park JS, Lee BR, Lee JM, Kim J-S, Kim SO, Song MH. Efficient hybrid organic-inorganic light emitting diodes with self-assembled dipole molecule deposited metal oxides. Appl Phys Lett 2010;96:243306–8.

[47] Padinger F, Rittberger RS, Sariciftci NS. Effects of postproduction treatment on plastic solar cells. Adv Funct Mater 2003;11:1–4.
[48] Chirvase D, Parisi J, Hummelen JC, Dyakonov V. Influence of nanomorphology on the photovoltaic action of polymer-fullerene composites. Nanotechnology 2004;15:1317–23.
[49] Chu CW, Yang HC, Hou WJ, Huang JS, Li G, Yang Y. Control of the nanoscale crystallinity and phase separation in polymer solar cells. Appl Phys Lett 2008;92:103306–8.
[50] Dante M, Peet J, Nguyen TQ. Nanoscale charge transport and internal structure of bulk heterojunction conjugated polymer/fullerene solar cells by scanning probe microscopy. J Phys Chem C 2008;112:7241–9.
[51] Montanari I, Nogueira AF, Nelson J, Durrant JR, Winder C, Loi MA, et al. Transient optical studies of charge recombination dynamics in a polymer/fullerene composite at room temperature. Appl Phys Lett 2002;81:3001–3.
[52] Nogueira AF, Montanari I, Nelson J, Durrant JR, Winder C, Sariciftci NS. Charge recombination in conjugated polymer/fullerene blended films studied by transient absorption spectroscopy. J Phys Chem B 2003;107:1567–73.
[53] Krebs FC. Stability and degradation of organic and polymer solar cells. Chichester: John Wiley & Sons; 2012.
[54] Dyakonov V, Zoriniants G, Scharber M, Brabec CJ, Janssen RAJ, Hummelen JC, et al. Photoinduced charge carriers in conjugated polymer-fullerene composites studied with light-induced electron-spin resonance. Phys Rev B 1999;59:8019–25.
[55] Westerling M, Osterbacka R, Stubb H. Recombination of long-lived photoexcitations in regioregular polyalkylthiophenes. Phys Rev B 2002;66:165220/01–165220/07.
[56] Brabec C, Dyakonov V, Parisi J, Sariciftci NS. Organic photovoltaic: concepts and realization. Berlin: Springer; 2003.
[57] Marumoto K, Muramatsu Y, Kuroda S. Quadrimolecular recombination kinetics of photogenerated charge carriers in regioregular poly(3-alkylthiophene)/fullerene composites. Appl Phys Lett 2004;84:1317–19.
[58] Bassler H. Charge transport in disordered organic photoconductors. Phys Status Solidi B 1993;175:15–56.
[59] Sensfuss S, Konkin A, Roth HK, Al-Ibrahim M, Zhokhavets U, Gobsch G, et al. Optical and ESR studies on poly(3-alkylthiophene)/fullerene composites for solar cells. Synth Metals 2003;137:1433–4.
[60] Schlick S, editor. Advanced ESR methods in polymer research. New York, NY: John Wiley & Sons, Inc.; 2006.
[61] Eaton GR, Eaton SS, Barr DP, Weber RT. Quantitative EPR. Wien, New York, NY: Springer; 2010.
[62] Ranby B, Rabek JF. ESR spectroscopy in polymer research. New York, NY: Springer; 2011.
[63] Misra SK, editor. Multifrequency electron paramagnetic resonance: theory and applications. Weinheim: Wiley-VCH; 2011.
[64] Lund A, Shiotani M, Shimada S. Principles and applications of ESR spectroscopy. New York, NY: Springer; 2011.
[65] Lund A, Shiotan M, editors. EPR of free radicals in solids I: trends in methods and applications, vol. 1. Amsterdam: Springer; 2013.

[66] Lund A, Shiotan M, editors. EPR of free radicals in solids II: progress in theoretical chemistry and physics, vol. 2. Amsterdam: Springer; 2013.
[67] Baranov P. Magnetic resonance of semiconductors and semiconductor nanostructures. New York, NY: Springer; 2016.
[68] Aguirre A, Gast P, Orlinskii S, Akimoto I, Groenen EJJ, El Mkami H, et al. Multifrequency EPR analysis of the positive polaron in I_2-doped poly(3-hexylthiophene) and in poly[2-methoxy-5-(3,7-dimethyloctyloxy)]-1,4-phenylenevinylene. Phys Chem Chem Phys 2008;10:7129−38.
[69] Behrends J, Sperlich A, Schnegg A, Biskup T, Teutloff C, Lips K, et al. Direct detection of photoinduced charge transfer complexes in polymer fullerene blends. Phys Rev B 2012;85:125206/01−125206/06.
[70] Uvarov MN, Kulik LV. Electron spin echo of photoinduced spin-correlated polaron pairs in P3HT:PCBM composite. Appl Magn Reson 2013;44:97−106.
[71] Uvarov MN, Popov AG, Lukina EA, Kulik LV. Spin relaxation and structure of light-induced spin-correlated PCBM-/P3HT(+) radical pairs. J Struct Chem 2014;55:644−50.
[72] Assenheim HM. Introduction to electron spin resonance. New York, NY: Springer; 2014.
[73] Buchachenko AL, Turton CN, Turton TI. Stable radicals. New York, NY: Consultants Bureau; 1995.
[74] Misra SK, editor. Handbook of multifrequency electron paramagnetic resonance: data and techniques. New York, NY: Wiley; 2014.
[75] Kim Y, Cook S, Tuladhar SM, Choulis SA, Nelson J, Durrant JR, et al. A strong regioregularity effect in self-organizing conjugated polymer films and high-efficiency polythiophene: fullerene solar cells. Nat Mater 2006;5:197−203.
[76] Krinichnyi VI. 2-mm wave band EPR spectroscopy of condensed systems. Boca Raton, FL: CRC Press; 1995. See also <http://hf-epr.awardspace.us/publications.htm>.
[77] Krinichnyi VI. 2-mm Waveband electron paramagnetic resonance spectroscopy of conducting polymers (review). Synth Metals 2000;108:173−222 See also the references therein.
[78] Krinichnyi VI. Advanced ESR methods. In: Schlick S, editor. Polymer research. Hoboken, NJ: Wiley; 2006. p. 307−38. See also the references therein.
[79] Silinsh EA, Kurik MV, Chapek V. Electronic processes in organic molecular crystals: the phenomena of localization and polarization (Russian). Riga: Zinatne; 1988.
[80] Vonsovskii SV. Magnetism. Magnetic properties of dia-, para-, ferro-, antiferro-, and ferrimagnetics, vol. 1. New York, NY: John Wiley & Sons; 1974.
[81] Mizoguchi K, Kuroda S. Magnetic properties of conducting polymers. In: Nalwa HS, editor. Handbook of organic conductive molecules and polymers. Chichester, New York: John Wiley & Sons; 1997. p. 251−317.
[82] Raghunathan A, Kahol PK, Ho JC, Chen YY, Yao YD, Lin YS, et al. Low-temperature heat capacities of polyaniline and polyaniline polymethylmethacrylate blends. Phys Rev B 1998;58:R15955−8.
[83] Kahol PK, Mehring M. Exchange-coupled pair model for the non-curie-like susceptibility in conducting polymers. Synth Metals 1986;16:257−64.
[84] Clark WG, Tippie LC. Exchange-coupled pair model for the random-exchange Heisenberg antiferromagnetic chain. Phys Rev B 1979;20:2914−23.
[85] Jonston DC. Thermodynamics of charge-density waves in quasi one-dimensional conductors. Phys Rev Lett 1984;52:2049−52.

[86] Barnes SE. Theory of electron spin resonance of magnetic ions in metals. Adv Phys 1981;30:801–938.
[87] Nelson J. Diffusion-limited recombination in polymer-fullerene blends and its influence on photocurrent collection. Phys Rev B 2003;67:155209/1–155209/10.
[88] Schultz NA, Scharber MC, Brabec CJ, Sariciftci NS. Low-temperature recombination kinetics of photoexcited persistent charge carriers in conjugated polymer/fullerene composite films. Phys Rev B 2001;64:245210/01–245210/07.
[89] Tanaka H, Hasegawa N, Sakamoto T, Marumoto K, Kuroda SI. Light-induced ESR studies of quadrimolecular recombination kinetics of photogenerated charge carriers in regioregular poly(3-alkylthiophene)/C-60 composites: alkyl chain dependence. Jpn J Appl Phys Part 1-Regular Pap Brief Commun Rev Pap 2007;46:5187–92.
[90] Devreux F, Genoud F, Nechtschein M, Villeret B. On polaron and bipolaron formation in conducting polymers. In: Kuzmany H, et al., editors. Electronic properties of conjugated polymers. Berlin: Springer-Verlag; 1987. p. 270–6.
[91] Krinichnyi VI. LEPR spectroscopy of charge carriers photoinduced in polymer/fullerene composites. In: Lechkov M, Prandzheva S, editors. Encyclopedia of polymer composites: properties, performance and applications. Hauppauge, New York, NY: Nova Science Publishers; 2009. p. 417–46.
[92] Tachiya M, Seki K. Theory of bulk electron-hole recombination in a medium with energetic disorder. Phys Rev B 2010;82:085201/01–085201/08.
[93] Molin YN, Salikhov KM, Zamaraev KI. Spin exchange. Berlin: Springer; 1980.
[94] Houze E, Nechtschein M. ESR in conducting polymers: oxygen-induced contribution to the linewidth. Phys Rev B 1996;53:14309–18.
[95] Roth HK, Keller F, Schneider H. Hochfrequenzspectroskopie in der Polymerforschung. Berlin: Academie Verlag; 1984.
[96] Blumenfeld LA, Voevodski VV, Semenov AG. Application of electron paramagnetic resonance in chemistry (Russ). Novosibirsk: Izdat. SO AN SSSR); 1962.
[97] Weil JA, Bolton JR, Wertz JE. Electron paramagnetic resonance: elementary theory and practical applications, vol. 2d. New York, NY: Wiley-Interscience; 2007.
[98] Lebedev YS, Muromtsev VI. EPR and relaxation of stabilized radicals (Russ). Moscow: Khimija); 1972.
[99] Wertz JE, Bolton JR. Electron spin resonance: elementary theory and practical applications. London: Springer Verlag; 2013.
[100] Krinichnyi VI, Roth HK, Schrödner M, Wessling B. EPR study of polyaniline highly doped by p-toluenesulfonic acid. Polymer 2006;47:7460–8.
[101] Krinichnyi VI, Tokarev SV, Roth HK, Schrödner M, Wessling B. EPR study of charge transfer in polyaniline highly doped by p-toluenesulfonic acid. Synth Metals 2006;156:1368–77.
[102] Krinichnyi VI, Yudanova EI, Wessling B. Influence of spin–spin exchange on charge transfer in PANI-ES/P3DDT/PCBM composite. Synth Metals 2013;179:67–73.
[103] Van Vooren A, Kim J-S, Cornil J. Intrachain versus interchain electron transport in poly(fluorene-alt-benzothiadiazole): a quantum-chemical insight. Eur J Chem Phys Phys Chem 2008;9:989–93.
[104] Lan Y-K, Huang C-I. A theoretical study of the charge transfer behavior of the highly regioregular poly-3-hexylthiophene in the ordered state. J Phys Chem B 2008;112:14857–62.

[105] Cheung DL, McMahon DP, Troisi A. Computational study of the structure and charge-transfer parameters in low-molecular-mass P3HT. J Phys Chem B 2009;113:9393–401.
[106] Troisi A, Orlandi GJ. Dynamics of the intermolecular transfer integral in crystalline organic semiconductors. J Phys Chem A 2006;110:4065–70.
[107] Kirkpatrick J, Marcon V, Nelson J, Kremer K, Andrienko D. Charge mobility of discotic mesophases: a multiscale quantum and classical study. Phys Rev Lett 2007;98:227402/01–227402/04.
[108] Butler MA, Walker LR, Soos ZG. Dimensionality of spin fluctuations in highly anisotropic TCNQ salts. J Chem Phys 1976;64:3592–601.
[109] Krasicky PD, Silsbee RH, Scott JC. Studies of a polymeric chromium phosphinate—electron-spin resonance and spin dynamics. Phys Rev B 1982;25:5607–26.
[110] Hennessy MJ, McElwee CD, Richards PM. Effect of interchain coupling on electron-spin resonance in nearly one-dimensional systems. Phys Rev B 1973;7:930–47.
[111] Dyson FJ. Electron spin resonance absorbtion in metals. II. Theory of electron diffusion and the skin effect. Phys Rev B 1955;98:349–59.
[112] Bernier P. The magnetic properties of conjugated polymers: ESR studies of undoped and doped systems. In: Scotheim TE, editor. Handbook of conducting polymers. New York, NY: Marcel Deccer, Inc.; 1986. p. 1099–125.
[113] Krinichnyi VI. Dynamics of spin charge carriers in polyaniline. Appl Phys Rev 2014;1:021305/01–021305/40.
[114] Chapman AC, Rhodes P, Seymour EFW. The effect of eddy currents on nuclear magnetic resonance in metals. Proc Phys Soc B 1957;70:345–60.
[115] Poole CP. Electron spin resonance, a comprehensive treatise on experimental techniques. New York, NY: John Wiley & Sons; 1983.
[116] Krinichnyi VI, Pelekh AE, Tkachenko LI, Kozub GI. Study of spin dynamics in trans-polyacetylene at 2-mm waveband EPR. Synth Metals 1992;46:1–12.
[117] Carrington F, McLachlan AD. Introduction to magnetic resonance with application to chemistry and chemical physics. New York, Evanston, London: Harrer & Row, Publishers); 1967.
[118] Pietronero L. Ideal conductivity of carbon p-polymers and intercalation compounds. Synth Metals 1983;8:225–31.
[119] Kivelson S, Heeger AJ. Intrinsic conductivity of conducting polymers. Synth Metals 1988;22:371–84.
[120] Long AR, Balkan N. AC loss in amorphous germanium. Philos Mag B 1980;41:287–305.
[121] Fishchuk II, Kadashchuk AK, Bässler H, Weiss DS. Nondispersive charge-carrier transport in disordered organic materials containing traps. Phys Rev B 2002;66:205208/01–205208/12.
[122] Roth HK, Krinichnyi VI. Spin and charge transport in poly(3-octylthiophene). Synth Metals 2003;137:1431–2.
[123] Krinichnyi VI, Roth HK, Konkin AL. Multifrequency EPR study of charge transfer in poly(3-alkylthiophenes). Phys B 2004;344:430–5.
[124] Krinichnyi VI, Roth HK. EPR study of spin and charge dynamics in slightly doped poly(3-octylthiophene). Appl Magn Reson 2004;26:395–415.
[125] Konkin A, Ritter U, Scharff P, Roth H-K, Aganov A, Sariciftci NS, et al. Photo-induced charge separation process in (PCBM-$C_{120}O$)/(M3EH-PPV) blend solid film

studied by means of X- and K-bands ESR at 77 and 120 K. Synth Metals 2010;160:485–9.

[126] Poluektov OG, Filippone S, Martín N, Sperlich A, Deibel C, Dyakonov V. Spin signatures of photogenerated radical anions in polymer-[70]fullerene bulk heterojunctions: high frequency pulsed EPR spectroscopy. J Phys Chem B 2010;114:14426–9.

[127] Krinichnyi VI, Yudanova EI, Denisov NN. The role of spin exchange in charge transfer in low-bandgap polymer:fullerene bulk heterojunctions. J Chem Phys 2014;141:044906/01–044906/11.

[128] Niklas J, Mardis KL, Banks BP, Grooms GM, Sperlich A, Dyakonov V, et al. Highly-efficient charge separation and polaron delocalization in polymer–fullerene bulk-heterojunctions: a comparative multi-frequency EPR and DFT study. Phys Chem Chem Phys 2013;15:9562–74.

[129] De Ceuster J, Goovaerts E, Bouwen A, Hummelen JC, Dyakonov V. High-frequency (95 GHz) electron paramagnetic resonance study of the photoinduced charge transfer in conjugated polymer-fullerene composites. Phys Rev B 2001;64:195206/01–195206/06.

[130] Krinichnyi VI, Yudanova EI. Light-induced EPR study of charge transfer in P3HT/bis-PCBM bulk heterojunctions. AIP Adv 2011;1:022131/01–022131/15.

[131] Krinichnyi VI, Yudanova EI. Light-induced EPR study of charge transfer in P3HT/$PC_{71}BM$ bulk heterojunctions. J Phys Chem C 2012;116:9189–95.

[132] Sensfuss S, Blankenburg L, Schache H, Shokhovets S, Erb T, Konkin A, et al. Thienopyrazine-based low-bandgap polymers for flexible polymer solar cells. Eur Phys J-Appl Phys 2010;51:303204/1–303204/5.

[133] Eaton SS, Eaton GR. EPR spectra of C-60 anions. Appl Magn Reson 1996;11:155–70.

[134] Allemand PM, Srdanov G, Koch A, Khemani K, Wudl F, Rubin Y, et al. The unusual electron-spin-resonance of fullerene C_{60}. J Am Chem Soc 1991;113:2780–1.

[135] Bietsch W, Bao J, Ludecke J, van Smaalen S. Jahn-Teller distortion and merohedral disorder of C-60(-) as observed by ESR. Chem Phys Lett 2000;324:37–42.

[136] Deibel C, Mack D, Gorenflot J, Schöll A, Krause S, Reinert F, et al. Energetics of excited states in the conjugated polymer poly(3-hexylthiophene). Phys Rev B 2010;81:085202–6.

[137] Chen TA, Wu XM, Rieke RD. Regiocontrolled synthesis of poly(3-alkylthiophenes) mediated by Rieke zink—their characterization and solid-state properties. J Am Chem Soc 1995;117:233–44.

[138] Wienk MM, Kroon JM, Verhees WJH, Knol J, Hummelen JC, van Hal PA, et al. Efficient methano[70]fullerene/MDMO-PPV bulk heterojunction photovoltaic cells. Angewandte Chemie-Int Edn 2003;42:3371–5.

[139] Yamanari T, Taima T, Sakai J, Saito K. Highly efficient organic thin-film solar cells based on poly(3-hexylthiophene) and soluble C-70 fullerene derivative. Jpn J Appl Phys 2008;47:1230–3.

[140] Boland P, Sunkavalli SS, Chennuri S, Foe K, Abdel-Fattah T, Namkoong G. Investigation of structural, optical, and electrical properties of regioregular poly(3-hexylthiophene)/fullerene blend nanocomposites for organic solar cells. Thin Solid Films 2010;518:1728–31.

[141] Sperlich A, Liedtke M, Kern J, Kraus H, Deibel C, Filippone S, et al. Photoinduced C(70) radical anions in polymer:fullerene blends. Phys Status Solidi-Rapid Res Lett 2011;5:128–30.
[142] Krinichnyi VI, Yudanova EI. Structural effect of electron acceptor on charge transfer in poly(3-hexylthiophene)/methanofullerene bulk heterojunctions. Solar Energy Mater Solar Cells 2011;95:2302–13.
[143] Pénicaud A, Peréz-Benitez A, Escudero R, Coulon C. Single crystal synthesis of $[(C_6H_5)_4P]_2[C_{70}][I]$ by electrocrystallization and experimental determination of the g-value anisotropy of C_{70}•- and C_{60}•- at 4.2 K. Solid State Commun 1995;96:147–50.
[144] Reed CA, Bolskar RD. Discrete fulleride anions and fullerenium cations. Chem Rev 2000;100:1075–120.
[145] Tanaka K, Zakhidov AA, Yoshizawa K, Okahara K, Yamabe T, Yakushi K, et al. Magnetic properties of TDAE-C-60 add TDAE-C-70 where TDAE is tetrakis (dimethylamino)ethylene. Phys Rev B 1993;47:7554–9.
[146] Friedrich J, Schweitzer P, Dinse KP, Rapta P, Stasko A. EPR study of radical-anions of C-60 and C-70. Appl Magn Reson 1994;7:415–25.
[147] Hase H, Miyatake Y. Comparative ESR study of C-60 and C-70 radical-anions produced in gamma-irradiated organic-solid solutions at 77 K. Chem Phys Lett 1995;245:95–101.
[148] Adrian FJ. Spin-orbit effects in fullerenes. Chem Phys 1996;211:73–80.
[149] Stone AJ. Gauge invariance of the g tensor. Proc R Soc A: Math Phys Eng Sci 1963;A271:424–34.
[150] Dubois D, Kadish KM, Flanagan S, Haufler RE, Chibante LPF, Wilson LJ. Spectroelectrochemical study of the C60 and C70 fullerenes and their monoanions, dianions, trianions, and tetraanions. J Am Chem Soc 1999;113:4364–6.
[151] Krinichnyii VI, Yudanova EI. Influence of morphology of low-band-gap PCDTBT: PC71BM composite on photoinduced charge transfer: LEPR spectroscopy study. Synth Metals 2015. Available from: http://dx.doi.org/10.1016/j.synthmet.2015.09.019.
[152] Krinichnyi VI. Relaxation and dynamics of spin charge carriers in polyaniline. In: Wythers MC, editor. Advances in materials science research. Hauppauge, New York, NY: Nova Science Publishers; 2014. p. 109–60.
[153] Krinichnyi VI, Roth HK, Sensfuss S, Schrödner M, Al Ibrahim M. Dynamics of photoinduced radical pairs in poly(3-dodecylthiophene)/fullerene composite. Phys E 2007;36:98–101.
[154] Krinichnyi VI. Dynamics of charge carriers photoinduced in poly(3-dodecylthiophene)/fullerene composite. Acta Mater 2008;56:1427–34.
[155] Krinichnyi VI. Dynamics of charge carriers photoinduced in poly(3-dodecylthiophene)/fullerene bulk heterojunction. Solar Energy Mater Solar Cells 2008;92:942–8.
[156] Krinichnyi VI. An ESR study of photoinduced charge transport in the polymer/fullerene system. High Energy Chem 2008;42:572–5.
[157] Krinichnyi VI, Yudanova EI. LEPR spectroscopy of charge carriers photoinduced in polymer/fullerene bulk heterojunctions. J Renewable Sustain Energy 2009;1:043110/01–043110/18.

[158] Krinichnyi VI, Balakai AA. Light-induced spin localization in poly(3-dodecylthiophen)/PCBM composite. Appl Magn Reson 2010;39:319–28.
[159] Krinichnyi VI. EPR study of charge transfer in the poly-3-dodecylthiophene-fullerene system. Polym Sci, Ser A 2010;52:26–32.
[160] Yudanova EI, Krinichnyi VI. Influence of ultrasonic, microwave, and thermal effects on photoinduced charge transfer in poly(3-hexylthiophene)-methanofullerene composites: EPR study. Polym Sci Ser A 2013;55:233–43.
[161] Marumoto K, Muramatsu Y, Takeuchi N, Kuroda S. Light-induced ESR studies of polarons in regioregular poly(3-alkylthiophene)-fullerene composites. Synth Metals 2003;135:433–4.
[162] Janssen RAJ, Moses D, Sariciftci NS. Electron and energy transfer processes of photoexcited oligothiophenes onto tetracyanoethylene and C60. J Chem Phys 1994;101:9519–27.
[163] Tong MH, Coates NE, Moses D, Heeger AJ, Beaupre S, Leclerc M. Charge carrier photogeneration and decay dynamics in the poly(2,7-carbazole) copolymer PCDTBT and in bulk heterojunction composites with PC70BM. Phys Rev B 2010;81:125210–15.
[164] Kočka J, Elliott SR, Davis EA. AC conductivity and photo-induced states in amorphous semiconductors. J Phys C—Solid State Phys 1979;12:2589–96.
[165] Tanaka K, Sato T, Kuga T, Yamabe T, Yoschizawa K, Okahara K, et al. Weak suppression of ferromagnetism in tetrakis(dimethylamino)ethylene-(C60)1-x(C70)x. Phys Rev B Solid State 1995;51:990–5.
[166] Gotschya B, Gompper R, Klos H, Schilder A, Schütz W, Völkel G. Ferromagnetic versus molecular ordering in C60 charge transfer complexes. Synth Metals 1996;77:287–90.
[167] Conwell EM, Duke CB, Paton A, Jeyadev S. Molecular conformation of polyaniline oligomers: optical absorption and photoemission of three-phenyl molecules. J Chem Phys 1988;88:3331–7.
[168] Harigaya K. Long-range excitons in conjugated polymers with ring torsions: poly (para-phenylene) and polyaniline. J Phys Condensed Matter 1998;10:7679–90.
[169] Łuźny W, Trznadel M, Proń A. X-Ray diffraction study of reoregular poly(3-alkylthiophenes). Synth Metals 1996;81:71–4.
[170] Buchachenko AL, Vasserman AM. Stable radicals (Russ). Moscow: Khimija); 1973.
[171] Williams JM, Ferraro JR, Thorn RJ, Carlson KD, Geiser U, Wang HH, et al. Organic superconductors (including fullerenes): synthesis, structure, properties, and theory. Englewood Cliffs, NJ: (Prentice-Hall, Inc.; 1992.
[172] Yazawa K, Inoue Y, Shimizu T, Tansho M, Asakawa N. Molecular dynamics of regioregular poly(3-hexylthiophene) investigated by NMR relaxation and an interpretation of temperature dependent optical absorption. J Phys Chem B 2010;114:1241–8.
[173] Breiby DW, Sato S, Samuelsen EJ, Mizoguchi K. Electron spin resonance studies of anisotropy in semiconducting polymeric films. J Polym Sci Part B-Polym Phys 2003;41:3011–25.
[174] Marchant S, Foot PJS. Poly(3-hexylthiophene)-zinc oxide rectifying junctions. J Mater Sci-Mater Electron 1995;6:144–8.
[175] Al Ibrahim M, Roth HK, Schrödner M, Konkin A, Zhokhavets U, Gobsch G, et al. The influence of the optoelectronic properties of poly(3-alkylthiophenes) on the device parameters in flexible polymer solar cells. Org Electron 2005;6:65–77.

[176] So F, Kido J, Burrows P. Organic light-emitting devices for solid-state lighting. Mater Res Soc Bull 2008;33:663–9.
[177] Sharma GD. Advances in nano-structured organic solar cells. In: Badescu V, Paulescu M, editors. Physics of nanostructured solar cells. New York, NY: Nova Science Publishers; 2010. p. 361–460.
[178] Krinichnyi VI, Yudanova EI, Denisov NN. Light-induced EPR study of charge transfer in poly(3-hexylthiophene)/fullerene bulk heterojunction. J Chem Phys 2009;131:044515/01–044515/11.
[179] Krinichnyi VI, Yudanova EI, Denisov NN. EPR study of charge transfer photoinduced in poly(3-hexylthiophene)/fullerene composite. Polym Sci Ser A 2010;52:715–26.
[180] Krinichnyi VI, Grinberg OY, Nazarova IB, Kozub GI, Tkachenko LI, Khidekel ML, et al. Polythiophene and polyacetylene conductors in the 3-cm and 2-mm electron spin resonance bands. Bull Acad Sci USSR Div Chem Sci 1985;34:425–7.
[181] Obrzut J, Page KA. Electrical conductivity and relaxation in poly(3-hexylthiophene). Phys Rev B 2009;80:195211/01–195211/07.
[182] Shklovskii BI, Efros AL. Electronic properties of doped semiconductors. New York, NY: Springer-Verlag; 1984.
[183] Tycko R, Dabbagh G, Fleming RM, Haddon RC, Makhija AV, Zahurak SM. Molecular dynamics and the phase transition in solid C_{60}. Phys Rev Lett 1991;67:1886–9.
[184] Denisov NN, Krinichnyi VI, Nadtochenko VA. Spin properties of paramagnetic centers photogenerated in crystals of complexes between C60 and TPA. In: Kadish K, Ruoff R, editors. Fullerenes. Recent advances in the chemistry and physics of fullerenes and related materials. Pennington, NJ: The Electrochemical Society, Inc.; 1997. p. 139–47.
[185] Pike GE. AC conductivity of scandium oxide and a new hopping model for conductivity. Phys Rev B 1972;6:1572–80.
[186] Elliott SR. On the super-linear frequency dependent conductivity of amorphous semiconductors. Solid State Commun 1978;28:939–42.
[187] Parneix JP, El Kadiri M. Frequency- and temperature-dependent dielectric losses in lightly doped conducting polymers. In: Kuzmany H, et al., editors. Electronic properties of conjugated polymers. Berlin: Springer-Verlag; 1987. p. 23–6.
[188] Agostini G, Corvaja C, Pasimeni L. EPR studies of the excited triplet states of $C_{60}O$ and $C_{60}C_2H_4N(CH_3)$ fullerene derivatives and C_{70} in toluene and polymethylmethacrylate glasses and as films. Chem Phys 1996;202:349–56.
[189] Morosin B, Hu ZB, Jorgensen JD, Short S, Schirber JE, Kwei GH. Ne intercalated C-60: diffusion kinetics. Phys Rev B 1999;59:6051–7.
[190] Harsanyi G. Polymer films in sensor applications. Boca Raton, FL: CRC Press; 1995.
[191] ElKaoutit M. Application of conducting polymers in electroanalysis. In: Motheo AJ, editor. Aspects on fundaments and applications of conducting polymers. Rijeka: InTech; 2011. p. 43–66.
[192] Lubentsov BZ, Timofeeva ON, Saratovskikh SL, Krinichnyi VI, Pelekh AE, Dmitrenko VV, et al. The study of conducting polymer interaction with gaseous substances. 4. The water-content influence on polyaniline crystal structure and conductivity. Synth Metals 1992;47:187–92.

[193] Krinichnyi VI. Investigation of biological systems by high-resolution 2-mm wave band ESR. J Biochem Biophys Methods 1991;23:1–30.
[194] Krinichnyi VI. Investigation of biological systems by high resolution 2-mm wave band EPR. Appl Magn Reson 1991;2:29–60.
[195] Goldenberg LM, Krinichnyi VI. Water-sensitive sensor based on modified poly (vinylchloride). Synth Metals 1993;53:403–7.
[196] Davydov AS. Solitons in molecular systems (Russ.). Kiev: Naukova Dumka); 1984.
[197] Krinichnyi VI, Eremenko ON, Rukhman GG, Letuchii YA, Geskin VM. Sensors based on conducting organic polymers. Polyaniline. Polym Sci USSR 1989;31:1819–25.
[198] Schuhmann W. Conducting polymers and their application in amperometric biosensors. In: Usmani AM, Akmal N, editors. Diagnostic biosensor polymers, ACS symposium series. Washington, DC: American Chemical Society; 1994. p. 110–23.
[199] Arshak K, Velusamy V, Korostynska O, Oliwa-Stasiak K, Adley C. Conducting polymers and their applications to biosensors: emphasizing on foodborne pathogen detection. IEEE Sens J 2009;9:1942–51.
[200] Goldenberg LM, Krinichnyi VI, Nazarova IB. The Schottky device based on doped poly(para-phenylene). Synth Metals 1991;44:199–203.
[201] Nazarova IB, Krinichnyi VI, Goldenberg LM. Schottky diodes based on poly(para-phenylene) and poly(1,4-dipyrrolobenzene). Synth Metals 1993;53:399–402.
[202] Cosnier S, Karyakin A, editors. Electropolymerization: concepts, materials and applications. New York, NY: Wiley; 2011.
[203] Lupton JM, McCamey DR, Boehme C. Coherent spin manipulation in molecular semiconductors: getting a handle on organic spintronics. Chem Phys Chem 2010;11:3040–58.
[204] Kinoshita M, Iwasaki N, Nishi N. Molecular spectroscopy of the triplet state through optical detection of zero-field magnetic resonance. Appl Spectrosc Rev 1981;17:1–94.
[205] Lee MK, Segal M, Soos ZG, Shinar J, Baldo MA. Yield of singlet excitons in organic light-emitting devices: a double modulation photoluminescence-detected magnetic resonance study. Phys Rev Lett 2005;94:137403–6.
[206] McCamey DR, van Schooten KJ, Baker WJ, Lee SY, Paik S-Y, Lupton JM, et al. Hyperfine-field-mediated spin beating in electrostatically bound charge carrier pairs. Phys Rev Lett 2010;104:017601–4.
[207] Krinichnyi VI, Tokarev SV, Roth HK, Schrödner M, Wessling B. Multifrequency EPR study of metal-like domains in polyaniline. Synth Metals 2005;152:165–8.
[208] Kahol PK. Magnetic susceptibility of polyaniline and polyaniline-polymethylmethacrylate blends. Phys Rev B 2000;62:13803–4.
[209] Wessling B, Srinivasan D, Rangarajan G, Mietzner T, Lennartz W. Dispersion-induced insulator-to-metal transition in polyaniline. Eur Phys J 2000;2:207–10.
[210] Kapil A, Taunk M, Chand S. Preparation and charge transport studies of chemically synthesized polyaniline. J Mater Sci-Mater Electron 2010;21:399–404.
[211] Krinichnyi VI. The nature and dynamics of nonlinear excitations in conducting polymers. Heteroaromatic polymers. Russ Chem Rev 1996;65:521–36.
[212] Krinichnyi VI. The nature and dynamics of nonlinear excitations in conducting polymers. Polyaniline. Russ Chem Bull 2000;49:207–33.
[213] Takeda K, Hikita H, Kimura Y, Yokomichi H, Morigaki K. Electron spin resonance study of light-induced annealing of dangling bonds in glow discharge hydrogenated

amorphous silicon: deconvolution of electron spin resonance spectra. Jpn J Appl Phys Part 1-Regular Papers Short Notes Rev Paps 1998;37:6309–17.

[214] Yanilkin VV, Nastapova NV, Morozov VI, Gubskaya VP, Sibgatullina FG, Berezhnaya LS, et al. Competitive conversions of carbonyl-containing methanofullerenes induced by electron transfer. Russ J Electrochem 2007;43:184–203.

[215] Wessling B. New insight into organic metal polyaniline morphology and structure. Polymers 2010;2:786–98.

[216] Wang ZH, Ray A, MacDiarmid AG, Epstein AJ. Electron localization and charge transport in poly(o-toluidine)—a model polyaniline derivative. Phys Rev B 1991;43:4373–84.

[217] Adrain FJ, Monchick L. Theory of chemically induced magnetic polarization. Effects of $S-T_{\pm 1}$ mixing in strong magnetic fields. J Chem Phys 1979;71:2600–10.

[218] Ginder JM, Richter AF, MacDiarmid AG, Epstein AJ. Insulator-to-metal transition in polyaniline. Solid State Commun 1987;63:97–101.

[219] Yan B, Schultz NA, Efros AL, Taylor PC. Universal distribution of residual carriers in tetrahedrally coordinated amorphous semiconductors. Phys Rev Lett 2000;84:4180–3.

[220] Krinichnyi VI, Roth HK, Hinrichsen G, Lux F, Lüders K. EPR and charge transfer in H_2SO_4-doped polyaniline. Phys Rev B 2002;65:155205/1–155205/14.

[221] Wang ZH, Scherr EM, MacDiarmid AG, Epstein AJ. Transport and EPR studies of polyaniline—a quasi-one-dimensional conductor with 3-dimensional metallic states. Phys Rev B 1992;45:4190–202.

A fundamental review of current knowledge about spectroscopy characterization techniques for polymer nanocomposites—a one-stop reference source for engineers and researchers.

Spectroscopy of Polymer Nanocomposites covers all aspects of the spectroscopic characterization of polymer nanocomposites. More than 25 spectroscopy characterization techniques—almost all used in materials science—are treated in the book, with discussion of their potentialities and limitations. By comparing the techniques with each other and presenting the techniques together with their specific application areas, the book provides scientists and engineers the information needed for solving specific problems and choosing the right technique for analyzing the material structure. From this, the dispersion structure of fillers, property relations, and filler–polymer interactions can be determined, and, ultimately, the right materials can be chosen for the right applications. This handpicked selection of topics, and the combined expertise of contributors from industry, academia, government, and private research organizations across the globe, makes this survey an outstanding reference source for anyone involved in the field of polymer nanocomposites in academia or industry.

- Comprehensive coverage of spectroscopy techniques for analyzing polymer nanocomposites
- Enables researchers and engineers to choose the right technique and make better materials decisions in research and a range of industries
- Provides the fundamentals, information on structure–property relations, and all other aspects relevant for understanding spectroscopic analyses of nanoreinforced polymers and their applications

About the Editors

Dr. Sabu Thomas is a Professor of Polymer Science & Technology and Honorary Director of the International and Inter University Centre for Nanoscience and Nanotechnology, at the School of Chemical Sciences, Mahatma Gandhi University, Kottayam, Kerala, India. Prof. Thomas is a prolific researcher with a total of over 625 publications to his name and is listed as one of the most productive researchers in India by the Council of Scientific and Industrial Research.

Dr. Didier Rouxel is Professor at the Institut Jean Lamour, CNRS, Université de Lorraine, Vandoeuvre-lès-Nancy, France. He has written 80 publications, 6 book chapters, and 138 communications.

Dr. Deepalekshmi Ponnamma is working as a postdoctoral researcher at the Center for Advanced Materials, Qatar University, Doha, Qatar. She has written 6 publications in international journals and 8 book chapters, and has edited 2 books.

Related Titles

Gao (ed.), Advances in Polymer Nanocomposites: Types and Applications, 9781845699406
Tjong & Mai (eds.), Physical Properties and Applications of Polymer Nanocomposites, 9781845696726
Thomas, Shanks & Sarathchandran (eds.), Nanostructured Polymer Blends, 9781455731596

ELSEVIER
William Andrew
Applied Science Publishers
www.williamandrew.com

NANOTECHNOLOGY

ISBN 978-0-323-40183-8
9 780323 401838